

BIOPOLYMER MODIFIED POLYPROPYLENE MESH FOR HERNIA
TREATMENT

A THESIS SUBMITTED TO
THE GRADUATE SCHOOL OF NATURAL AND APPLIED SCIENCES
OF
MIDDLE EAST TECHNICAL UNIVERSITY

BY

SEMA AKBABA

IN PARTIAL FULFILLMENT OF THE REQUIREMENTS
FOR
THE DEGREE OF MASTER OF SCIENCE
IN
BIOTECHNOLOGY

SEPTEMBER 2018

Approval of the thesis:

**BIOPOLYMER MODIFIED POLYPROPYLENE MESH FOR
HERNIA TREATMENT**

Submitted by **SEMA AKBABA** in partial fulfillment of the requirements for the degree of **Master of Science in Biotechnology Department, Middle East Technical University** by,

Prof. Dr. Halil Kalıpçılar
Dean, Graduate School of **Natural and Applied Sciences** _____

Assoc. Prof. Dr. Can Özen
Head of Department, **Biotechnology** _____

Prof. Dr. Ayşen Tezcaner
Supervisor, **Engineering Sciences Dept., METU** _____

Assist. Prof. Dr. Tugan Tezcaner
Co-Supervisor, **General Surg. Dept., Başkent University** _____

Examining Committee Members:

Prof. Dr. Dilek Keskin (Head of Committee)
Engineering Sciences Dept., METU _____

Prof. Dr. Ayşen Tezcaner (Supervisor)
Engineering Sciences Dept., METU _____

Prof. Dr. Sreeparna Banerjee
Biological Sciences Dept., METU _____

Assoc. Prof. Dr. Can Özen
Biotechnology Dept., METU _____

Assist. Prof. Dr. Tugan Tezcaner
General Surgery Dept., Başkent University _____

Date: 07.09.2018

I hereby declare that all information in this document has been obtained and presented in accordance with academic rules and ethical conduct. I also declare that, as required by these rules and conduct, I have fully cited and referenced all material and results that are not original to this work.

Name, Last name: Sema Akbaba

Signature:

ABSTRACT

BIOPOLYMER MODIFIED POLYPROPYLENE MESH FOR HERNIA TREATMENT

Akbaba, Sema

MSc., Department of Biotechnology

Supervisor: Prof. Dr. Ayşen Tezcaner

Co-Supervisor: Assist. Prof. Dr. Tugan Tezcaner

September 2018, 95 pages

Displacement of a tissue through any aperture on the abdominal wall is defined as hernia. Only effective treatment of hernia is surgery, in which an intraperitoneal mesh or membrane is placed to support defected tissue. Ideal intraperitoneal implant should both promote regeneration and prevent intraperitoneal adhesions. Consequently, aim of this thesis was to develop a 3-layered intraperitoneal patch which has immunomodulatory, regenerative and anti-adhesive properties. For this purpose, polypropylene mesh was modified with anti-adhesive pullulan (PUL) hydrogel layer and immunomodulatory electrospun fibroin: chitosan oligosaccharide lactate layer (F: COS). Anti-adhesive potential of PUL hydrogel was tested by cell viability of fibroblasts and 25% (w/v) PUL hydrogel successfully prevented cell adhesion. Furthermore, mechanical testing and degradation revealed that hydrogels with higher than 25% (w/v) concentration would result in inefficient cross-linking whereas water uptake and dimensional change revealed that hydrogels lower than 25% (w/v) concentration were impractical. Additionally, effect of different F: COS ratios on immunomodulatory and regenerative properties of electrospun layer was investigated. Regenerative potential was assessed by cell viability of fibroblasts while immunomodulatory property was determined by the amount of nitric oxide produced

by seeded RAW 264.7 macrophage cells. Cell viability assay revealed that electrospun F: COS 90:10 (w/w) was ideal for cell attachment and proliferation. Electrospun F: COS 90:10 (w/w) was shown to reduce amount of nitric oxide produced by macrophage cells. Based on in vitro results, it was concluded that intraperitoneal patch composed of PP mesh within 25% (w/v) PUL hydrogel with F: COS 90:10 (w/w) electrospun layer on one side holds promise for treatment of hernia and prevention of intraperitoneal adhesions.

Keywords: Hernia, Intraperitoneal Adhesion, Immunomodulation, Regeneration

ÖZ

HERNİ TEDAVİSİ İÇİN BİYOPOLİMER İLE MODİFİYE EDİLMİŞ POLİPROPİLEN ÖRTÜ

Akbaba, Sema
Yüksek Lisans, Biyoteknoloji
Tez Yöneticisi: Prof. Dr. Ayşen Tezcaner
Ortak Tez Yöneticisi: Dr. Öğretim Üyesi Tugan Tezcaner

Eylül 2018, 95 sayfa

Bir organın karın duvarında bulunan bir açıklıktan dolayı yer değiştirmesine hernia adı verilir. Herninin tek etkin tedavisi intraperitoneal yamanın hasarlı bölgeye destek amaçlı dikildiği cerrahi operasyonlardır. İdeal bir intraperitoneal implant hem rejenerasyonu desteklemeli hem de intraperitoneal adezyonları önleyebilmelidir. Bu sebeple bu tezde, yenilenmeyi destekleyici, immünomodülatör, ve adezyon önleyici özelliklere sahip 3 katmanlı bir yama geliştirilmesi hedeflenmiştir. Bu amaçla, polipopilen yama adezyonu engelleyici pullulan (PUL) hidrojel ve immünomodülatör özellikteki elektro eğirilmiş fibroin:kitosan oligosakkaride laktat (F: COS) ile güçlendirilmiştir. PUL hidrojelin adezyon önleyici etkisi fibroblastların canlılığı ile tespit edilmiş ve in vitro çalışmalar %25'lik PUL hidrojelin ümit vadettiğini göstermiştir. Ayrıca, mekanik test ve degradasyon analizi ile konsantrasyonunu %25'den yüksek hidrojellerin yeteri kadar iyi çapraz bağlanamadığı ve su tutma ölçümleri ile konsantrasyonunu %25'den düşük hidrojellerin jellerin kullanışsız olduğu tespit edilmiştir. Ek olarak, değişik oranlardaki F: COS'un immünomodülatör ve rejeneratif etkisi araştırıldı. Rejeneratif potansiyel hücre canlılık analizi ile gerçekleştirilirken immünomodülatör etki taşıyıcılara ekilen makrofaj hücrelerinin ürettiği nitrik oksit miktarı ile blirlendi. Hücre canlılık analizi elektro-eğirilmiş F: COS 90:10'ın hücre

yapışması ve çoğalması için uygun bir ortam sağladığını gösterdi. Aynı zamanda elektro-eğirilmiş F: COS 90:10'ın üretilen nitrik oksit miktarını azalttığı da saptandı. İn vitro çalışma sonuçlarına göre üretilmiş olan karın içi yamasının herni tedavisi ve intraperitoneal adezyonun önlenmesinde potansiyele sahiptir.

Anahtar Kelimeler: Herni, İntraperitoneal Yapışıklık, İmmünomodülasyon, Rejenerasyon

to my cats, Sora & Haru

ACKNOWLEDGEMENTS

I consider myself very lucky to be able to conduct a research on a topic that I deeply love. I have experienced this period as very interesting and instructive. Therefore, I would like to express my gratitude to all the people who helped me throughout this journey.

First and foremost, my deepest appreciation goes to Prof. Ayşen Tezcaner, my thesis advisor, for her support and guidance throughout my study with her knowledge and experience. Her valuable insights and directions gave me needful guidance to complete the research and write this thesis. I am also thankful for her encouragement and endless patience. Many thanks for her close mentorship and contribution to my education in every sense.

I am grateful to Assist. Prof. Tugan Tezcaner, my co-supervisor, for the perspective he brought to my view on tissue engineering. Topic of this thesis and research the strategy were chosen thanks to his knowledge of medicine.

I would also like to express my sincere gratitude to my co-supervisor in disguise, Prof. Dilek Keskin. She was always supportive and positive. I am very thankful for her valuable advices and guidance.

I would like to thank my thesis committee members Prof. Dr. Sreeperna Banerjee, Assoc. Prof. Dr. Can Özen for participating in my thesis defence and for their interest and comments.

I am also grateful to Research Assistant Deniz Atila, my research mentor, for his great contributions during experiments and discussion of results.

I feel very lucky to be surrounded by many good people. I am very thankful to Gülhan Işık, Engin Pazarçeviren, Bahadır Güner, Yasemin Pazarçeviren and Milad Fathi for their contributions in my experiments and thesis as well as their friendship. I am also grateful to Büşra Yıldız, Emine Gökçe and Zehra Kılıç for their never ending love and motivation for many years.

Last but not least, my special thanks go to my mother, Ayten Akbaba, and father, Muharrem Akbaba, for their endless love and support. I am deeply grateful to my parents for the effort they put in my education. I would also like to my brother, Serhat Akbaba, and sister, Sena Akbaba, for always encouraging me to do my best.

TABLE OF CONTENTS

ABSTRACT	v
ÖZ	vii
ACKNOWLEDGEMENTS	x
TABLE OF CONTENTS	xiii
LIST OF TABLES	xvii
LIST OF FIGURES	xviii
LIST OF ABBREVIATIONS	xxi
CHAPTERS	
INTRODUCTION	1
1.1 Physiology of Abdomen.....	1
1.1.1 Abdominal Wall.....	1
1.1.2 Peritoneum	2
1.1.2.1 Peritoneal Complications	3
1.1.2.1.1 Hernia.....	3
1.1.2.1.2 Intraperitoneal Adhesions	5
1.2 Biomaterials	6
1.2.1 Pullulan	8
1.2.2 Chitosan Oligosaccharide Lactate.....	8
1.2.3 Fibroin	9
1.2.4 Polypropylene	10

1.3 Tissue Engineering.....	11
1.4 Immunomodulation.....	12
1.5 Studies on Biomaterials Subjecting Abdominal Wall Treatment	13
1.6 Aim of the Study.....	21
MATERIALS AND METHODS.....	23
2.1 Materials	23
2.2 Methods.....	24
2.2.1 Isolation of Fibroin	24
2.2.2 Fabrication of Intraperitoneal Patch.....	24
2.2.2.1 Modification of Polypropylene Mesh	24
2.2.2.2 Preparation of Electrospun Fibroin: Chitosan Oligosaccharide Lactate Layer	25
2.2.2.3 Preparation of Pullulan Hydrogel Layer	29
2.2.3 Characterization of Intraperitoneal Patch	30
2.2.3.1 Assessment of Physical Properties.....	30
2.2.3.1.1 Analysis of Fiber Morphology.....	30
2.2.3.1.2 Water Uptake Analysis	30
2.2.3.1.3 Degradation Analysis.....	32
2.2.3.1.4 Determination of Dimensional Change	33
2.2.3.2 Water Contact Angle.....	33
2.2.3.3 Assessment of Mechanical Properties	34
2.2.3.3.1 Compression Test.....	34
2.2.3.3.2 Tensile Test.....	34
2.2.4 Cell Culture Studies	34

2.2.4.1 Assessment of Cell Viability.....	35
2.2.4.2 Assessment of Immunomodulatory Properties	36
2.2.4.3 Assessment of Cell Morphology	36
2.2.5 Statistical Analysis	37
RESULTS AND DISCUSSION	39
3.1 Modification of PP Layer.....	39
3.1.1 X-Ray Photoelectron Spectroscopy Scanning Analysis	39
3.2 Characterization of Intraperitoneal Patch.....	41
3.2.1 Assessment of Physical Properties.....	41
3.2.1.1 Analysis of Fiber Morphology	41
3.2.1.2 Water Uptake Analysis	48
3.2.1.3 Degradation Analysis	50
3.2.1.3.1 Degradation of PUL Layer.....	50
3.2.1.3.2 Degradation of F: COS Layer	55
3.2.1.4 Determination of Dimensional Change.....	59
3.2.2 Assessment of Mechanical Properties.....	61
3.2.2.1 Compression Test.....	61
3.2.2.2 Tensile Test	62
3.3 Water Contact Angle Measurement	63
3.4 Cell Culture Studies	65
3.4.1 Assessment of Cell Viability.....	65
3.4.1.1 Cell Viability on PUL Layer	65
3.4.1.2 Cell Viability on F: COS Layer	67
3.4.1.3 Assessment of Cell Morphology	69

3.4.2 Assessment of Immunomodulatory Properties	71
CONCLUSION.....	75
REFERENCES	77
APPENDIX.....	95

LIST OF TABLES

Table 1. 1 Commercially available intraperitoneal meshes used for treatment of hernia (Fragiskos, 2007, Chapter 35).....	5
Table 2. 1 Parameters used for electrospinning of F: COS with different w/w ratios using HFIP:DMEM (9:1 v/v) solvent system.....	26
Table 2. 2 Parameters used for electrospinning of F: COS with different w/w ratios using TFA: DCM (7:3 v/v) solvent system.	27
Table 2. 3 Parameters used for electrospinning of F: COS with different w/w ratios using HFIP: TFA (9:1 v/v) solvent system.....	28
Table 2. 4 Amounts of components used for a 200 µL gel of different concentrations.	29
Table 2. 5 Ingredients of Tyrode’s solution.	31
Table 3. 1 Atomic ratios of C, O ₂ and P on PP mesh before and after plasma treatment.	40
Table 3. 2 Mean fiber diameter of samples with different F: COS ratios that were electrospun using HFIP:TFA (9:1 v/v) solvent system. “*” indicates that the group was significantly different than other groups (n=50, p<0.05).....	47
Table 3. 3 Calculated Young’s modulus (E), compressive strength (σ) and total strain (ε) values for PUL15, PUL20, PUL25, PUL30 and PUL35 hydrogels. Young’s modulus and compressive strength increases significantly with increasing hydrogel concentration, except for PUL 30. There was no significance between PUL25 and PUL30 in terms of Young’s modulus and compressive strength (n=6, p<0.05).	61
Table 3. 4 Calculated tensile strength for PP and PUL25-PP. (n=4).	62

LIST OF FIGURES

Figure 1. 1 Anatomy of abdominal wall.	2
Figure 1. 2 Classification of biomaterials.	7
Figure 1. 3 Structure of PUL repeating unit.....	8
Figure 1. 4 Structure of COS repeating unit.	9
Figure 1. 5 Structure of N terminal domain of Bombyx mori silk fibroin.....	10
Figure 1. 6 Structure of PP repeating unit.....	11
Figure 3. 1 XPS analysis XPS spectra of (a) non-treated PP mesh and (b) air plasma treated PP mesh.....	40
Figure 3. 2 SEM images of electrospun F: COS 100:0 (^{w/w}) fibers with a) HFIP:1XDMEM, b) HFIP:5XDMEM or c) HFIP:10XDMEM (9:1 ^{v/v}) as solvent. Ribbon-like fiber morphology was observed in all meshes that were electrospun in different solvent systems (Scale bar:100 μ m).....	42
Figure 3. 3 SEM images of electrospun F: COS a) 100:0, b)95:5, c) 90:10, d)80:20, e)70:30 and f) 60:40 (^{w/w}) fibers. TFA: DCM (7:3 ^{v/v}) was used as solvent system (Scale bar:100 μ m).....	43
Figure 3. 4 SEM images of electrospun F: COS a) 100:0, b) 95:5, c) 90:10, d) 80:20, e) 70:30 and f) 60:40 g) 50:50 (^{w/w}) fibers. HFIP: TFA (9:1 ^{v/v}) was used as the solvent system (Scale bar: 20 μ m).....	45
Figure 3. 5 Water uptake percentages of PUL15, PUL20, PUL25, PUL30 and PUL35 hydrogels in Tyrode's solution (pH 7.4) at 37°C. Water uptake was calculated as the ratio of amount of water conserved in hydrogel to dry weight of hydrogel. PUL15 showed the highest water uptake at all given time points. At all time points, water uptake percentage of PUL15 hydrogels were significantly highest. From 5 th hr	

onwards, water uptake percentage of PUL25 group was significantly lower than PUL20 group and significantly higher than PUL30 group. (n=6, p<0.05).48

Figure 3. 6 Weight loss of PUL15, PUL20, PUL25, PUL30 and PUL35 hydrogels in Tyrode’s solution (pH 7.4) at 37°C. From day 4 onwards, there was no statistical difference between weight loss percentages of PUL15 and PUL20 as well as PUL25 and PUL30. “*” indicates statistical significance between groups whereas “#” stands for non-significant difference between groups (n=6, p<0.05).51

Figure 3. 7 Weight loss percentages of PUL20 and PUL25 hydrogels in PBS solution (0.1M pH 7.4) or PBS solution containing 57.4 ng/mL trypsin (T) or 339 ng/mL α -amylase (A) at 37°C. “*” indicates significant difference between groups whereas “#” stands for non-significant difference between groups (n=6, p<0.05).53

Figure 3. 8 pH values recorded during enzymatic degradation of PUL20 and PUL25 hydrogels in PBS solution (pH 7.4) or PBS solution containing 57.4 ng/mL trypsin (T) 339 ng/mL α -amylase (A) at 37°C.55

Figure 3. 9 SEM images of F: COS 90:10 (w/w) fibers incubated (a-d) in PBS, (e-h) in PBS containing 339 ng/mL α -Amylase and in PBS containing 57.4 ng/mL Trypsin at days 1, 4, 7 and 10 (Scale bar: 20 μ m).56

Figure 3. 10 pH values of degradation media containing PBS, 339 ng/mL α -Amylase in PBS and in 57.4 ng/mL Trypsin in PBS at days 1, 4, 7 and 14 (n=4 p<0.05).59

Figure 3. 11 (a) Diameter and (b) thickness change percentages of freeze-dried PUL20 and PUL25 hydrogels, at different stages of production. “*” was used as a notification for statistically significant values (n=6, p<0.05).60

Figure 3. 12 Image of a PUL25-PP sample breaking after tensile test.62

Figure 3. 13 Water contact angle values of PUL-side and F: COS-side of intraperitoneal patch and F: COS layer alone. PUL25 hydrogel was chosen for PUL-side while electrospun F: COS 90:10 (^w/_w) was chosen for F: COS-side of the intraperitoneal patch. “*” indicates statistical difference among groups whereas “#” stands for non-significant difference between groups (n=4, p<0.05).64

Figure 3. 14 Percent reduction of Alamar Blue for L929 cells seeded (25,000 cells/cm²) on TCPS, air-dried PUL20 hydrogels, PUL25, PUL30 and PUL35

hydrogels. Percent reduction Alamar Blue showed highest value at all given time points. Percent reduction of PUL hydrogels were non-significant at days 1,4 and 7. “*” indicates statistical significance whereas “#” stands for non-significant values (n=6, p<0.05). 65

Figure 3. 15 Percent reduction of Alamar Blue by L929 cells seeded (25,000 cells/cm²) on TCPS, freeze-dried PUL20 hydrogels and freeze-dried PUL25 hydrogels. There was no statistical difference between percent reduction values observed between PUL20 and PUL25 hydrogel groups at all time points. Moreover, percent reduction values observed in both hydrogel groups was lower than observed in TCPS group, at all given time points. “*” indicates statistical difference between groups whereas “#” stands for non-significant difference between groups (n=6, p<0.05). 66

Figure 3. 16 Percent reduction of Alamar Blue by L929 cells seeded (25,000 cells/cm²) on TCPS and electrospun F: COS 100:0, 95:5, 90:10, 80:20, 70:30, 60:40 and 50:50 groups. “*” indicates significant difference between groups (n=6, p<0.05). 68

Figure 3. 17 SEM images of L929 cells seeded (25,000 cells/cm²) on electrospun F: COS with different polymer ratios. (Scale bar: 100 μm). 69

Figure 3. 18 Concentration of NO₂ produced by RAW 264.7 cells seeded on electrospun F: COS layers with different polymer ratios. “*” was used as a notification for statistically significant difference between the groups (n=6, p<0.05). “#” stands for non-significant difference between groups (n=6, p<0.05). 72

Figure A. 1 Standard curve for NO⁻ detection assay constructed with nitrite (NO₂) standards (0-10ng) 95

LIST OF ABBREVIATIONS

A	Absorbance at given wavelength
COS	Chitosan Oligosaccharide Lactate
dH₂O	Distilled Water
E	Young's Modulus
ECM	Extracellular Matrix
F: COS	Fibroin: Chitosan Oligosaccharide Lactate
hr	Hour
IFN-α	Interferon- α
IFN-β1	Interferon- β 1
IFN-γ	Interferon- γ
IL-1	Interleukin-1
IL-2	Interleukin-2
IL-10	Interleukin-10
IL-12	Interleukin-12
IL-13	Interleukin-13
LPS	Lipopolysaccharide
min	Minute
PBS	Phosphate Buffered Saline
PP	poly(propylene)
PUL	Pullulan
PUL-PP	poly(propylene) Embedded Pullulan Hydrogel
PUL-PP-A	poly(propylene) Embedded Pullulan Hydrogel Treated with α -Amylase
PUL-PP-T	poly(propylene) Embedded Pullulan Hydrogel Treated with Trypsin
SEM	Scanning Electron Microscopy

TCPS	Tissue Culture Polystyrene
TNF-α	Tumor Necrosis Factor- α
UV	Ultraviolet
V/v	Volume per volume
W/v	Weight per volume
W/w	Weight per weight
W_{dry}	Dry weight
W_f	Final weight
W_i	Initial weight
W_{wet}	Wet weight
X_f	Final measurement
X_i	Initial Measurement
XPS	X-ray photoelectron spectroscopy
γ_{lv}	Liquid-vapor interfacial energy
γ_{sl}	Solid-liquid interfacial energy
γ_{sv}	Solid-vapor interfacial energy
ϵ	Total strain
σ	Compressive strength

CHAPTER 1

INTRODUCTION

1.1 Physiology of Abdomen

1.1.1 Abdominal Wall

Abdominal wall is an enclosed structure covering the boundaries of abdomen. Abdominal wall is from mesothelial descent as it forms from somites, in early stages of embryonic development (Fragiskos, 2007, Chapter 35; Smith, 2002, Chapter 43). Abdominal wall presents an anatomically organized structure constituting multiple layers with innervation and vascularization (Fragiskos, 2007, Chapter 35). Abdominal wall consists of 9 consecutive layers which are peritoneum, preperitoneal areolar and adipose tissue, transversalis fascia, transversus abdominis muscle, internal oblique muscle, external oblique muscle, superficial fascia, subcutaneous tissue and skin. Figure 1.1 reveals anatomy of abdominal wall. Abdominal wall's blood supply is provided by superior and inferior epigastric arteries while venous drainage is carried through superficial veins above umbilicus to vena cava, in harmony with lymphatic vessels. Abdominal wall is also innervated by branches of thoracic nerves reaching out to the midline (Smith, 2002, Chapter 43).

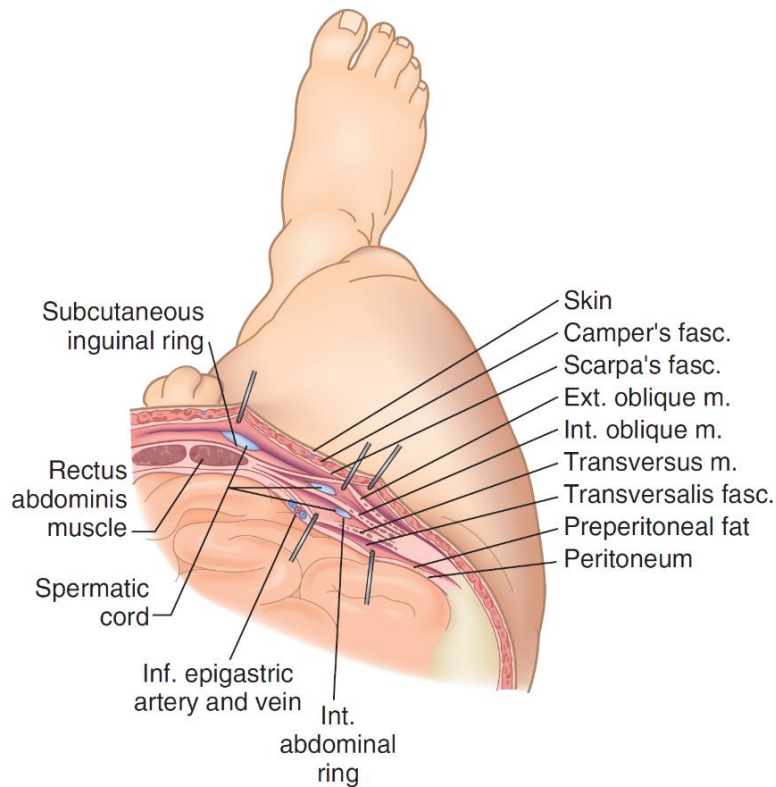


Figure 1. 1 Anatomy of abdominal wall (Smith, 2002, Chapter 43).

1.1.2 Peritoneum

Peritoneum is a semipermeable structure consisting of single layer of mesothelium. Peritoneum has a bilayer structure which allows transfer of chemokines, cells and peritoneal fluid as well as removal of bacteria. Surface area of peritoneum is increased by microvilli on the apical surface of mesothelium. Peritoneum boards visceral peritoneum and parietal peritoneum. Visceral peritoneum covers organs present in abdominal cavity whereas parietal peritoneum lies as the innermost layer of abdominal wall, covering abdominal cavity. Visceral and parietal peritoneum are separated by peritoneal cavity, containing peritoneal fluid. A healthy body contains about 100mL peritoneal fluid, though the amount may increase due to an infection or a disorder (Fragiskos, 2007, Chapter 35; Smith, 2002, Chapter 43).

In case of infection, macrophages are transferred to peritoneal fluid through lymphatic vessels, leading release of pro-inflammatory chemokines and formation of foreign body giant cells. In the meantime, bacteria are removed by lymphatic vessels or opsonized by proteins in peritoneal fluid. Infection of peritoneum also leads to fibrinization of tissue, resulting in entrapment of bacteria in these layers (Smith, 2002, Chapter 43). Permanency of this fibrinization is referred as a disorder named retroperitoneal fibrosis and is considered as an auto-immune disorder (Fragiskos, 2007, Chapter 35).

1.1.2.1 Peritoneal Complications

1.1.2.1.1 Hernia

Hernia can be defined as displacement of an organ, partially or completely, through any aperture on the abdominal wall. Hernia can be congenital or acquired and classified according to its localization (Smith, 2002, Chapter 44). Hernia types include inguinal, femoral, umbilical, incisional, epigastric, Spigelian, obturator, sciatic, perineal and lumbar hernias, with most common types being incisional, umbilical, femoral and inguinal hernias (Fragiskos, 2007, Chapter 35). Incisional hernia refers hernias formed after a surgery. It was reported that up to 20% of patients who undergoes any abdominal surgery would develop incisional hernia (Fragiskos, 2007, Chapter 35). A hernia that is larger than its orifice is classified as strangulated hernia. Strangulated hernia possesses life threatening risk due to its potential to lead gangrene (Smith, 2002, Chapter 44).

Healing of hernia occurs through 4 stages: clotting, inflammation, proliferation and remodeling as in other types of wounds. Different than other types of wounds, in hernia, regeneration of abdominal wall is independent from wound size, as cells migrate from other parallel layers (Sadava, Krpata, Gao, Rosen, & Novitsky, 2014a).

Healing takes 5 to 10 days in cases there is no complication (Brochhausen et al., 2012). Effective treatment of hernia is only with surgery. Although an open surgery can be performed, most of surgeries are done laparoscopically. During surgery, an intra-abdominal mesh is placed as an underlay to ensure closure (Ławniczak, Grobelski, & Pasięka, 2011). However, level of inflammation tends to increase if intra-abdominal mesh is placed. It was stated that long period of inflammation can lead fibrotic encapsulation, resulting in rejection of mesh and failure of treatment. Thus, immunomodulation of wound site is considered important for regeneration of abdominal wall (Sadava et al., 2014a). Commonly used and commercially available meshes and their materials can be found in Table 1.1. Intraperitoneal meshes can be biodegradable, non-biodegradable or partially biodegradable. Biodegradable meshes are biocompatible, yet mechanically insufficient when degraded. It must also be noted that decellularized meshes possess risk of causing immunogenic reaction. On the other hand, non-biodegradable meshes provide mechanical support although they increase fibrotic capsule formation (Fragiskos, 2007, Chapter 35). It was stated that Proceed[®] (Ethicon, USA) was sufficient for prevention of intraperitoneal adhesions, however its usage was limited by its high cost (Deeken, Faucher, & Matthews, 2012). Prolene[®] (Ethicon, USA) is another non-biodegradable mesh that is widely used thanks to its low-cost. Nevertheless, it was reported that Prolene fails to encourage regeneration and prevents intraperitoneal adhesions as it is made of polypropylene (PP) (Arung, Meurisse, & Detry, 2011).

Table 1. 1 Commercially available intraperitoneal meshes used for treatment of hernia (Fragiskos, 2007, Chapter 35).

Biodegradability	Mesh	Material
non-Biodegradable	Composix	PP/poly(tetrafluoroethylene)
	DualMesh	poly(tetrafluoroethylene)
	Proceed	PP/Polydioxanone
	Prolene	Polypropylene
	Ti-MESH	PP/Titanium
Partially Biodegradable	C-Qur	PP/Omega-3 Fatty Acid
	Parietex	Polyester/Collagen
	Sepramesh IP	PP/Hyaluronan
Biodegradable	AlloDerm	Human Dermis
	CollaMend	Porcine Dermis
	Dexon	Polyglycolic acid
	Gore Bio-A	Polyglycolide/Trimethylene Carbonate
	SurgiMend	Fetal Bovine Dermis
	Surgisis Gold	Porcine Small Intestine Submucosa
	Veritas	Bovine Pericardium
	Vicryl	Polyglactin 910

1.1.2.1.2 Intraperitoneal Adhesions

Intraperitoneal adhesions are another complication related to hernia that can be defined as fibrotic attachments forming between parietal peritoneum and outer surface of intestines (Brochhausen et al., 2011). As mentioned earlier, fibrin is released from mesothelial cells, during inflammatory stage of abdominal wall regeneration (Sadava, Krpata, Gao, Rosen, & Novitsky, 2014b) Later in remodeling phase, fibrin stripes are formed and intraperitoneal adhesion forms with vascularization and innervation (Ar'Rajab et al., 1996). Intraperitoneal adhesions possess risks such as chronic pain, obstruction, strangulation and infertility. Thus, it is important for an intra-abdominal

mesh to prevent formation of intraperitoneal adhesions (Lin, Yuan, Zhang, & Sun, 2017).

1.2 Biomaterials

Biomaterial refers to any type of material that is intended to be used in contact with body, in order to replace or enhance tissues or biological systems. Therefore, it can be said that biomaterials must implement biocompatibility (J. B. Park & Lakes, 2007, sec. Preface). Biocompatibility stands for a materials being able to coexist with living systems. On that account, biocompatibility includes biomaterial's being non-toxic, non-carcinogenic, and non-immunogenic (Basu, Katti, & Kumar, 2009, Chapter 1). A biomaterial can be either biodegradable which means that it can be degraded in body by time or non-biodegradable which would stay where it's implanted, permanently. Biodegradable implants are used when complete replacement of regenerated tissue is desired whereas non-biodegradable implants are widely used in hard tissue engineering. Biomaterials also require to have a certain degree of tensile strength, elastic modulus, water uptake capacity or host response all of which depending on tissue they are going to interact or replace (J. B. Park & Lakes, 2007).

Biomaterials can be classified as polymers, ceramics, metals and composites (J. B. Park & Lakes, 2007, sec. Preface). Different subgroups of biomaterials can be found in Figure 1.2. Polymers refer biomaterials with repetitive subunits. Polymeric biomaterials can be natural such as fibroin and pullulan or synthetic like polypropylene. Polymers encompass a wide range of biomaterials with different physical and chemical structures. Ceramics are mostly inorganic biomaterials with high crystallinity and low ductility. Thus, they are often used in hard tissue engineering. Ceramics can be grouped as Metals are also a class of biomaterials that are widely used in hard tissue engineering. Metals are used in the form of alloys to improve overall biomaterial's thermal and electrical conductivity as well as its susceptibility to corrosion. Main types of metals can be summed as stainless steel,

cobalt alloys, chromium alloys and titanium alloys. Composites are final group of biomaterials which can be defined as biphasic biomaterials. Composites can occur naturally or can be obtained as a reinforced biomaterial in order to overcome drawbacks related to that biomaterial (J. B. Park & Lakes, 2007, Chapter 4). After all, biomaterials possess different types of properties leading to both advantages and disadvantages. Thus choice of biomaterial plays important role in order to mimic accurate cellular microenvironment (Lanza, Langer, & Vacanti, 2013, Chapter 19).

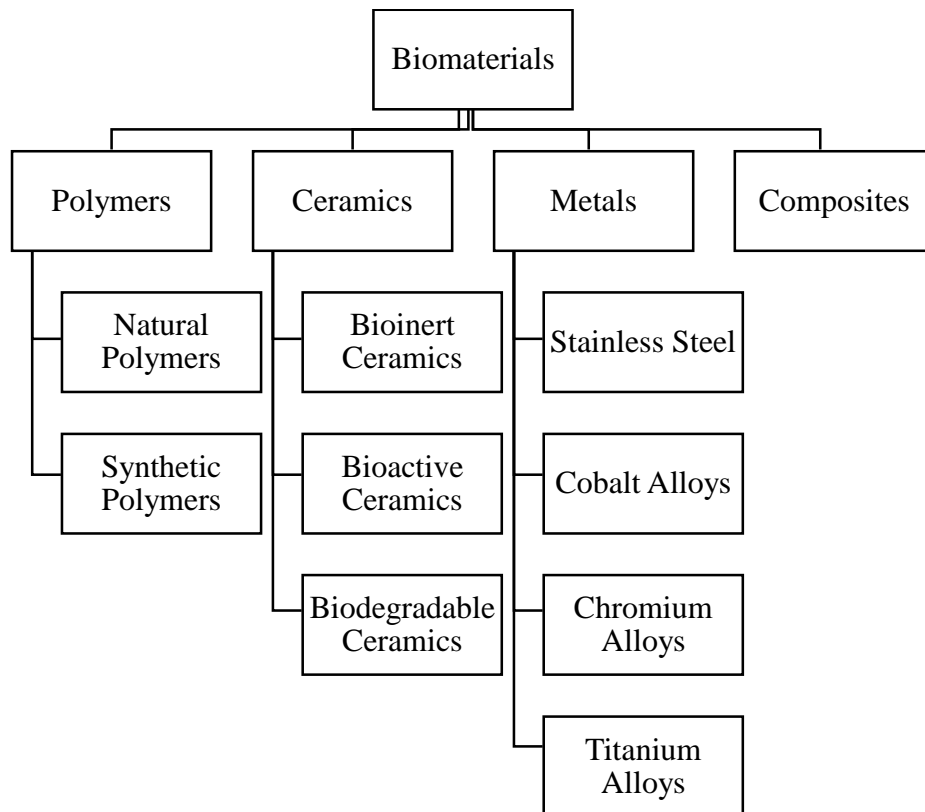


Figure 1. 2 Classification of biomaterials.

1.2.1 Pullulan

Pullulan (PUL) is a homopolysaccharide produced by *Aureobasidium pullulans*. PUL consists of maltotriose units where glucose units are linked by α -1,6 glycosidic bond and maltotriose units are linked by α -1,4 glycosidic bond (Singh, Kaur, Rana, & Kennedy, 2017). Figure 1.3 reveals the structure of PUL subunit. PUL is widely used in food industry as it is water soluble, non-ionic, non-toxic and non-immunogenic (Tabasum et al., 2018). Due to these properties, PUL is also used in tissue engineering, drug delivery and gene delivery (Naseri-Nosar & Ziora, 2018; Singh, Kaur, & Kennedy, 2015). PUL was also referred as one of the immunomodulatory biomaterials. Wang et al. (2016) compared immunomodulatory potential of alkaline PUL pellets in comparison to immunomodulatory drug Resiquimod. It was reported that pellets made of alkaline PUL was able to increase proinflammatory proteins IFN- α and IFN- β 1 (Wang et al., 2016).

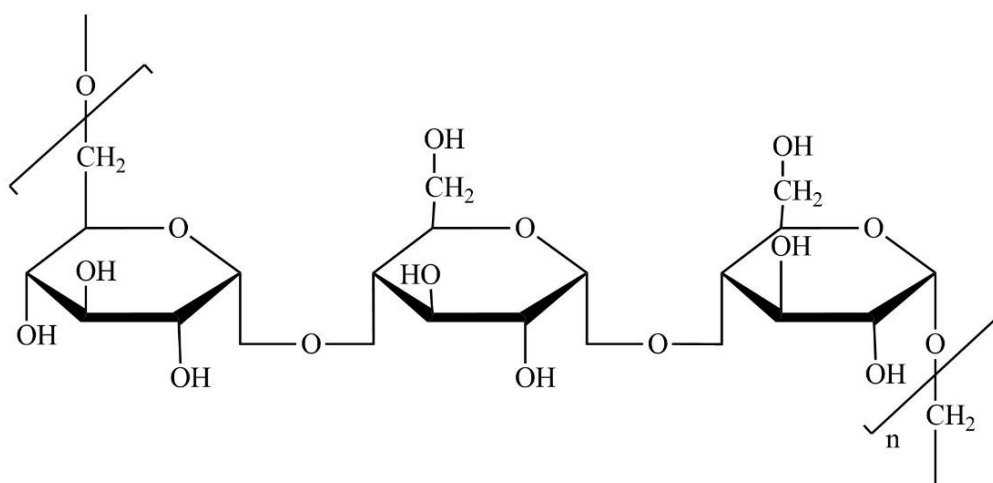


Figure 1. 3 Chemical structure of PUL repeating unit.

1.2.2 Chitosan Oligosaccharide Lactate

Chitosan oligosaccharide lactate (COS) is a depolymerized oligomer derivative of chitosan (Norowski, Mishra, Adatrow, Haggard, & Bumgardner, 2012). Chitosan is

abundant as it is present in exoskeleton of crustaceans, cell wall of fungi etc. COS consists of n-glucosamine and n-acetyl-glucosamine linked through β -(1-4) glycosidic bond (Azuma, Osaki, Minami, & Okamoto, 2015). Structure of COS can be found in Figure 1.4. Unlike chitosan, COS is water soluble, which makes it easier to incorporate into different structures and blends (J. H. Park et al., 2009). Moreover, COS attracts attention due to its anti-cancer and antimicrobial properties (Azuma et al., 2015). Immunomodulatory effect of COS was also reported (Norowski et al., 2012). *In vitro* studies showed that COS containing culture media reduced nitric oxide (NO⁻) production of human colorectal adenocarcinoma cells (Nam, Kim, & Shon, 2007).

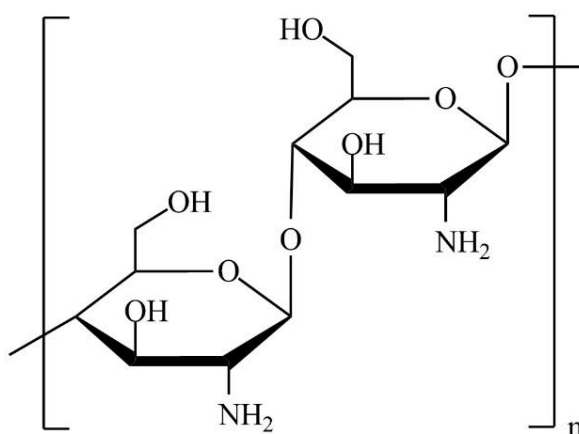


Figure 1. 4 Chemical structure of COS repeating unit.

1.2.3 Fibroin

Fibroin (F) is a protein type polymeric biomaterial retrieved from silk produced by various arthropods. Domestic mulberry silkworm *Bombyx mori* can be addressed as the most common source of fibroin (Qi et al., 2017). Fibroin consists of 390 kDa heavy light chain and 26 kDa light chain connected by a disulfide bond. Due to its unique amino acid content, fibroin presents a semi-crystalline structure which can be turned into more crystalline version by ethanol or methanol treatment. Glycine, alanine, serine, threonine and serine-rich N-terminal part of fibroin forms β -sheet structure in response to pH, temperature, electricity or sonication (Rockwood et al., 2011). Figure

1.5 reveals the secondary structure of N-terminal domain of Bombyx mori fibroin (He et al., 2012). Due to its source, availability and cost fibroin is more advantageous compared to xenogeneic proteins such as collagen (Kundu, Rajkhowa, Kundu, & Wang, 2013). Moreover, fibroin was also reported as one of the immunomodulatory biomaterials. In the study, fibroin nanoparticles present in cell culture media were shown to reduce nitrite levels produced by RAW 264.7 macrophage cells (Chon et al., 2012).

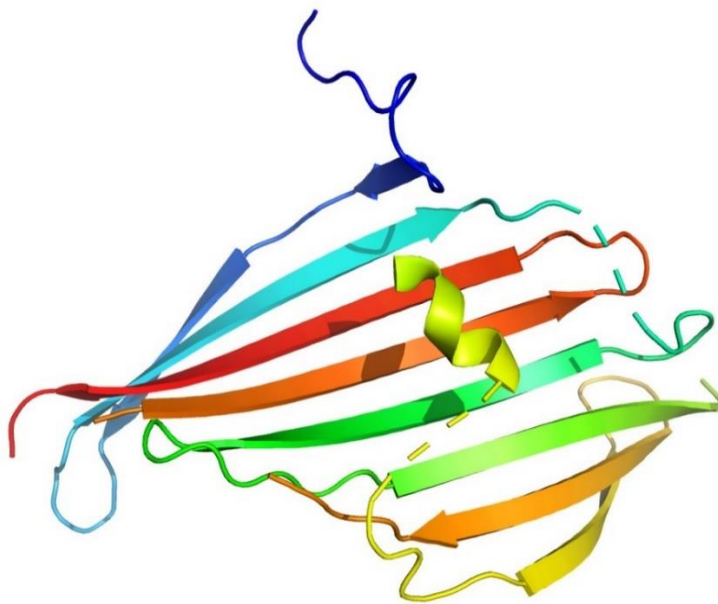


Figure 1. 5 Structure of N terminal domain of Bombyx mori silk fibroin(He et al., 2012).

1.2.4 Polypropylene

Polypropylene (PP) is a thermoplastic polymer produced through polymerization of its monomer, propylene. Molecular structure of repetitive PP chain can be found in Figure 1.6. PP is widely used in surgery in the form of sutures and meshes due to its low cost, availability, ease of processing, high mechanical strength and ease of sterilization (Kelly, Macdougall, Olabisi, & McGuire, 2017). Main issue related with use of PP in surgery is its immunogenicity. It was reported that, after recovery of hernia with PP mesh, immune response was higher during initial periods after

implantation rather than prolonged time. Thus, PP can be reinforced with less immunogenic materials to prevent this issue (Prudente, Fávoro, Filho, & Riccetto, 2016). PP can be modified with various plasma treatment application (Jaleh, Parvin, Wanichapichart, Saffar, & Reyhani, 2010; Yu et al., 2008). For instance, microporous PP membranes were treated with carbon dioxide (CO₂) plasma treatment. Due to introduction of polar groups to polymer chain, fouling index of membranes was lowered (Yu et al., 2008). In another study, PP membranes were subjected to oxygen (O₂) plasma. X-ray photoelectron spectroscopy revealed that hydrophilicity was induced (Jaleh et al., 2010).

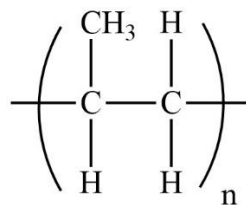


Figure 1. 6 Chemical structure of PP repeating unit.

1.3 Tissue Engineering

Tissue engineering can be defined as a multidisciplinary field encompassing embryology, materials science, pharmacology cell biology and immunology. Tissue engineering aims to overcome organ shortage by generating functional tissues through principles of engineering. For this purpose, tissue engineering employs 3 main elements: tissue scaffolds, cells and growth factors to imitate the original tissue. Tissue engineering requires at least one of the aforesaid elements though they may also be combined together (Lanza et al., 2013, Chapter 1).

Tissue scaffolds are considered as carriers of cells. In that sense, scaffolds are intended to take place of extracellular matrix (ECM). It was stated that, cellular responses are guided through microenvironmental cues (Y. Kim, Ko, Kwon, & Shin, 2016). For this purpose, scaffold types presenting different types of microenvironments were

developed such as 3D printed scaffolds which enable high precision custom designs, electrospun fibers resembling fibrous proteins in ECM, hydrogels supplying entangled hydrophilic microenvironment and so on (Geckil, Xu, Zhang, Moon, & Demirci, 2010; Gizaw et al., 2018; Jammalamadaka & Tappa, 2018). It was noted that an ideal scaffold needs to promote cell adhesion, proliferation and maintenance, provide mechanical support and allow transport of molecules such as nutrients, growth factor and metabolic waste (Geckil et al., 2010).

Cells are another element of tissue engineering. Tissue engineering employs cells to regenerate or replenish tissues. These cells can be cell lines, adult cells or stem cells. Cell lines are used only *in vitro* studies whereas adult cells and stem cells can be used both *in vitro* and *in vivo*. Stem cells can be obtained from embryos, tissues, blood or by induction of somatic cells. Categorization of stem cells are done according to their potency: totipotent, pluripotent and multipotent. In general, choice of cell depends on, cells present in original tissue, accessibility, delivery method, capacity of differentiation, etc. (Howard, Buttery, Shakesheff, & Roberts, 2008).

Growth factors consist final pillar of tissue engineering. During embryonic development, generation of different types of tissues from stem cells is achieved by guidance of growth factors. Consequently, tissue engineering aims to mimic embryological development and employs growth factors. Moreover, delivery system of growth factors possesses importance since dosage and exposure time are considered as important as choice of growth factor (K. Lee, Silva, & Mooney, 2011).

1.4 Immunomodulation

Healing is a complex process involving immune cells as well as native cells of tissue. Healing starts with immediate immune response at the time of injury and takes about 4 hours. During this period, blood proteins and platelets coagulate on site of injury and/or on surface of implant. Then, second stage, induced innate immune response

takes over until day 4. Meantime, macrophages and other immune cells recruit wound site and release proinflammatory cytokines such as TNF- α , IL-1 β , IL-12 and IFN- γ . Finally, adaptive immune response takes place with the activity of lymphocytes releasing TNF- α , IFN- γ , IL1, IL2, IL10 and IL13 (Vishwakarma et al., 2016).

Immune response is considered as biggest challenge for tissue engineering applications (Christo, Diener, Bachhuka, Vasilev, & Hayball, 2015). Prolonged time of immune reaction potentially leads to fibrotic encapsulation of implant Biomaterials and tissue scaffolds carry risk of causing immune reaction. A biomaterial's immunogenic potential is affected by its chemical structure, molecular weight, net charge and hydrophilicity whereas size, shape and surface topography are considered as important factors for a scaffold (Andorko & Jewell, 2017). Healing is started by pro-inflammatory M1 phenotype of macrophages and followed by M2 phenotype for complete regeneration. It was also stated that, macrophage activity is indeed needed for healing since lack of macrophage activation would only result in scar tissue formation (Christo et al., 2015). Hence, immunomodulation, promotion of transition from M1 to M2 phenotype gains importance. Immunomodulation can be achieved on biomaterial level by employing immunomodulatory biomaterials or changing chemical properties of biomaterials. Use of scaffolds releasing pro-inflammatory cytokines and implant surface modifications are also immunomodulation strategies (Vasconcelos et al., 2016; Vishwakarma et al., 2016).

1.5 Studies on Biomaterials Subjecting Abdominal Wall Treatment

Treatment of hernia and prevention of intraperitoneal adhesions were studied by several research groups. In general, designed products can be classified into 3 groups: liquid barriers, sealant glues and solid barriers (Hu et al., 2018; Klink et al., 2013; Thornton, Johns, Campeau, Hoehler, & Dizerega, 1998). Applicability of liquid barriers and injectable gels were investigated as they are easy to apply. These barriers were often combined with antibiotics, chemicals, peptides and enzymes, in order to

prevent intraperitoneal adhesions. Thornton et al. (1998) tested iron cross-linked hyaluronan gels on 13 patients. It was asserted that severity of adhesions was lowered, although number of adhesions were not significantly different than observed in control group consisting of 10 patients (Thornton et al., 1998). In another study, Sonmez et al. (2000) investigated the effect of intraperitoneal pantothenic acid administration on adhesions. *In vivo* study results involving 36 rats showed that, pantothenic acid had no visible effect on prevention of intraperitoneal adhesions (Sonmez et al., 2000). Nehéz et al. (2006) used mice to test the potential of intraperitoneal administration of poly-lysine and poly-glutamate for prevention of intraperitoneal adhesions. Histological evaluations revealed that PP mesh and poly-lysine and poly-glutamate injection reduced the risk of adhesion compared to polypropylene only (Nehéz et al., 2006). In another study, collagen Type-I or melatonin was injected to intraperitoneal cavity of rats. For this purpose, abdominal incisions were created followed by no treatment, collagen solution injection or melatonin solution injection. Results showed that the risk of adhesion formation was lowered with the presence of collagen or melatonin solutions (Koc et al., 2009).

Yetkin et al. (2009) investigated the potential of amniotic membrane implantation supported by intraperitoneal vitamin E administration in rats. Group asserted that amniotic membrane implantation supported by vitamin E administration was more successful than olive oil administration (Yetkin et al., 2009). Contrarily, another study performed on rats reported that amniotic membrane implantation had no significant effect on prevention of intraperitoneal adhesions (Pomilio Di Loreto et al., 2013). As another liquid barrier, Emre et al (2009) reported the effect of intraperitoneal administration of honey on prevention of adhesions in rats. Histological analysis revealed that intraperitoneal injection of honey reduced the risk of intraperitoneal adhesions, yet results were not comparable to routinely used intraperitoneal meshes (Emre et al., 2009). Moreover, efficacy of injectable poly(ϵ -caprolactone-co-lactide)-b-poly(ethyleneglycol)-b-poly(ϵ -caprolactone-co-lactide) copolymer hydrogel was assessed. For this purpose, *in vitro* toxicity of the copolymer hydrogel was tested with

mouse osteoblast cell line MC-3T3. Additionally, abrasions were created in rabbit model and copolymer hydrogel was injected into intraperitoneal cavity. It was concluded that copolymer hydrogel was not toxic and was more effective compared to commercially available poly(lactic acid)-based mesh (Z. Zhang et al., 2011). Another study conducted by the same group showed that aforesaid hydrogels loaded with arginylglycylaspartic acid also reduced the risk of intraperitoneal adhesions. The group noted that arginylglycylaspartic acid incorporated would bind cells while hydrogel acted as physical barrier (Z. Zhang et al., 2012). Although effectivity of the method was reported, its high cost due to incorporated arginylglycylaspartic acid might hinder its usage.

Intraperitoneal administration of icodextrin solution was studied by Klink et al. (2013). Comparison of defected rat abdominal walls revealed that icodextrin solution was more effective than saline solution. However, it was also revealed that there was no significant difference in terms of immune response and regeneration of abdominal wall (Klink et al., 2013). Another study investigated the effect of intraperitoneal injection of garlic oil. Prior to testing, abdominal wall abrasion was created on rats by scraping. According to *in vivo* experiment, it was reported that garlic oil was superior to untreated group in terms of number of intraperitoneal adhesions formed (Sahbaz, Isik, Aynioglu, Gungorduk, & Gun, 2014). The potential of ethyl pyruvate to prevent intraperitoneal adhesions was studied by Artis et al. (2016). Ethyl pyruvate solution and saline solution were injected into intraperitoneal cavity whereas Seprafilm[®] (Genzyme, USA) was implanted in the abdominal wall. *in vivo* study performed on rats showed that ethyl pyruvate was significantly more effective than saline solution. It was also reported that adhesion scoring was the lowest for Seprafilm[®]. However, there was no significant difference between Seprafilm[®] and ethyl pyruvate (Artis et al., 2016). Overall, it was concluded that use of only liquid barrier or hydrogels was insufficient as they do not possess any mechanical support for abdominal wall (Ławniczak et al., 2011).

Sealant glues are also proposed for treatment of hernia and prevention of intraperitoneal adhesions. Rather than being used alone, sealant glues are advised as supportive elements to fix solid barriers (Blázquez et al., 2018). Clarke et al.(2011) evaluated feasibility of the fibrin glue for fixation of Proceed[®] (Ethicon Inc., USA) and compared with fixation by suture and/or tacks in an *in vivo* study using pigs. It was observed that glue applied mesh significantly shrunk more than the meshes fixed with suture and tacks. Additionally, it was reported that there was no significant difference between these two groups in terms of tensile strength and adhesion score (Clarke et al., 2011). Fixation with fibrin glue was also compared with poly(ethylene glycol) glue fixation through implantation of small intestine submucosa membrane to pigs. Study concluded that both sealants were equally effective in considering shear strength, fixation strength and promotion of regeneration (Jenkins et al., 2011). Another study done by Martín-Cartes et al. (2008) examined anti adhesive potential of hyaluronidase cream. For this purpose, Dualmesh[®] and PP mesh were sealed with hyaluronidase cream on pigs with infraumbilical midline incision. Results revealed that hyaluronidase cream reduced adhesion formation in both groups, compared to mesh only groups (Martín-Cartes et al., 2008). Moreover, effectivity of cyanoacrylate glue for mesh fixation was investigated. PP meshes fixed with cyanoacrylate or absorbable strap Securestrap[®] (Ethicon Inc., USA) were implanted in sheep. It was revealed that intraperitoneal adhesions were detected 2 weeks after implantation. Moreover, foreign body giant cell formation was shown to be significantly higher in fixations made with glue (Reynvoet et al., 2015). Although sealant glues are considered to have promising results, their use is hindered as they are expensive and hard to apply (Kukleta, Freytag, & Weber, 2012).

Solid barriers including meshes and membranes consist of products that are widely studied and proposed for treatment of hernia. Hyaluronan was studied by various groups as it is present in native tissue and has regenerative potential (Tsai et al., 2005). Effectivity of hyaluronan/collagen membrane was tested by Tsai et al. For this purpose, 1-ethyl-3-(3-dimethylaminopropyl) carbodiimide hydrochloride cross-linked

collagen/hyaluronan membranes were implanted to animals with midline incisions. Commercially available hyaluronan carboxymethyl cellulose mesh was used as control. *In vivo* studies performed in rats revealed that hyaluronan/collagen membrane delayed formation of intraperitoneal adhesions, however adhesion formation started 4 weeks after implantation (Tsai et al., 2005). In another study, electrospun bilayer membrane consisting of hyaluronic acid/poly(ϵ -caprolactone) and electrospun poly(ϵ -caprolactone) layers was tested for its effectivity against intraperitoneal adhesions. For this purpose, bilayer membrane and electrospun poly(ϵ -caprolactone) membrane were implanted in rats with midline incisions. *In vitro* studies revealed bilayer membrane was more effective compared to both electrospun poly(ϵ -caprolactone) membrane and untreated group. However, membrane was not tested against any commercial product (Jiang, Wang, Yan, & Fan, 2013). In addition to hyaluronic acid, collagen was also studied to investigate its potential for prevention of intraperitoneal adhesions. Kaleya et al. (2005) compared Permacol[®] (Medtronic, USA) to PP Mesh. Midline incisions were formed in rats and treated with either Permacol[®] or PP mesh. Histology analysis showed that Permacol[®] created less foreign body reaction than PP mesh. Adhesions were also shown to be more on PP mesh (Kaleya, 2005). On the other hand, Wotton & Akoh (2009) made a case report on rejection of Permacol[®] due to foreign body reaction by a 72 year old man.

Another study investigated the effect of dried irradiated amniotic membrane reinforced with PP mesh. Incisions created in rats were treated with either PP mesh or dried irradiated amniotic membrane reinforced with PP mesh. Macroscopic evaluation showed that dried irradiated amniotic membrane reinforced with PP mesh had no positive effect on preventing intraperitoneal adhesions (Pomilio Di Loreto et al., 2013). Furthermore, anti-adhesive property of poly(lactide-co-glycolic acid) nanofibers loaded with epigallocatechin gallate was tested on rats. For this purpose, abraded peritoneal incisions were closed with poly(lactide-co-glycolic acid) nanofibers loaded epigallocatechin gallate, poly(lactide-co-glycolic acid) nanofibers or Interceed[®] (Ethicon, USA). Results showed that effectivity of poly(lactide-co-

glycolic acid) nanofibers loaded epigallocatechin gallate was comparable to Interceed[®] and superior to poly(lactide-co-glycolic acid) nanofibers (Shin et al., 2014). Additionally, utility of poly(vinylidene fluoride)/PP mesh was tested. For this purpose, poly(vinylidene fluoride)/PP mesh, PP mesh and PP mesh with oxidized collagen film were implanted in rats with abdominal incision. It was reported that both mesh shrinkage percentage and adhesion formation were higher in PP mesh group and lower in PP mesh with oxidized collagen film group and poly(vinylidene fluoride)/PP monofilament mesh group (Junge et al., 2009). Another study investigated the use of combination of the growth factors with PP mesh coated with electrospun poly(ϵ -caprolactone) for hernia treatment. Electrospun poly(ϵ -caprolactone) fibers were dip coated with insulin-like growth factor-1, basic fibroblast growth factor and transforming growth factor beta-2. Potential of mesh was assessed through implantation in incisional hernia model on chinchilla rabbits and PP mesh and PP mesh coated with electrospun poly(ϵ -caprolactone) were used as control groups. Results showed that poly(ϵ -caprolactone) coating decreased adhesion formation whereas growth factors accelerated regeneration (Plencner et al., 2014). Although study revealed positive results, high cost of growth factors may limit its routine use.

In a study done by Hu et al. (2018) the effect of poly(dopamine) coated PP mesh on prevention of intraperitoneal adhesions was assessed in rat midline incision model. Parietex[®] (Medtronic, USA) mesh, PP mesh and poly(dopamine) coated PP mesh were implanted in abdominal wall. 60 days post implantation results revealed that poly(dopamine) coated PP mesh was superior to PP mesh and similar to Parietex[®], in terms of adhesion prevention (Hu et al., 2018). Furthermore, Fatkhudinov et al., (2018) evaluated the performance of knitted poly(dioxanone) and poly(glycolic acid) meshes. 3cm² defects were closed with either Permacol[®] (Medtronic, USA), knitted poly(dioxanone) mesh or knitted poly(glycolic acid) mesh. Histological analysis showed that poly(glycolic acid) group had more foreign body giant cells compared to Permacol[®] mesh. Additionally, knitted poly(dioxanone) mesh presented the best biocompatibility among all three meshes (Fatkhudinov et al., 2018).

In another study, Dória et al. (2018) investigated adhesion prevention potential of polyamide mesh in rabbit model. Comparison against PP mesh showed that polyamide mesh caused less adhesions and foreign body reaction. Finally, Piasecka-Zelga et al. (2018) evaluated the anti-adhesive potential of bacterial cellulose/chitosan enhanced PP mesh. For this purpose, 4cm² of PP mesh, PP mesh reinforced with bacterial cellulose or PP mesh reinforced with bacterial cellulose/chitosan were implanted in rats. Evaluation after 3 months revealed that all 3 groups developed fibrotic capsule with PP mesh group having the thickest and PP mesh reinforced with bacterial cellulose/chitosan having the thinnest fibrotic capsule (Piasecka-Zelga et al., 2018). Literature was also checked for similar studies. Abed et al. (2008) tested PUL/Dextran hydrogel reinforced with PP mesh in order to alleviate foreign body reaction caused by PP mesh. For this purpose, PUL/dextran hydrogel reinforced PP mesh was compared to decellularized small intestinal submucosa, PP mesh, and PUL/Dextran hydrogel in rats through midline incision. Histological analysis after 30 days showed that PUL/dextran hydrogel reinforced PP mesh led to less inflammation compared to PP mesh. Additionally, level of inflammation was similar in PUL/dextran hydrogel reinforced PP mesh and decellularized small intestinal submucosa (Abed et al., 2008). Anti-adhesive property of PUL was also evaluated by Bang et al. (2016). PUL was functionalized with carboxyl and phenyl groups to become an injectable hydrogel. Prepared gels were injected into peritoneal cavity of rats and cross-linked with horseradish peroxidase and hydrogen peroxide (H₂O₂). Prior to injection, defects with 1 cm² area was created and serosa was abraded. Adhesion scoring of injectable PUL hydrogel group was found to be significantly lower than that of untreated group (Bang et al., 2016). Both studies revealed the potential of PUL for prevention of adhesions. However, PUL is not suitable for cell attachment and proliferation which makes it hindering regeneration (Shi, Le Visage, & Chew, 2011). Thus, in this thesis, need for an extra layer supporting regeneration and immunomodulation was suggested.

Fibroin was also investigated by several groups for treatment of hernia and prevention of intraperitoneal adhesions. First, Gobin, Butler & Mathur (2006) compared

fibroin/chitosan blend membranes to human acellular dermal matrix and PP mesh in guinea pigs in order to investigate its regenerative and anti-adhesive potential. For this purpose, prior to implantation, 8 cm² of abdominal wall was removed. Macroscopic and histological assessments were done 4 weeks post-implantation. Histological analysis showed that fibroin/chitosan membrane promoted ECM remodeling. Moreover, fibrotic capsule was found to be least dense in fibroin/chitosan membrane group. In another study, Guillaume et al. (2016) investigated feasibility of the woven fibroin mesh coated with lectin for hernia treatment. For this purpose, fibroblast cells were seeded on PP mesh, silk mesh and fibroin mesh coated with lectin. It was shown that lectin coating increased cell adhesion and viability. Moreover, immunogenic potential of PP mesh, silk mesh and lectin coated fibroin mesh was assessed through detection of Interleukin-6 level, secreted by peripheral blood mononuclear cells. In a similar study, Zhang et al. (2018) tested feasibility of the silk meshes with varying knitting patterns. For this purpose, differently knitted silk meshes were characterized in terms of tensile strength, suture pullout strength, shear resistance and stiffness. Commercially available PP mesh and PP/poly(ϵ -caprolactone) mesh were used for comparison. Following characterization *in vitro* test was performed by using fibroblastic cell line, L929, whereas *in vivo* study was done by employing rats with abdominal wall excision. *In vitro* experiments showed that highest level of cell attachment was observed on knitted silk mesh. Moreover, *in vivo* experiments revealed that knitted silk mesh group presented least amount of adhesions and thinnest fibrotic tissue among 3 groups.

Konar et al (2017) stated that fibroin hydrogel coated PP mesh was superior to PP mesh. Peritoneal explant cells were cultured on fibroin hydrogel and cell attachment was compared to peritoneum's cell habitat. Regenerative capacity of fibroin was shown via immunohistochemistry. Moreover, PP mesh and fibroin coated PP mesh were implanted in rabbits with ventral hernia. *In vivo* testing revealed that amount of adhesions was lower in fibroin hydrogel coated PP mesh group. Different from these studies, in this thesis, fibroin was used in electrospun form to promote adhesion.

Furthermore, fibroin was electrospun as a blend with chitosan oligosaccharide lactate to achieve immunomodulation. Moreover, electrospun fibroin/chitosan oligosaccharide lactate layer was separated from intraperitoneal cavity by PUL, to prevent intraperitoneal adhesions.

1.6 Aim of the Study

Aim of this thesis was to develop of an immunomodulatory, low-cost and effective intraperitoneal patch for treatment of hernia, regeneration of abdominal wall and prevention of intraperitoneal adhesions. With this objective in mind, a 3-layered intraperitoneal patch was designed so that each layer would contribute to a specific purpose. Electrospun F: COS layer was chosen as first layer to achieve immunomodulation and promote regeneration of abdominal wall. Traditional low-cost PP mesh was included as middle layer to provide mechanical strength. In order to have well integrated layers, highly hydrophobic PP mesh was subjected to air plasma treatment followed by incubation in STMP. As final layer, PUL hydrogel was employed to prevent formation of intraperitoneal adhesions. Prepared intraperitoneal patches were characterized in terms of, morphology, degradation kinetics, water uptake behavior, tensile strength and compressive strength. Finally, effectivity and immunomodulatory properties of developed intraperitoneal patch were confirmed *in vitro* by using L929 mouse fibroblast cells and RAW 264.7 mouse macrophage cells, respectively. Simplified experimental array can be found in Figure 1.7.

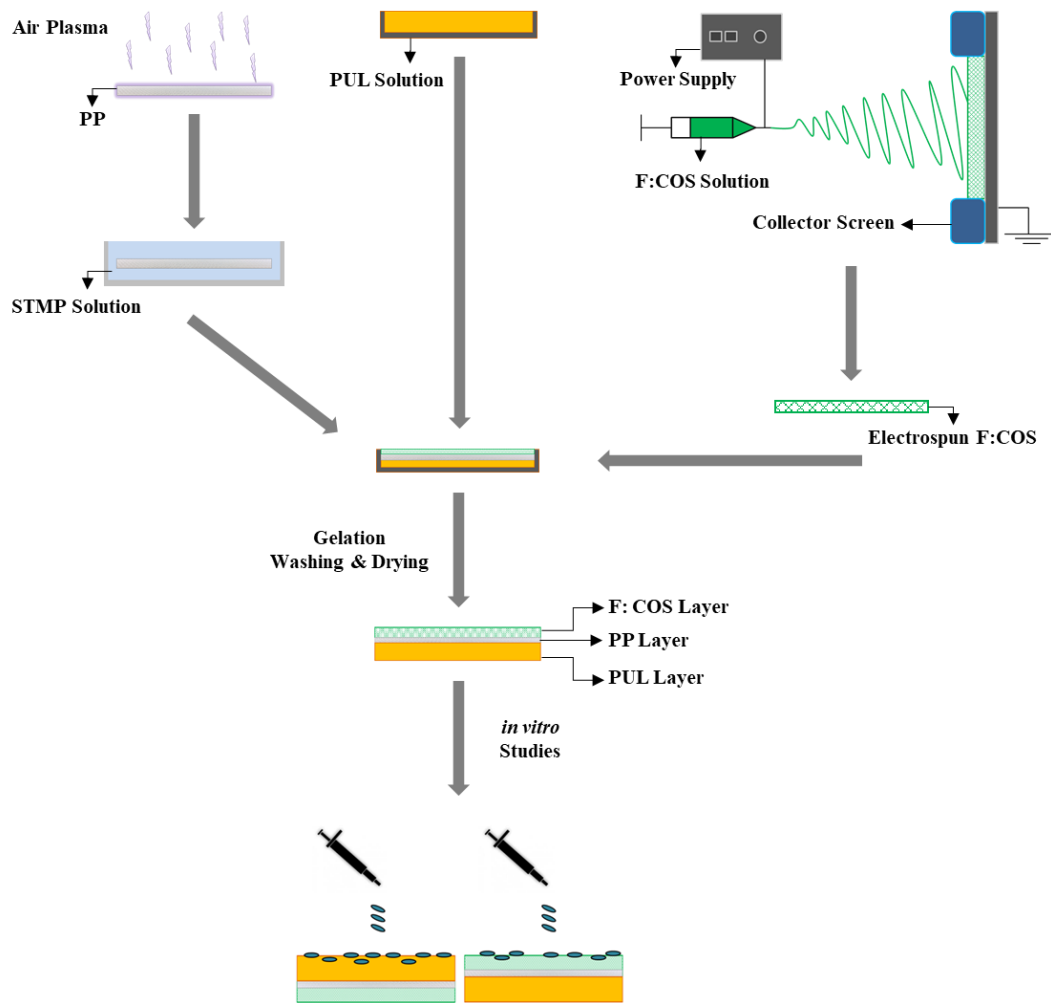


Figure 1. 7 Simplified experimental array.

CHAPTER 2

MATERIALS AND METHODS

2.1 Materials

Bombyx mori silk cocoons were purchased from Kozabirlik (Bursa, Turkey). Pullulan (MW 200,000 Da) was kindly donated by Hayashibara Co., Ltd. (Japan). NO⁻ detection kit was purchased from Biovision, Inc. (USA). Fetal bovine serum (FBS), penicillin/streptomycin (Pen/Strep) and trypsin/ethylenediaminetetraacetic acid (Trypsin/EDTA) were from Biowest (France). Polypropylene meshes were obtained from Venaporta (Turkey). Chitosan oligosaccharide lactate (MW 5,000 Da), Lipopolysaccharide from *Escherichia coli* O55:B5, low glucose Dulbecco's Modified Eagle Media (DMEM) without Phenol Red, Dialysis tubing (MWCO 12,000 Da), trypsin from porcine pancreas, α -amylase from porcine pancreas, sodium bicarbonate (NaHCO₃), lithium bromide (LiBr), sodium trimetaphosphate (STMP), sodium hydroxide (NaOH), ethanol (EtOH), trifluoroacetic acid (TFA) and dichloromethane (DCM) were purchased from Sigma-Aldrich (Germany). 1,1,1,3,3,3-hexafluoro-2-propanol (HFIP), glucose, calcium chloride (CaCl₂), magnesium chloride (MgCl₂), 4-(2-hydroxyethyl)-1-piperazineethanesulfonic acid (HEPES), sodium chloride (NaCl), potassium chloride (KCl), di-sodium hydrogen phosphate (Na₂HPO₄), sodium dihydrogen phosphate (NaH₂PO₄), glutaraldehyde (GTA) and hexamethyldisilazane (HDMS) were obtained from Merck (Germany). Alamar Blue[®] was purchased from Invitrogen (Germany). Mouse fibroblast cell line L929 and mouse macrophage cell line RAW 264.7 were obtained from ATCC (USA).

2.2 Methods

2.2.1 Isolation of Fibroin

Fibroin was isolated from *Bombyx mori* silk cocoons (Rockwood et al., 2011). Briefly, cocoons were cut in 3 mm thick circular pieces and silkworm was disposed. In the meantime, 2 L of 0.02 M sodium bicarbonate (NaHCO_3) solution was prepared and set to 100°C. Following, 5 g of cocoon pieces were degummed in boiling solution, for 30 minutes with occasional stirring. After degumming, obtained silk cotton was rinsed 3 times by sequentially incubating in 1 L of distilled water (dH_2O) for 20 minutes each. Afterwards, silk cotton was removed from dH_2O and excess water was eliminated by squeezing. Sequentially, degummed silk cotton was dried overnight at room temperature. Following, dried silk cotton was dissolved in lithium bromide (LiBr) to yield fibroin solution. For this purpose, 9.3 M of LiBr solution was prepared so that volume of LiBr solution would be 4 times of weight of silk cotton. Then, silk cotton was placed in 80mL beaker and pressed down as much as possible. Following, LiBr was added on top of silk cotton and incubated at 60°C for 4 hours. After dissolution, obtained amber colored fibroin solution was placed in dialysis tubing and dialyzed against dH_2O for 48 hours by changing dH_2O 3 times a day. In the final part of extraction, fibroin solution was further purified by centrifugation. For this purpose, fibroin solution was centrifuged twice at 9000 rpm for 20 minutes at 4°C. After each centrifugation, supernatant was collected while pellet was discarded. Finally, extracted fibroin solution was freeze dried at -80°C, prior to storage at 4°C.

2.2.2 Fabrication of Intraperitoneal Patch

2.2.2.1 Modification of Polypropylene Mesh

PP mesh was modified with plasma treatment in order to obtain better integration between PUL hydrogel and PP mesh layers. For this purpose, each side of PP mesh

was subjected to air plasma treatment by using plasma system (Diener Pico, Germany) at 100 watts for 5 minutes. After modification, PP mesh was immediately placed in either 10% sodium trimetaphosphate (STMP) solution or 10% PUL solution followed by overnight incubation at 4°C. After incubation, samples were washed with distilled water and air dried, prior to storage at 4°C. Modification of meshes were confirmed by employing X-Ray Photoelectron Spectroscopy (PHI 5000 Versaprobe, USA).

2.2.2.2 Preparation of Electrospun Fibroin: Chitosan Oligosaccharide Lactate Layer

In order to determine best immunomodulatory effect, fibroin: chitosan oligosaccharide lactate (F: COS) solutions with 100:0, 95:5, 90:10, 80:20, 70:30, 60:40 and 50:50 F: COS ratios (w/w) were electrospun. Solutions were prepared so that final polymer concentration would be 10% (w/v). With this objective in mind, first, suitability of different solvent systems was investigated. Solution preparation was followed by electrospinning. During this process, electrospinning system consisting of NE-1000 syringe pump (New Era, USA), ES30 power supply, collector screen and electrospinning cabinet was used. Briefly, prepared solution was placed on syringe pump and connected to power supply. Voltage was gradually increased until Taylor cone formation was observed. Subsequently, electrospinning process was initiated. Fiber optimization was carried out considering three parameters: flow rate, distance and voltage for each solvent system and concentration. Following electrospinning process, fibers were incubated in ethanol for 1 hour to enable cross-linking of fibroin (Su et al., 2017). Fiber morphology was visualized with the aid of SEM device (Quanta 400F Field Emission SEM, USA).

In preliminary studies, first, 1,1,1,3,3,3-hexafluoro-2-propanol (HFIP) and low glucose Dulbecco's Modified Eagle Media (DMEM) were chosen as solvents. HFIP:1XDMEM (9:1 v/v), HFIP:5XDMEM (9:1 v/v) and HFIP:10XDMEM (9:1 v/v) solvent systems were prepared. F was dissolved in HFIP whereas COS was dissolved

in either 1X, 5X or 10X DMEM. After complete dissolution, solvents were mixed together. HFIP: DMEM solvent systems were used only for F: COS 100:0 due to instant precipitation of COS after mixing. Parameters used during optimization study for electrospinning can be found in Table 2.1.

Table 2. 1 Parameters used for electrospinning of F: COS with different w/w ratios using HFIP:DMEM (9:1 ^{v/v}) solvent system.

Solvent System	F: COS Ratio	Batch Number	Flow Rate (mL/h)	Voltage (kV)	Distance (cm)
HFIP:1XDMEM	100:0	1-1	6	20	15
		1-2	4	20	15
		1-3	4	20	10
HFIP:5XDMEM	100:0	2-1	6	20	15
		2-2	4	20	15
		2-3	6	20	20
		2-4	6	16	20
		2-5	6	16	17
HFIP:10XDMEM	100:0	3-1	6	20	15
		3-2	6	20	20
		3-3	4	20	15
		3-4	6	16	15

Secondly, suitability of trifluoroacetic acid (TFA): dichloromethane (DCM) (7:3 ^{v/v}) solvent system was investigated. For this purpose, both F and COS were dissolved in TFA. Following, DCM was added, right before electrospinning. F: COS (50:50) (^{w/w}) could not be spun due to precipitation of COS after addition of DCM. Parameters used for electrospinning can be found in Table 2.2.

Table 2. 2 Parameters used for electrospinning of F: COS with different w/w ratios using TFA: DCM (7:3 v/v) solvent system.

F: COS Ratio	Batch Number	Flow Rate (mL/h)	Voltage (kV)	Distance (cm)
100:0	4-1	1	15	12
	4-2	1	20	12
	4-3	1	20	25
95:5	5-1	1	17	22
	5-2	1	19	22
90:10	6-1	2	15	22
	6-2	2	15	20
	6-3	2	15	15
80:20	7-1	2	15	15
	7-2	2	13	15
70:30	8-1	2	13	15
	8-2	2	13	12
60:40	9-1	2	15	15
	9-2	2	15	12

Finally, HFIP: TFA (9:1 v/v) system was prepared by dissolving F in HFIP and COS in TFA. Subsequently, two solutions were mixed. Parameters used for electrospinning can be found in Table 2.3.

Table 2. 3 Parameters used for electrospinning of F: COS with different ^{w/w} ratios using HFIP: TFA (9:1 ^{v/v}) solvent system.

F: COS Ratio	Batch Number	Flow Rate (mL/h)	Voltage (kV)	Distance (cm)
100:0	10-1	1	20	25
	10-2	1	20	20
95:5	11-1	1	20	20
	11-2	1	19	25
	11-3	1	18	25
90:10	12-1	1	18	25
	12-2	1	17	25
80:20	13-1	1	17	25
	13-2	1	16	25
70:30	14-1	1	16	25
	14-2	1	17	25
	14-3	1	18	25
60:40	15-1	1	18	25
	15-2	1	17	25
50:50	16-1	1	18	20
	16-2	1	19	20
	16-3	1	18	25
	16-4	1	19	25

2.2.2.3 Preparation of Pullulan Hydrogel Layer

PUL hydrogel layer was prepared as described by Dulong et al. (2011) by using STMP as cross-linker, with some modifications. Briefly, 15%, 20%, 25%, 30% and 35% (w/v) PUL solutions were prepared in dH₂O. STMP was then added to solutions so that PUL: STMP ratio (w/w) would be 30:10. After complete dissolution, hydrogels with or without PP layer were prepared. For the preparation of hydrogels with PP layer (PUL-PP), 100 µL Pul solution was casted in teflon molds, by using 1mL syringe. Then, cross-linking was initiated with the addition of sodium hydroxide (NaOH). For this purpose, 10% NaOH solution was added so that final PUL: STMP: NaOH weight ratio would be 30:10:1. Solution was stirred thoroughly with syringe needle and incubated at 25°C for 1h, to obtain pre-gel solution. Subsequently, PP mesh was cut in a disc of 1 cm in diameter and placed on top of pre-gel. Then, another 100 µL PUL solution was added and cross-linked as the first layer. For experiments requiring whole 3-layered structure, Electrospun F: COS was placed on top of PUL-PP hydrogel, right after cross-linking of the second layer. For the preparation of hydrogels without PP, 200 µL portions of Pul solutions were casted in teflon molds. Following, PUL hydrogels were cross-linked with the same method and PUL: STMP: NaOH ratio as PUL-PP hydrogels. Afterwards, gels were incubated overnight at 4°C, for complete gelation. Amounts of components for a 200 µL gel are given in Table 2.4, below.

Table 2. 4 Amounts of components used for a 200 µL gel of different concentrations.

Hydrogel	Concentration (w/v%)	dH₂O (µL)	Pul (mg)	STMP (mg)	10% NaOH (µL)
PUL15	15	200	30	10.0	10.0
PUL20	20	200	40	13.3	13.3
PUL25	25	200	50	16.7	16.7
PUL30	30	200	60	20.0	20.0
PUL35	35	200	70	23.3	23.3

After gelation was complete, gels were thoroughly washed with distilled water in order to eliminate NaOH and unbound STMP. Finally, gels were either freeze-dried or air-dried at 25°C, prior to storage at 25°C, in desiccator.

2.2.3 Characterization of Intraperitoneal Patch

2.2.3.1 Assessment of Physical Properties

2.2.3.1.1 Analysis of Fiber Morphology

Electrospun F: COS fibers with different polymer ratios were visualized through SEM (Quanta 400F Field Emission SEM, USA). Prior to visualization, samples were coated with Au/Pd by using sputter coating device (Hummle IV, Turkey). After visualization, fiber diameters were measured from the images using ImageJ (USA). Finally, fiber diameter distribution was obtained. For this purpose, 80 fibers were chosen from 4 images, for each group.

2.2.3.1.2 Water Uptake Analysis

Water uptake percentages of PUL and PUL-PP hydrogels were calculated by using a general gravimetric method (Wittaya-Areekul & Prahsarn, 2006). Tyrode's solution was chosen for this experiment as it is considered as peritoneal fluid simulation (Gokal & Nolph, 2009, Chapter 1). Ingredients of Tyrode's solution can be found in Table 2.5 (Cold Spring Harbor Protocols, 2007). Briefly, given amounts of sodium chloride (NaCl), potassium chloride (KCl), 4-(2-hydroxyethyl)-1-piperazineethanesulfonic acid (HEPES), calcium chloride (CaCl₂), magnesium chloride (MgCl₂) and glucose were added, respectively. Following, 0.02% (w/v) Sodium azide was added to prevent contamination. Finally, pH was set to 7.4 with the aid of 1M NaOH.

Table 2. 5 Ingredients of Tyrode's solution.

Ingredient	Concentration
NaCl	119 mM
KCl	5 mM
HEPES	25 mM
CaCl ₂	2 mM
MgCl ₂	2 mM
Glucose	6 g/L

In the first step, the effect of hydrogel concentration on water uptake was investigated. For this purpose, freeze dried PUL15, PUL20, PUL25, PUL30 and PUL35 hydrogels were cut into cylinders of 1cm in diameter and 2.5 cm in height. Dry weights of samples were recorded at predetermined incubation periods. Samples were then placed in falcon tubes containing Tyrode's solution with pH 7.4 and incubated at 37°C in orbital shaker set at 80 rpm. Afterwards, wet weight of each sample was recorded at each hour from 1st hour to 12nd hour and at 24th hour. By using recorded values water uptake percentage was calculated for each sample, by using Equation (2.1), W_{dry} refers weight of dry hydrogel and W_{wet} stands for weight of wet hydrogel at given time.

$$Water\ Uptake\ \% = \frac{W_{wet} - W_{dry}}{W_{dry}} \times 100\% \quad (2.1)$$

In the second step, the effect of PP placement in hydrogels on water uptake percentage was investigated. With this objective in mind, PUL and PUL-PP hydrogels were prepared at 20% and 25% (w/v) concentrations with aforesaid dimensions. First, dry weight of each sample was recorded and samples were placed in falcon tubes containing PBS with pH 7.4. Subsequently, samples were incubated at 37°C in orbital shaker at 80 rpm. Later, wet weight of each sample was recorded at the end of 1, 4, 7, and 14 days of incubation. Finally, as before, water uptake percentage was calculated by using Equation (2.1) (Wittaya-Areekul & Prahsarn, 2006).

2.2.3.1.3 Degradation Analysis

Analysis of degradation for the hydrogel layer was done by the gravimetric method in Tyrode's solution (Gokal & Nolph, 2009). In general, degradation analysis of PUL hydrogels were carried in 2 steps. In first step, the effect of hydrogel concentration on degradation was investigated in Tyrode's solution, whereas in the second step, enzymes present in peritoneal fluid was added into Tyrode's solution.

For the first step, freeze dried PUL15, PUL20, PUL25, PUL30 and PUL35 hydrogels with aforesaid dimensions were weighed. Then, PUL hydrogel samples were placed in falcon tubes containing Tyrode's solution (pH 7.4). Subsequently, samples were incubated at 37°C in orbital shaker at 80 rpm. Afterwards, samples were taken out, washed with dH₂O and lyophilized at the end of days 1, 4, 7, and 14. Then, samples were weighed and weight loss percentages were calculated by using Equation (2.2), (You et al., 2014) where W_i refers initial weight of hydrogel and W_f stands for weight of hydrogel at given time.

$$\% \text{ Weight loss} = \frac{W_i - W_f}{W_i} \times 100\% \quad (2.2)$$

In the second step, PUL and PUL-PP samples with 20% and 25% (w/v) concentrations with same dimensions as before were used. After recording initial dry weights, PUL samples were placed in PBS, while PUL-PP and F: COS samples were placed in either PBS, 57.4 ng/mL Trypsin or 339 ng/mL α -Amylase (Dubick et al., 1987). Enzyme solutions were prepared by dissolving aforesaid amounts in PBS followed by filtration with 0.3 μ m filter. Later, samples were incubated at 37°C in orbital shaker at 80 rpm. Then, at the end of days 1, 4, 7, and 14, samples were taken out, washed with dH₂O and lyophilized. Afterwards, samples were weighed and degradation percentage was calculated for each sample by using Equation 3, as in the first step (You et al., 2014).

Degradation of F: COS 90:10 (^{w/w}) layer was also assessed by observing changes in fiber morphology with SEM examination. F: COS 90:10 (^{w/w}) samples was placed in either PBS, 57.4 ng/mL Trypsin or 339 ng/mL α -Amylase in PBS (Dubick et al., 1987). Samples were then placed in orbital shaker set at 37°C and 80 rpm. At day 1, samples were taken out, washed and lyophilized. Dried samples were coated with Au/Pd by using sputter coating device and visualized via SEM device (Quanta 400F Field Emission SEM, USA).

2.2.3.1.4 Determination of Dimensional Change

Dimensional change of PUL hydrogels during production was determined in order to gain perspective for a well-integrated intraperitoneal patch. For this purpose, diameter and thickness of PUL20 and PUL25 hydrogels were recorded as casted and after gelation, washing, freeze drying and wetting steps. Percent change in diameter and thickness were calculated with Equation (2.3), where x_i refers initial measurement of hydrogel dimension and x_f stands for measurement of hydrogel dimension after given application.

$$\% \text{ Change} = \frac{x_f}{x_i} \times 100\% \quad (2.3)$$

2.2.3.2 Water Contact Angle

Water contact angle was measured in order to determine surface hydrophilicity of electrospun F: COS 90:10 (^{w/w}) layer and 2 sides of final assembled three layered mesh. Water contact angle was determined by goniometer (Attension, Biolin Scientific, Sweden) at 25°C. dH₂O was chosen as testing liquid and droplets were set to 7 μ L. After measurements, contact angles were calculated using Young-Laplace formula, given below in the equation (2.4) (Taylor, Urquhart, Zelzer, Davies, & Alexander, 2007).

$$\gamma_{sv} = \gamma_{sl} + \gamma_{lv} \times \cos\theta\gamma \quad (2.4)$$

2.2.3.3 Assessment of Mechanical Properties

2.2.3.3.1 Compression Test

Tensile test was performed on wet PUL15, PUL20, PUL25, PUL30 and PUL35 hydrogels with 4 mm thickness and 10 mm radius. Test was executed by using Lloyd LS500 Univert mechanical tester (CellScale, Canada). Data analysis was done by using the computer program Univert (CellScale, Canada). Tests were performed at a speed of 1 mm/min with 10 N load cell. The compressive strength, Young's modulus and strain values were determined from obtained stress–strain curves.

2.2.3.3.2 Tensile Test

Tensile test was performed on designed intraperitoneal patch consisting of PUL30 hydrogel, PP mesh and electrospun F: COS 90:10 (^{w/w}) Test was executed by using Lloyd LS500 Univert mechanical tester (CellScale, Canada). Data analysis was done by using the computer program Univert (CellScale, Canada). First, ends of 40 mm to 10 mm samples in the shape of dog bone were grinded in order to prevent slipping. Samples were placed in the grips so that gauge length would be 20 mm. Afterwards, tensile test was performed with a crosshead velocity of 1 mm/min and under 1N load. Finally, elastic modulus, tensile strength and elongation at break were calculated by using stress-strain data (Wittaya-Areekul & Prahsarn, 2006).

2.2.4 Cell Culture Studies

Cell attachment and proliferation was tested by using L929 cell line as both peritoneal tissue and L929 cell line was from mesothelial lineage (Smith, 2002, Chapter 43; Thonemann, Schmalz, Hiller, & Schweikl, 2002). Immunomodulation was tested via

RAW 264.7 cells as it is an adherent macrophage line. Both L929 and RAW 264.7 cells were cultivated with Low Glucose DMEM without Phenol Red, supplemented with 10% (v/v) fetal bovine serum (FBS) and 10 U/mL penicillin/streptomycin (Pen/Strep) in an incubator (5215, Shel Lab, USA) at 37°C with 5% CO₂ and 95% humidity. Cells were passaged when they reached at least 80% confluency, via 0.1% Trypsin/ethylenediaminetetraacetic acid (EDTA).

2.2.4.1 Assessment of Cell Viability

Cell viability was assessed via Alamar Blue Assay. For PUL hydrogel layer, in preliminary studies air dried PUL20, PUL25, PUL30 and PUL35 hydrogels which were 8 mm in diameter and 2mm in thickness were used. During experiments, hydrogels revealed significant change in dimension. Thus, considering integrity of layers, experiment was repeated with 20% and 25% (w/v) freeze dried PUL hydrogels. For electrospun F: COS layer, samples with 8 mm in diameter with F: COS 100:0, 95:5, 90:10, 80:20, 70:30, 60:40 and 50:50 were used. Samples were sterilized by incubation in 70% (v/v) EtOH for 1 hr, followed by ultraviolet (UV) light exposure for 1hr, each side. Afterwards, samples were placed in 48-well plates and seeded with L929 cells with a seeding density of 25,000 cells/cm². Tissue culture polystyrene (TCPS) was used as control whereas not seeded scaffolds served as scaffold negatives. After seeding, scaffolds were placed in incubator and cultivated for 14 days as mentioned above. Alamar Blue Assay was performed at days 1, 4 and 7. For the assay, first culture media was removed from wells. Subsequently, media was replaced by 300 μL of 10% (v/v) AlamarBlue™ reagent, in Low Glucose DMEM without Phenol Red. Subsequently, scaffolds were placed in incubator and incubated for 4 hrs at 37°C. After 4 hrs, Alamar Blue solutions were transferred to a new 48-well plate. Then, emptied wells were washed with PBS, prior to fresh media addition. Subsequently, scaffolds were placed in incubator until next time point. Absorbance of transferred Alamar Blue solutions were read at 570 and 600nm by using spectrophotometer (Paradigm Fluorescence Plate Reader, Molecular Devices, ABD). By using these absorbance

values, percent reduction of AlamarBlue™ reagent was calculated. Calculation was done according to Equation (2.5).

$$\%Reduction = \frac{(117.216 \times A570) - (80.586 \times A600)}{(155.677 \times N600) - (14.652 \times N570)} \times 100\% \quad (2.4)$$

2.2.4.2 Assessment of Immunomodulatory Properties

Immunomodulatory property of F: COS layer of intraperitoneal patch was investigated by measuring NO⁻ concentration in culture media, by using NO⁻ detection kit (Biovision, Inc., USA). For this purpose, electrospun F: COS 100:0, 95:5, 90:10, 80:20, 70:30, 60:40 and 50:50 samples with 1 cm² area were sterilized as mentioned before. Following, scaffolds were placed in 48-well plates and RAW 264.7 cells were seeded with a seeding density of 5x10⁴ cells/scaffold. Then, scaffolds were incubated for 24 hrs, in culture media to allow cells to adhere. Afterwards, macrophage cells were stimulated by 100ng/mL lipopolysaccharide (LPS) in cell culture media (Panilaitis et al., 2003). Following, NO⁻ amount in culture media was measured with the kit after 8 and 24 hours of incubation. Absorbance values were recorded at 540nm via spectrophotometer (Paradigm Fluorescence Plate Reader, Molecular Devices, ABD).

2.2.4.3 Assessment of Cell Morphology

Morphology of L929 cells seeded on F: COS layers were visualized by SEM. electrospun F: COS 100:0, 95:5, 90:10, 80:20, 70:30, 60:40 and 50:50 (w/w) samples were cultivated with L929 cells, as aforesaid. At days 1, 4, 7 and 14, samples were fixed with PBS containing 2.5% glutaraldehyde at 25°C for 20 min. Following, fixed samples were washed with PBS and dehydrated with increasing series of ethanol from 20% to 100% (v/v). Afterwards samples were dried in hexamethyldisilazane for 20 min. Finally, dried samples were stored in desiccator at 25°C, until analysis. Prior to imaging, samples were coated with 10 nm ultra-fine gold particles by using precision

etching coating system (Gatan 682 PECS, Gatan, Inc., USA). Coated samples were visualized by using SEM (Quanta 400F Field Emission SEM, USA) in order to detect cell attachment and morphology on scaffolds.

2.2.5 Statistical Analysis

All experiments were performed with n=6, except for analysis of fiber morphology. Fiber morphology was assessed with n=40. Significant differences between groups were assessed by using One-way analysis of variance (ANOVA). Multiple comparisons were conducted with Tukey's Comparison Test (SPSS-22 Software, SPPS Inc., USA).

CHAPTER 3

RESULTS AND DISCUSSION

3.1 Modification of PP Layer

3.1.1 X-Ray Photoelectron Spectroscopy Scanning Analysis

It was reported that plasma treatment can introduce modifications on the surface of PP (Morent, De Geyter, Leys, Gengembre, & Payen, 2008). With this in mind, PP mesh was modified with air plasma, in order to promote its integrity with PUL hydrogel. For this purpose, PP was immersed in 20% (w/v) STMP solution immediately after treatment. As preparing STMP solution, pH was increased to 10 by using NaOH, in order to open ring structure of STMP (Lack, Dulong, Picton, Cerf, & Condamine, 2007). Success of modification was assessed with XPS. Ratios of Carbon (C), oxygen (O₂) and phosphorus (P) were traced to detect STMP incorporation. Figure 3.1 reveals XPS spectra of non-treated PP mesh and air plasma treated PP mesh. Figure 3.1a shows major peak indicating C with atomic ratio 70.6%. Additionally, a negligible P and O₂ peaks were observed which was expected due to analysis conditions and contamination. Figure 3.1b shows a shift of atomic ratio of C to 50.1% whereas O₂ peak constitutes 41.2% and P peak constitutes 3.4% atomic ratio of the total. XPS results confirmed that surface of PP mesh was coated with STMP. Change in atomic ratios of C, O and P before and after plasma treatment is given in Table 3.1.

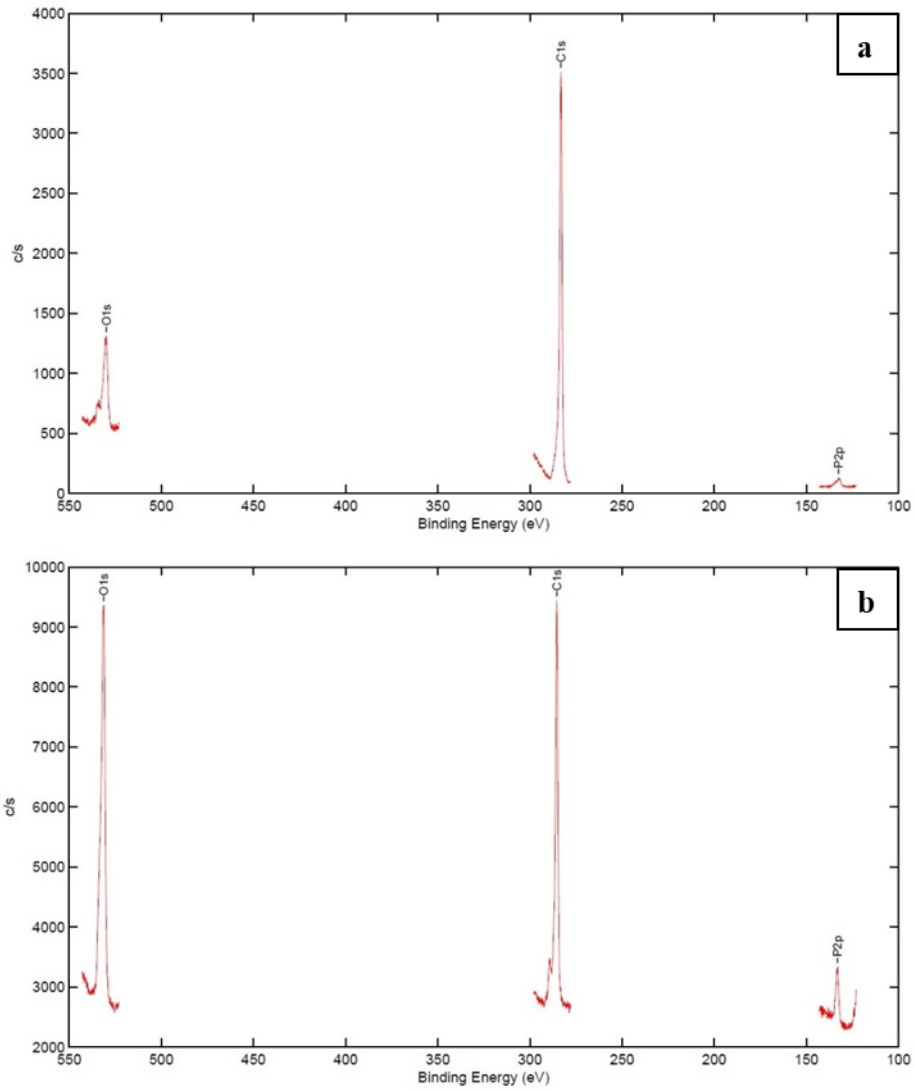


Figure 3. 1 XPS analysis XPS spectra of (a) non-treated PP mesh and (b) air plasma treated PP mesh.

Table 3. 1 Atomic ratios of C, O₂ and P on PP mesh before and after plasma treatment.

Atom	Atomic Ratio Before Plasma Treatment (%)	Atomic Ratio After Plasma Treatment (%)
C	70.6	50.1
O	18.9	41.2
P	2.2	3.4

3.2 Characterization of Intraperitoneal Patch

3.2.1 Assessment of Physical Properties

Physical properties of intraperitoneal patch were assessed by evaluation of fiber morphology, water uptake and degradation properties, determination of dimensional change and water contact angle of the hydrogel and electrospun layers. PUL hydrogels were subjected to water uptake analysis, degradation analysis, determination of dimensional change and water contact angle measurement whereas electrospun F: COS was subjected to fiber morphology analysis, degradation analysis and water contact angle measurement.

3.2.1.1 Analysis of Fiber Morphology

Fiber morphology of electrospun fibers was visualized by SEM device (Quanta 400F Field Emission SEM, USA). SEM images of samples electrospun with different solvent systems, namely HFIP: DMEM solvent systems (Figure 3.2), TFA: DCM solvent system (Figure 3.3) and HFIP: TFA solvent system (Figure 3.4). Additionally, diameter distribution was obtained from SEM images of electrospun fibers obtained with HFIP: TFA solvent system, by using the software ImageJ (USA). Mean fiber diameters of different batches are given in Table 3.1.

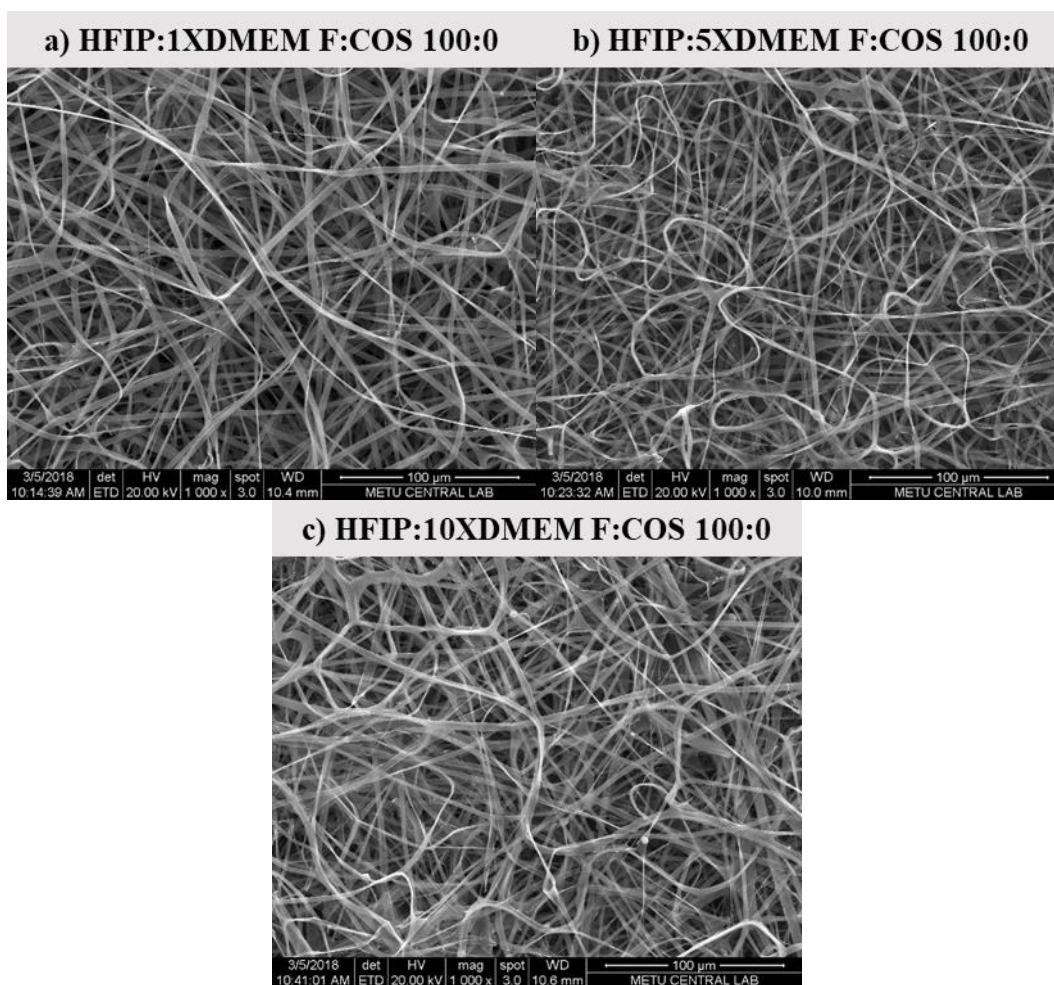


Figure 3. 2 SEM images of electrospun F: COS 100:0 (^{w/w}) fibers with a) HFIP:1XDMEM, b) HFIP:5XDMEM or c) HFIP:10XDMEM (9:1 ^{v/v}) as solvent. Ribbon-like fiber morphology was observed in all meshes that were electrospun in different solvent systems (Scale bar:100 μm).

As seen in Figure 3.2, Ribbon-like fibers with branches were obtained when HFIP was mixed with DMEM at different DMEM concentrations. Figure 3.2b and Figure 3.2c reveals formation of branched fibers that could be related with the change of charge per unit ejected from the needle tip (Garg & Bowlin, 2011). Salt precipitation occurred when HFIP: DMEM blends were prepared by mixing. Therefore, branching of fibers might be related to the presence of salts coming from DMEM. HFIP: DMEM solvent systems could not be carried on for all F: COS ratios as COS precipitated. Therefore,

only F: COS 100:0 (^{w/w}) fibers could be produced. As seen in Figure 3.3, F: COS 100:0 (^{w/w}) fibers presented ribbon shape for all HFIP: DMEM solvent systems. Koombhongse, Liu & Reneker (2001) relates fiber morphology with material, solvent, voltage and distance between needle tip and collector. Ribbon-like fibers are stated to result in evaporation behavior of solvent through a biomaterial. Formation of ribbon fibers occur by skin formation of fiber due to rapid evaporation. Evaporation of middle solvent occurs by diffusion through aforesaid skin layer, leaving collapsed ribbon-like fiber (Koombhongse et al., 2001). As a result, solvent system was switched to TFA: DCM (7:3 ^{v/v}).

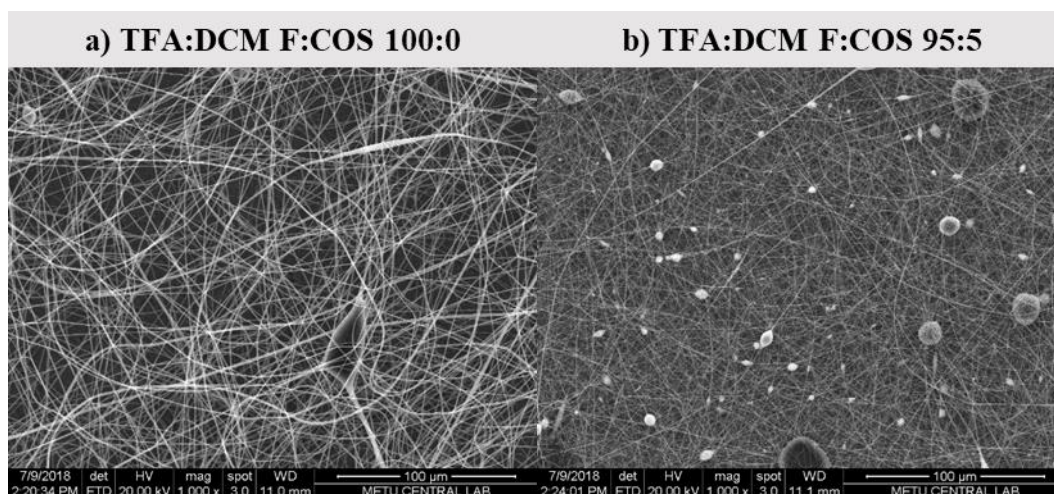


Figure 3. 3 SEM images of electrospun F: COS a) 100:0, b)95:5, c) 90:10, d)80:20, e)70:30 and f) 60:40 (^{w/w}) fibers. TFA: DCM (7:3 ^{v/v}) was used as solvent system (Scale bar:100 μm).

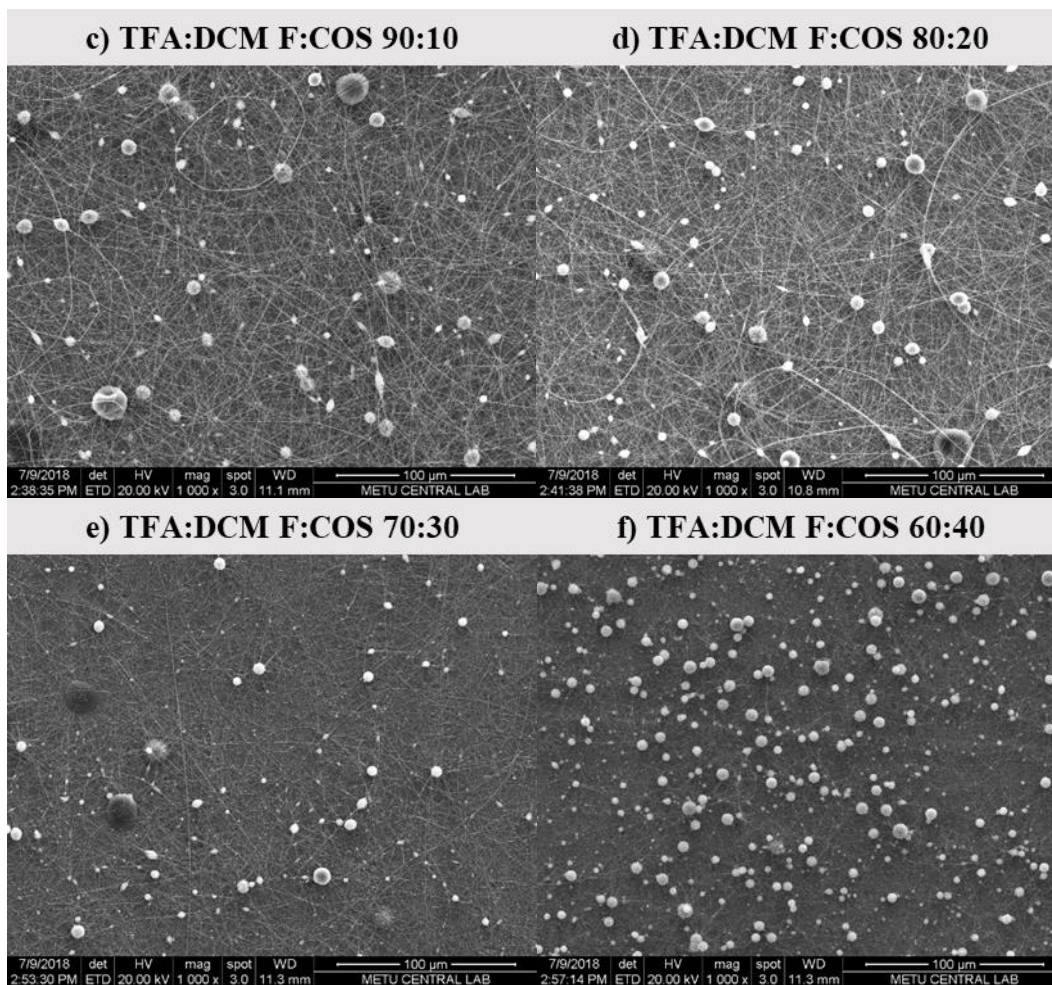


Figure 3.3 Continued SEM images of electrospun F: COS a) 100:0, b)95:5, c) 90:10, d)80:20, e)70:30 and f) 60:40 (^w/_w) fibers. TFA: DCM (7:3 ^v/_v) was used as solvent system (Scale bar:100 μm).

Successful fabrication of electrospun fibroin/chitosan blend with TFA:DCM (7:3, ^v/_v) was reported (Gu et al., 2013). However, TFA: DCM solvent system was not feasible as COS precipitated right after addition of DCM. Fibers of F: COS 100:0 (^w/_w) fibers electrospun with TFA:DCM was thinner than that of F: COS 100:0 (^w/_w) fibers electrospun with HFIP:DMEM which arises from solvent change (Kooombhongse et al., 2001). Moreover, as seen in Figure 3.3, spinning of precipitated solution resulted in particles on electrospun mat. Increasing COS concentration resulted in more deposited particles and thinner fibers. COS is a depolymerized oligomer derivative of

chitosan (Norowski et al., 2012). Therefore COS' lower molecular weight may play role in dielectric constant of final solution (Koombhongse et al., 2001). Due to mentioned problems solvent system was switched to HFIP: TFA (9:1 v/v).

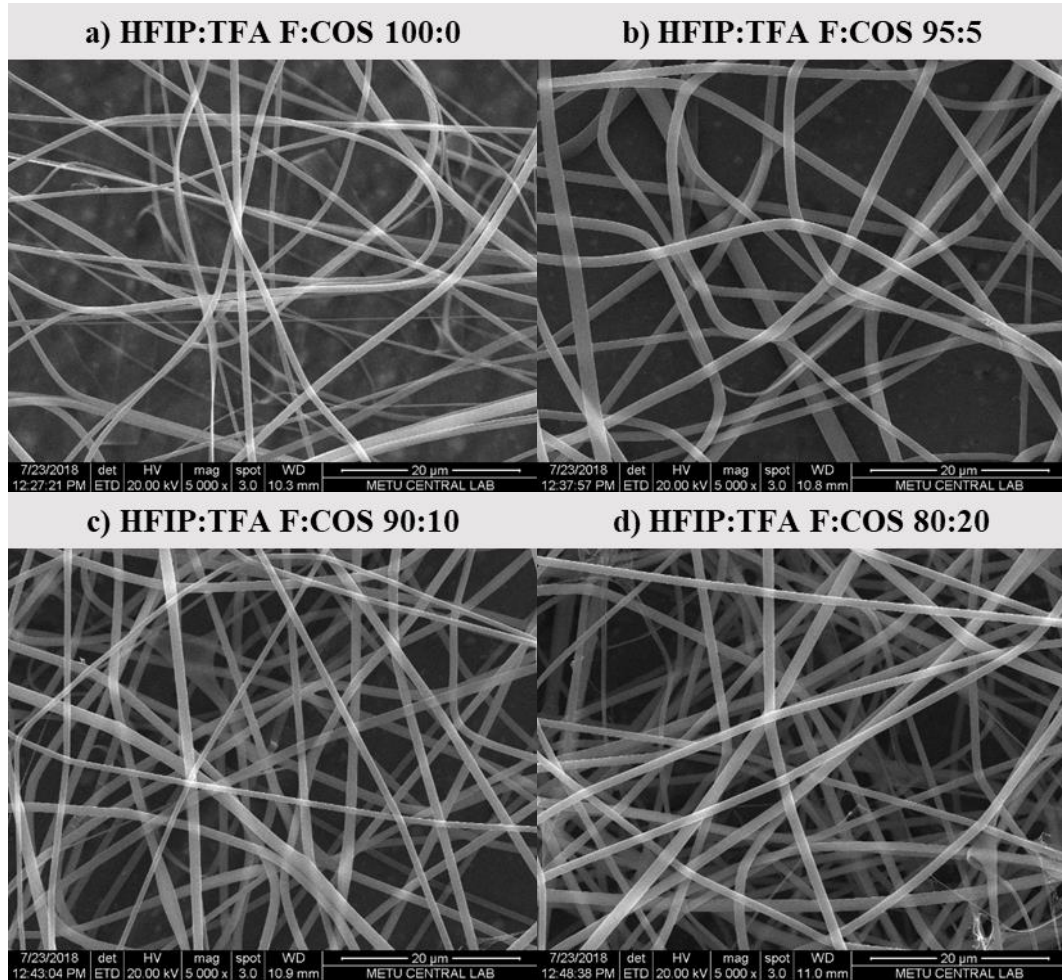


Figure 3. 4 SEM images of electrospun F: COS a) 100:0, b) 95:5, c) 90:10, d) 80:20, e) 70:30 and f) 60:40 g) 50:50 (w/w) fibers. HFIP: TFA (9:1 v/v) was used as the solvent system (Scale bar: 20 μ m).

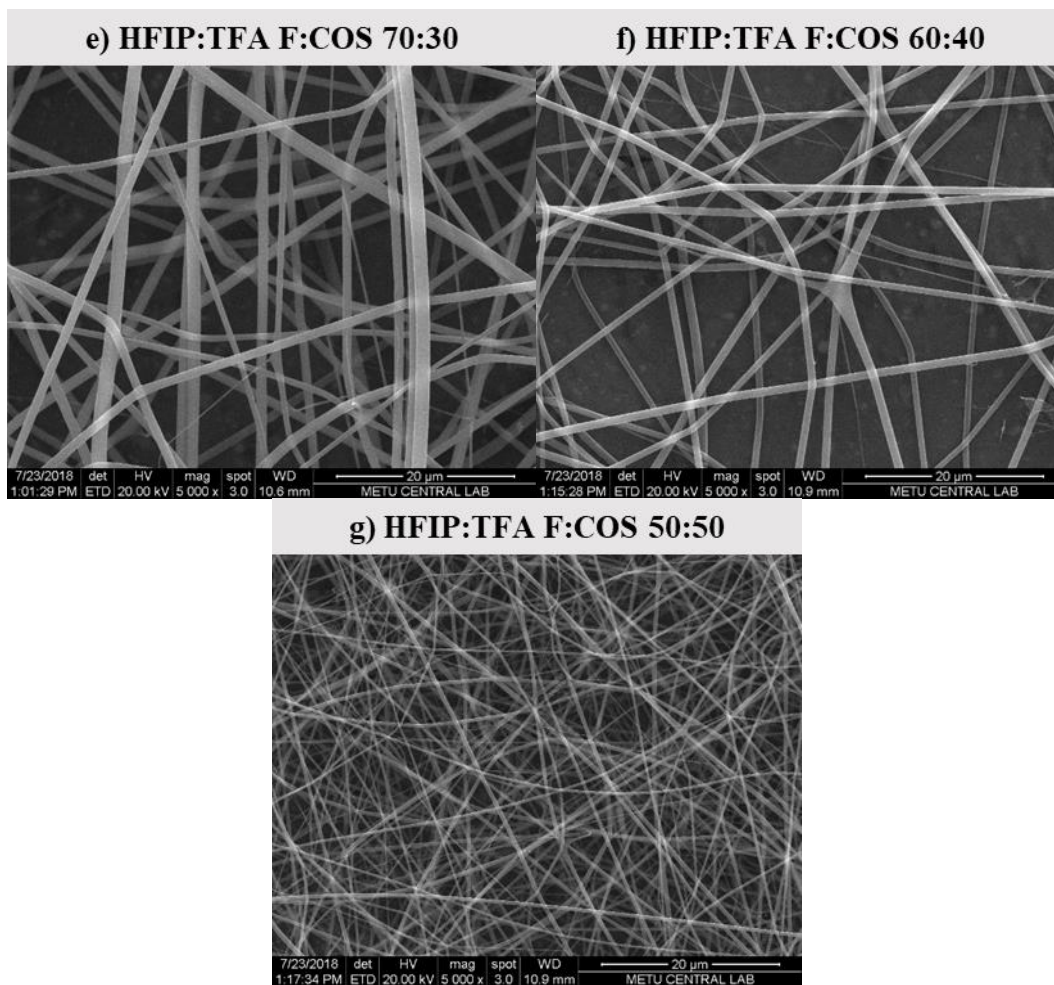


Figure 3.4 Continued SEM images of electrospun F: COS a) 100:0, b) 95:5, c) 90:10, d) 80:20, e) 70:30 and f) 60:40 g) 50:50 (^{w/w}) fibers. HFIP: TFA (9:1 ^{v/v}) was used as the solvent system (Scale bar: 20 μm).

Table 3. 2 Mean fiber diameter of samples with different F: COS ratios that were electrospun using HFIP:TFA (9:1 v/v) solvent system. “*” indicates that the group was significantly different than other groups (n=50, p<0.05).

F: COS Ratio	Fiber Diameter (nm)
100:0	1068±176
95:5	1243±159
90:10	969±95
80:20	1071±109
70:30	1025±152
60:40	957±92
50:50	565±92 *

Finally, F: COS fibers were produced by employing HFIP: TFA (9:1 v/v) solvent system. Precipitate or beading-free fibers were electrospun with varying F: COS ratios and electrospinning parameters. As seen in Figure 3.4, obtained fibers have ribbon-like morphology. In order to optimize electrospinning conditions, fiber diameter was determined by analyzing SEM images in ImageJ (USA). Overall fiber diameter was not affected from polymer ratio between except for F: COS 50:50 (w/w) which has significantly lower fiber diameter compared to other groups. Electrospinning parameters of F: COS 60:40 and F: COS 50:50 (w/w) were given in Table 2.3. When batches 15-1 and 16-3 considered, it can be seen that flow rate, collecting distance and voltage was same. Thus, lower diameter of F: COS 50:50 (w/w) group may be result polymer ratio (Koombhongse et al., 2001). As mentioned earlier, electrospun F: COS layer was intended to promote immunomodulation and regeneration. It was stated that surface topography is an important factor determining scaffold’s immunomodulatory property (Andorko & Jewell, 2017). Hence, different electrospinning parameters were tested in order to obtain uniform fibers. Considering reproducibility, batches with lower standard deviations were selected for further experiments which are 10-2, 11-1, 12-1, 13-1, 14-3, 15-2, 16-3 for F: COS ratios 100:0, 95:5, 90:10, 80:20, 70:30, 60:40, and 50:50 (w/w), respectively.

3.2.1.2 Water Uptake Analysis

Water uptake capacities of PUL15, PUL20, PUL25, PUL30 and PUL35 hydrogels were assessed by a gravimetric method described by Wittaya-arekul & Prahsarn (2006). Tyrode's solution was chosen as experiment media due to its resemblance of intraperitoneal fluid (Gokal & Nolph, 2009, Chapter 1). Water uptake percentages calculated at each hour from 1st to 12th and at 24th hour can be found in Figure 3.5.

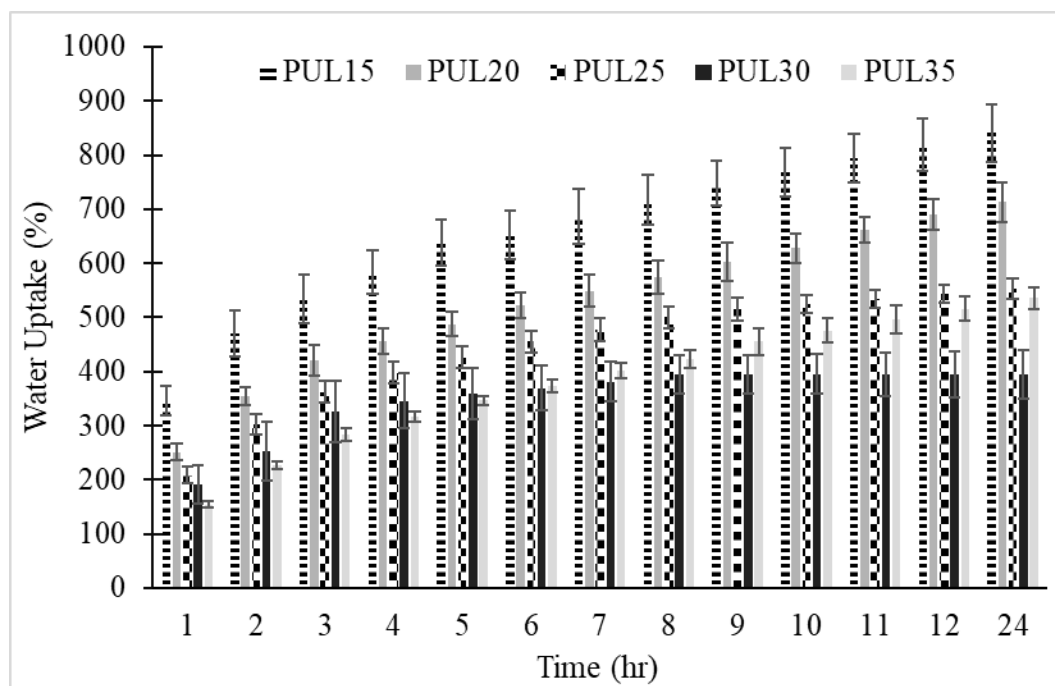


Figure 3. 5 Water uptake percentages of PUL15, PUL20, PUL25, PUL30 and PUL35 hydrogels in Tyrode's solution (pH 7.4) at 37°C. Water uptake was calculated as the ratio of amount of water conserved in hydrogel to dry weight of hydrogel. PUL15 showed the highest water uptake at all given time points. At all time points, water uptake percentage of PUL15 hydrogels were significantly highest. From 5th hr onwards, water uptake percentage of PUL15 group was significantly higher than PUL20 group and significantly higher than PUL30 group. (n=6, p<0.05).

It was observed that increasing hydrogel concentration resulted in decreasing water uptake, except for PUL35. PUL35's water uptake percentage reached its plateau at 12th hour and was statistically indifferent than PUL25. All PUL35 samples broke into pieces during first hour of incubation. As described in Chapter 2, hydrogels were mixed with syringe needles. Complete mixing of PUL35 was hard due to its high viscosity. This might be the result of non-uniform crosslinking resulting in disruption of samples.

It was also observed that at all time points, PUL15 had highest ($p < 0.05$) water uptake percentage. Water uptake percentages of PUL25 and PUL30 reached their plateau at 8th hour whereas PUL15, PUL20 and PUL35 reached their plateau at 12th hour. From 8th hour on, PUL25 had significantly higher water uptake percentage than PUL30. Following, at 12th hour, PUL15 had higher water uptake percentage ($818\% \pm 48\%$) than PUL20 ($690\% \pm 28\%$) followed by PUL25 ($544\% \pm 17\%$) and PUL30 ($394\% \pm 43\%$), respectively ($p < 0.05$).

In a study done by Wong et al. (2011), properties of PUL-collagen hydrogels cross-linked by STMP were investigated. 5% (w/v) hydrogels revealed $927\% \pm 129\%$ water uptake which reached the plateau at 12th hour. Our study also confirmed that low concentration PUL15 hydrogel reached its plateau at 12th hour, yielding compatible water uptake percentage. Another study subjected carboxymethyl-PUL hydrogels cross-linked with cystamine dihydrochloride. reported that water uptake percentage of 30% carboxymethyl-PUL hydrogels reached to 4000% having plateau at 8th hour (Li et al., 2011). Reported results were much higher than obtained results in this study which could be due to the difference in molecular structure and cross-linking mechanism. Finally, Lack et al (2004) determined water uptake percentage of hydrogels cross-linked with STMP. 20% (w/v) hydrogels prepared by the group with same STMP ratio as our study had around 700%. Considering PUL20 hydrogels, results were in concordance. Hence, hydrogel fabrication method was considered as successful.

Overall water uptake capacity decreased with increasing hydrogel concentration. It was stated that lower concentrations lead higher porosity and inner surface area (Haul, 1982, Chapter 1). Moreover, Wong et al. (2011) affirmed that water uptake is correlated to porosity. Hence, water uptake behavior of PUL hydrogels were expected to decrease with increasing concentration.

3.2.1.3 Degradation Analysis

3.2.1.3.1 Degradation of PUL Layer

Degradation analysis of PUL hydrogels were assessed by a gravimetric method (Wittaya-Areekul & Prahsarn, 2006). Degradation analysis was carried out by using Tyrode's solution as it was considered as peritoneal fluid simulation (Gokal & Nolph, 2009, Chapter 1). In the first part of analysis, weight loss percentages of PUL15, PUL20, PUL25, PUL30 and PUL35 hydrogels were determined for days 1, 4, 7, 14. Analysis was performed by using same samples from water uptake analysis. Degradation percentages calculated at days 1, 4, 7 and 14 can be found in Figure 3.6.

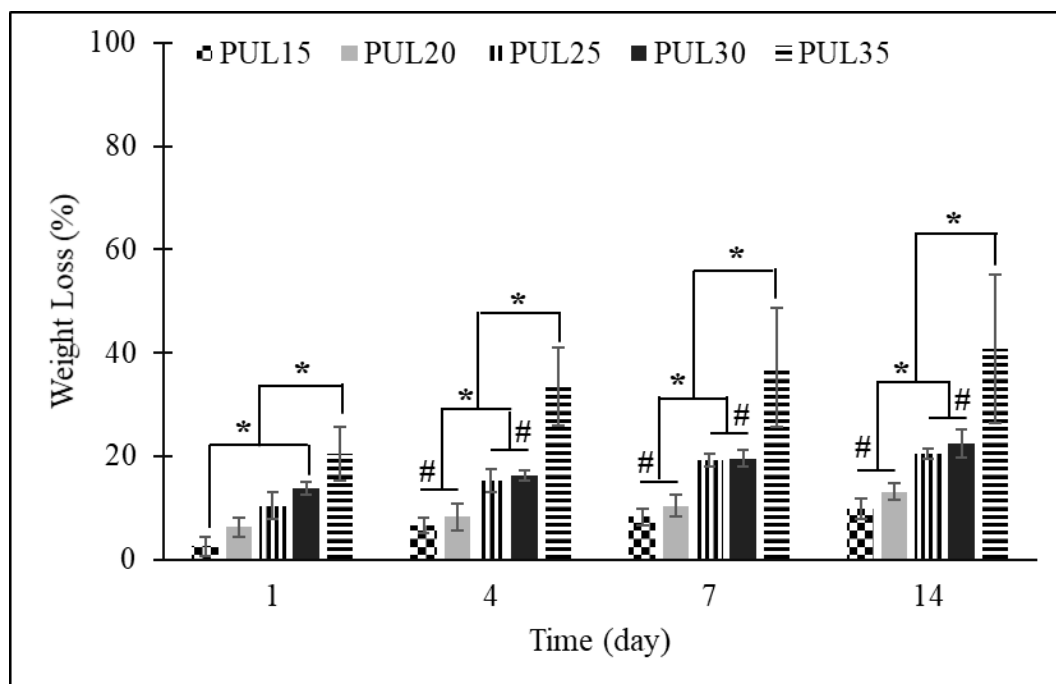


Figure 3. 6 Weight loss of PUL15, PUL20, PUL25, PUL30 and PUL35 hydrogels in Tyrode's solution (pH 7.4) at 37°C. From day 4 onwards, there was no statistical difference between weight loss percentages of PUL15 and PUL20 as well as PUL25 and PUL30. “*” indicates statistical significance between groups whereas “#” stands for non-significant difference between groups (n=6, p<0.05).

At day 1, PUL15 had the lowest weight loss whereas PUL35 had highest among all groups (p<0.05). From day 4 to day 14, PUL35 continued to have the highest weight loss percentage ($40.78 \pm 14.44\%$). Considering disruption of PUL35 hydrogels, highest degradation rate with a high value of standard deviation was an expected outcome. Also, there was no significant difference between PUL15 and PUL20 and between PUL25 and PUL30 at days between 4 and 14. Additionally, at day 14, weight loss percentages of PUL25 ($20.43\% \pm 1.08\%$) and PUL30 ($22.43\% \pm 2.73\%$) were significantly higher than degradation percentages of PUL15 ($9.76\% \pm 1.99\%$) and PUL20 ($13.14 \pm 1.66\%$).

High water uptake of PUL15 resulted in redundant swelling of hydrogels that might have caused the disintegration of PUL and PP layers. Additionally, PUL35 samples disrupted due to difficulty of crosslinking. Therefore, PUL15 and PUL35 were considered as inconvenient. Moreover, compared to PUL25, PUL30 had lower water uptake percentage and similar weight loss. Thus, PUL25 was considered more beneficial than PUL30. Combining results of water uptake and degradation analysis, PUL20 and PUL25 hydrogels were chosen for enzymatic degradation.

Enzymatic degradation analysis was done by using α -amylase and trypsin as both enzymes are present in intraperitoneal fluid (Dubick et al., 1987). PP was incorporated to PUL20 and PUL25 hydrogels (PUL20-PP and PUL25-PP, respectively). As control, PUL and PP incorporated PUL (PUL-PP) hydrogels incubated in PBS (0.1M pH7.4) only were used. Weight loss percentages calculated at days 1, 4, 7 and 14 can be found in Figure 3.7.

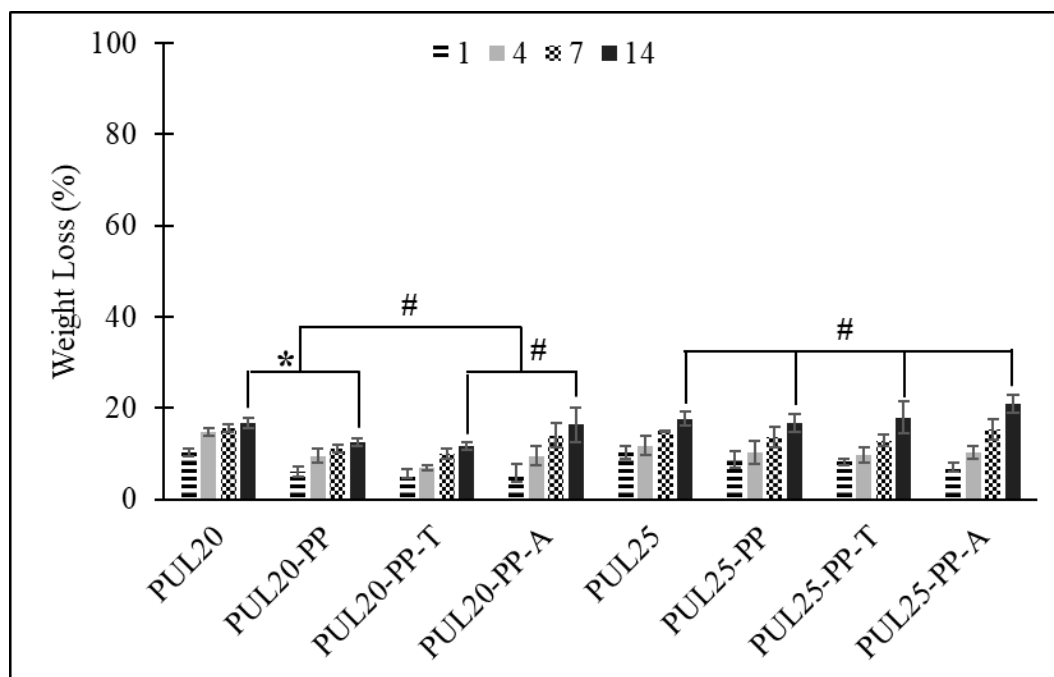


Figure 3. 7 Weight loss percentages of PUL20 and PUL25 hydrogels in PBS solution (0.1M pH 7.4) or PBS solution containing 57.4 ng/mL trypsin (T) or 339 ng/mL α -amylase (A) at 37°C. “*” indicates significant difference between groups whereas “#” stands for non-significant difference between groups (n=6, p<0.05).

During 14 days of enzymatic degradation analysis, neither disruption of samples nor disintegration of layers was observed. Degradation of PUL20-PP was significantly lower than that of PUL20. There was no significant difference between PUL25 and PUL25-PP. As mentioned, PUL20 had significantly higher water uptake compared to PUL25. Reduced water uptake due to PP incorporation may be the reason for lower weight loss of PUL-20. Accordingly, it was concluded that PP incorporation did not induce degradation. Furthermore, it was observed that PUL20 and PUL25 hydrogels were not degraded by α -amylase and trypsin. There was no statistical difference between weight loss percentages of PUL20-PP, PUL20-PP-T and PUL20-PP-A. Weight loss percentages of PUL25-PP, PUL25-PP-T and PUL25-PP-A were similar. Trypsin is a protease breaking carboxylic side of arginine or lysine if the amino acid is followed by proline, whereas α -amylase is a hydrolase breaking α -(1-4) linkages

(Olsen, Ong, & Mann, 2004; Van Der Maarel, Van Der Veen, Uitdehaag, Leemhuis, & Dijkhuizen, 2002). PUL consists of maltotriose units where glucose units are linked by α -1,6 glycosidic bond and maltotriose units are linked by α -1,4 glycosidic bond (Singh et al., 2017) Ability of different types of amylases to hydrolyze PUL was compiled by Jakovljevic et al. (2001). It was reported that fungal amylase and bacterial amylase were able to hydrolyze PUL whereas human saliva and porcine pancreas α -amylases lacked activity on PUL (Jakovljevic et al., 2001). Park et al. (2000) explained lack of activity of α -amylases on PUL arose from an amino acid sequence that is conserved in fungal amylase and bacterial amylase and not conserved in α -amylases (Park et al., 2000). Therefore, as expected, statistical difference was not present between degradation of hydrogels in PBS and α -amylase dissolved in PBS.

Lyu and Untereker (2009) define degradation behaviors as oxidation, physical degradation, enzymatic degradation and hydrolysis. In this study, PUL gels were not subjected to any oxidative or mechanical stress that may lead to oxidation or physical degradation. It was also stated that hydrolysis, breaking of chains due to interaction with water, is the major type of degradation taking place in polymeric biomaterials (Lyu & Untereker, 2009). It was observed that increasing concentration of PUL hydrogels resulted in increasing weight loss percentage. This was expected, as higher concentration would present more acidic chain ends which cause auto-acceleration of degradation (Leal-Serrano, Ruperez, & Leal, 1980; Lyu & Untereker, 2009). Göpferich (1996) states a biomaterial's hydrolysis can occur through surface or bulk erosion. There was no decrease in size of hydrogels during degradation analysis. As a result, it was concluded that PUL hydrogels degraded by hydrolysis through bulk erosion.

During enzymatic degradation, pH change of degradation media was monitored for PUL20 and PUL25 hydrogels in PBS solution (0.1M, pH 7.4) or PBS solution containing either 57.4 ng/mL trypsin 339 ng/mL α -amylase. Recorded pH values at days 1, 4, 7 and 14 can be found in Figure 3.8. pH of degradation media showed no

drastic change with time. In concordance with degradation analysis results, there was also no difference between pH values recorded from different groups as degradation of PUL was not effected by neither trypsin nor α -amylase. Lowest pH value amongst all groups recorded at day 14 was 7.26 which was still considered suitable for cell proliferation and wound healing (Kruse et al., 2017).

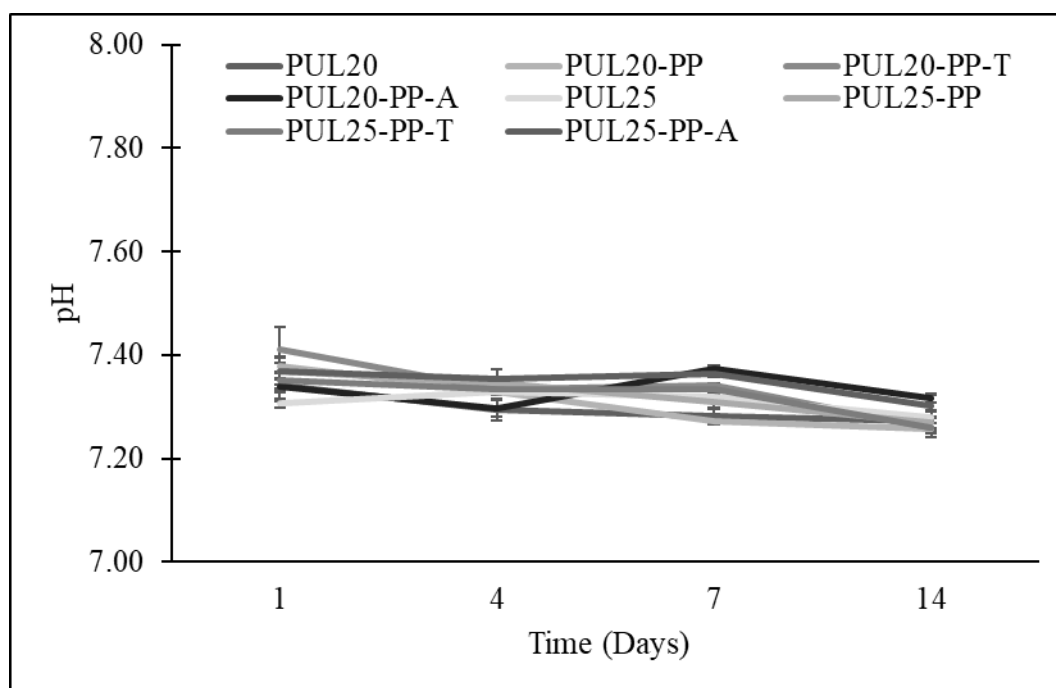


Figure 3. 8 pH values recorded during enzymatic degradation of PUL20 and PUL25 hydrogels in PBS solution (pH 7.4) or PBS solution containing 57.4 ng/mL trypsin (T) 339 ng/mL α -amylase (A) at 37°C.

3.2.1.3.2 Degradation of F: COS Layer

Degradation of F: COS 90:10 (^{w/w}) layer was assessed by examining change in fiber morphology. For this purpose, SEM images of fibers incubated in PBS (0.1M, pH7.4), 57.4 ng/mL Trypsin or 339 ng/mL α -Amylase in PBS were recorded at days 1,4,7 and 14 (Dubick et al., 1987). SEM images of F: COS 90:10 degraded in PBS, α -Amylase or Trypsin for given amounts of time are given in Figure 3.9.

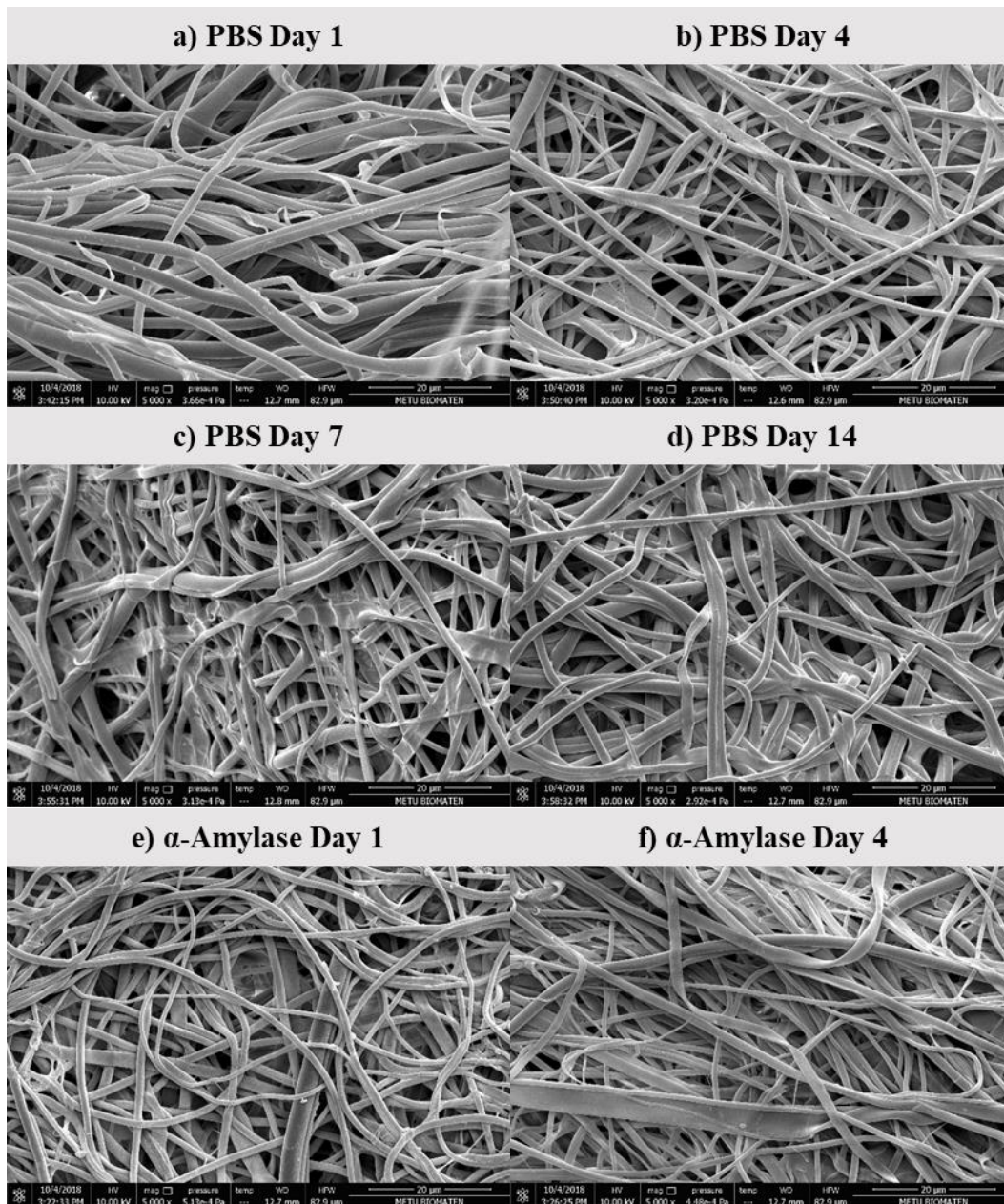


Figure 3. 9 SEM images of F: COS 90:10 (w/w) fibers incubated (a-d) in PBS, (e-h) in PBS containing 339 ng/mL α -Amylase and (i-l) in PBS containing 57.4 ng/mL Trypsin at days 1, 4, 7 and 10 (Scale bar: 20 μ m).

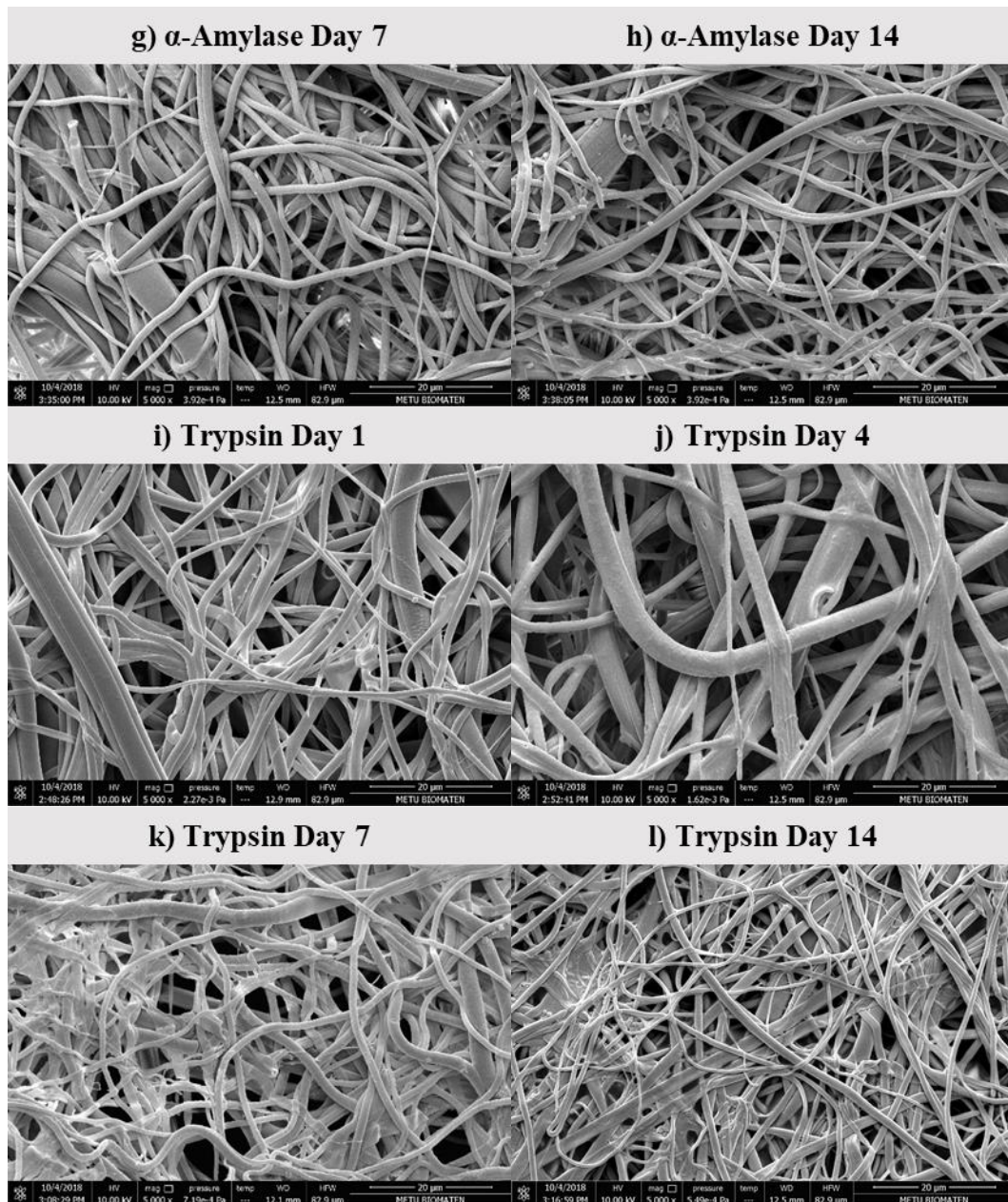


Figure 3.9 Continued SEM images of F: COS 90:10 (w/w) fibers incubated (a-d) in PBS, (e-h) in PBS containing 339 ng/mL α -Amylase and (i-l) in PBS containing 57.4 ng/mL Trypsin at days 1, 4, 7 and 10 (Scale bar: 20 μ m).

Fiber degradation can be identified with roughness on fiber surface, sticking of fibers to each other, disruption of roundness of fiber structure or rupture of fibers (Nagiah, Madhavi, Anitha, Srinivasan, & Sivagnanam, 2013; Schaub et al., 2015; Xu, Zou, Lu,

& Kang, 2017). As seen in Figure 3.9, all 3 degradation media led fiber disruption with time. Major change was observed from samples treated with trypsin. On the other hand, there was no significant change between fiber morphologies of samples incubated in PBS and α -amylase. Trypsin is a protease breaking carboxylic side of arginine or lysine if the amino acid is followed by proline, whereas α -amylase is a hydrolase breaking α -(1-4) linkages (Olsen et al., 2004; Van Der Maarel et al., 2002). Fibroin present in F: COS 90:10 (^{w/w}) fibers contains sequence that is available for trypsin digestion. After electrospun layer was incubated in ethanol which led to cross-linking of fibroin (Su et al., 2017). Hence, ethanol treatment was considered as the reason preventing complete degradation of F: COS scaffolds. The other component of fibers, COS, was not effected by degradation media as it contains n-glucosamine and n-acetyl-glucosamine linked through β -(1-4) glycosidic bond and was not cross-linked (Azuma et al., 2015). Therefore, change in terms of degradation was observed from Trypsin. COS may be released from fibers as it is water soluble and was not cross-linked (Norowski et al., 2012). Further research is advised for detection of COS in degradation media.

During degradation of F: COS fibers, pH change of degradation media was also monitored. Recorded pH values of degradation media containing PBS (0.1M pH7.4), 339 ng/mL α -Amylase in PBS and in 57.4 ng/mL Trypsin in PBS at days 1, 4, 7 and 14 are given in Figure 3.10. pH significantly dropped at day 1, which may be the result of immediate COS release in media. Moreover, from day 1 to 14, pH kept decreasing with lowest pH point among groups at day 14 being 7.22. Considering pH change, it was concluded that degradation of F: COS 90:10 (^{w/w}) fibers did not lead to an environment that would hinder cell proliferation (Kruse et al., 2017). However, intraperitoneal fluid contains other enzymes which may accelerate fiber degradation (Dubick et al., 1987). Hence, further enzymatic degradation may be performed for better a comprehension.

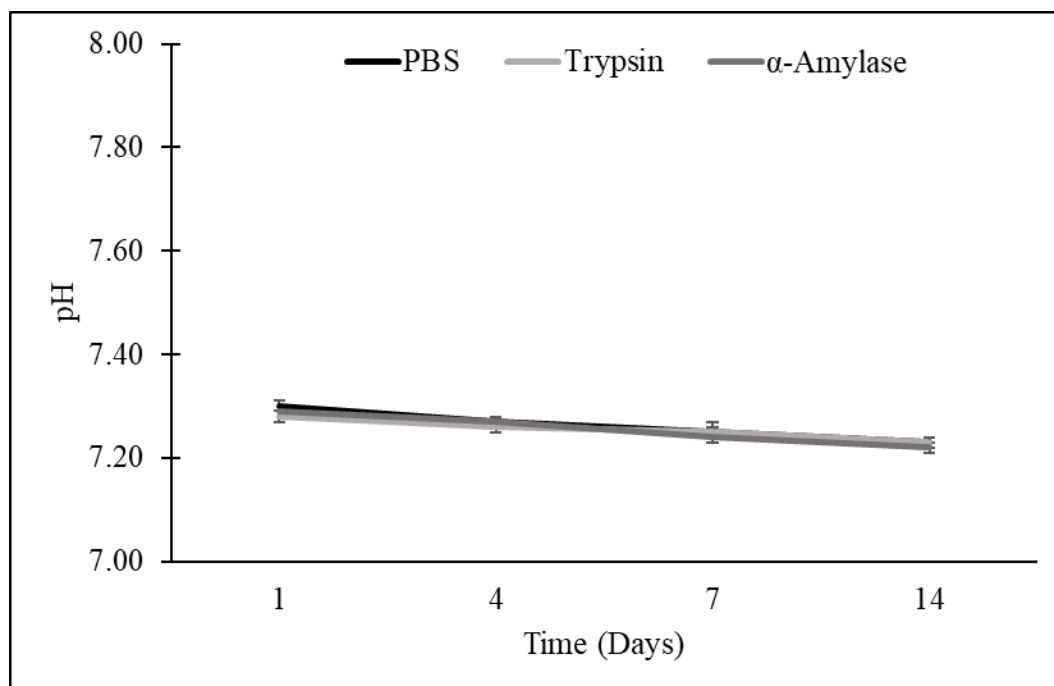


Figure 3. 10 pH values of degradation media containing PBS, 339 ng/mL α -Amylase in PBS and in 57.4 ng/mL Trypsin in PBS at days 1, 4, 7 and 14 (n=4 p<0.05).

3.2.1.4 Determination of Dimensional Change

Dimensional change of PUL20 and PUL25 hydrogels was monitored to gain perspective for a well-integrated intraperitoneal patch. Recorded diameter and thickness changes of PUL20 and PUL25 hydrogels at different stages of production are given in Figure 3.11. It was noted that diameter of both PUL20 and PUL25 hydrogels did no change upon crosslinking. Hydrogels were found to adhere on teflon mold. On the other hand, crosslinking caused decrease in thickness with PUL20's decrease being significantly higher than that of PUL25. Washing step significantly increased both diameter and thickness. On the contrary, freeze drying significantly decreased both diameter and thickness of PUL20 and PUL25 hydrogels. Upon wetting, PUL20 significantly increased in diameter more than that of PUL25 whereas PUL25 significantly increased in thickness more than that of PUL 20 (p<0.05). Change of diameter was considered as more critical for integration of layers. Thus, PUL25 was regarded as more practical.

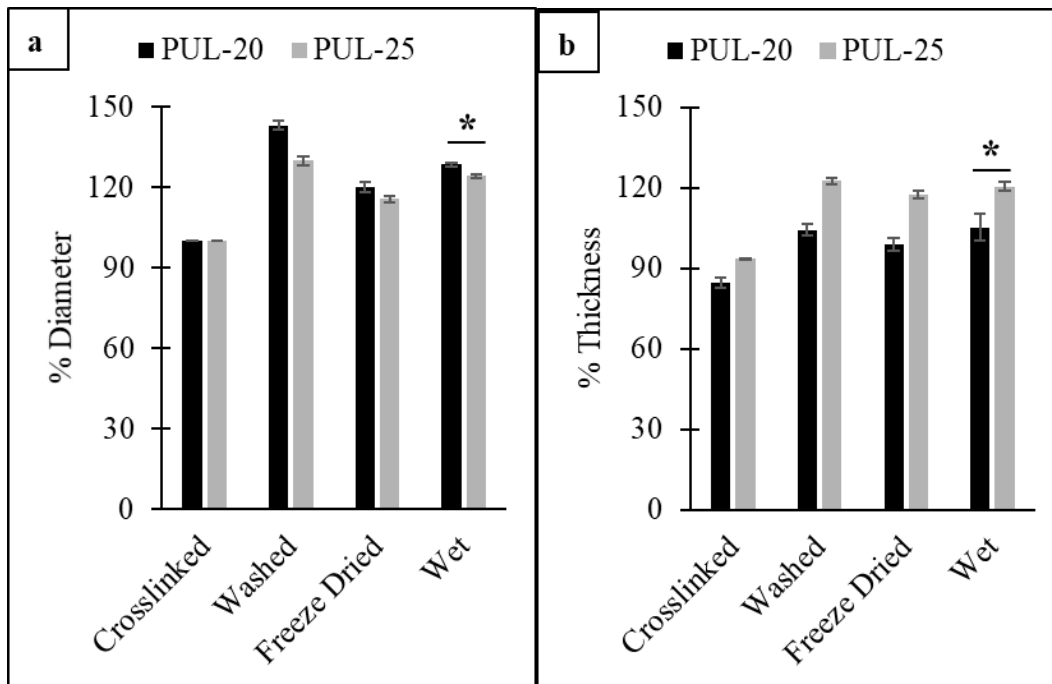


Figure 3. 11 (a) Diameter and (b) thickness change percentages of freeze-dried PUL20 and PUL25 hydrogels, at different stages of production. “*” was used as a notification for statistically significant values (n=6, p<0.05).

Dimensional change was acknowledged to be important to be able to keep layers of intraperitoneal patch well-integrated. Wong et al. (2011), demonstrated dimensional change of 5% (w/v) PUL-collagen hydrogels cross-linked by STMP upon wetting. Another study subjecting carboxymethyl-PUL hydrogels cross-linked with cystamine dihydrochloride also revealed excessive dimensional change of hydrogels, upon wetting (Li et al., 2011). Although exact measurements were not given, dimensional change was observed to be higher due to air drying of both hydrogels. In order to minimize excessive dimensional change, PUL hydrogels were freeze dried.

3.2.2 Assessment of Mechanical Properties

3.2.2.1 Compression Test

Compression test was performed on wet PUL15, PUL20, PUL25, PUL30 and PUL35 hydrogels. Tyrode's solution with pH 7.4 was used for wetting. Calculated values of Young's modulus, compressive strength and total strain are given in Table 3.3.

Table 3. 3 Calculated Young's modulus (E), compressive strength (σ) and total strain (ϵ) values for PUL15, PUL20, PUL25, PUL30 and PUL35 hydrogels. Young's modulus and compressive strength increases significantly with increasing hydrogel concentration, except for PUL 30. There was no significance between PUL25 and PUL30 in terms of Young's modulus and compressive strength (n=6, p<0.05).

Hydrogel	E (mPa)	σ (mPa)	E (%)
PUL15	26.39 \pm 2.23	5.57 \pm 0.79	50.64 \pm 0.71
PUL20	51.45 \pm 6.24	7.91 \pm 0.19	45.73 \pm 4.39
PUL25	78.69 \pm 0.81	16.97 \pm 0.75	51.41 \pm 2.97
PUL30	75.05 \pm 9.26	15.23 \pm 2.80	34.07 \pm 5.88
PUL35	91.97 \pm 2.29	18.56 \pm 0.61	46.58 \pm 0.69

Compression test revealed that increasing concentration of pullulan hydrogel yielded significantly higher Young's modulus and compressive strength values except for PUL30 whose Young's modulus and compressive strength was not significantly different than PUL25. Moreover, PUL30 presented the lowest strain. As mentioned earlier, PUL hydrogel preparation requires stirring which becomes harder and non-reproducible for high concentration hydrogels, due to high viscosity. Hence, PUL30 hydrogels' unexpected Young's modulus and compressive strength may be result of inadequate crosslinking. Abdominal wall was reported to bear a compressive pressure referred as intra-abdominal pressure. Intra-abdominal pressure was detected as between 5 to 10 kPa (Stokes, Gardner-Morse, & Henry, 2010). Considering

compressive strength of PUL hydrogels, PUL25, PUL30 and PUL35 hydrogels were considered to be able to withstand intra-abdominal pressure whereas PUL15 and PUL20 hydrogels were estimated to fail.

3.2.2.2 Tensile Test

Tensile test was performed on PP mesh embedded PUL25 hydrogel (PUL25-PP) and PP mesh in order to test integration between PUL and PP layers as well as assess adequacy of intraperitoneal patch for hernia treatment. Test was performed in transverse direction. Calculated tensile strength for PP and PUL25-PP are given in Table 3.4. Image of a PUL25-PP sample breaking after tensile test was also given in Figure 3.12.

Table 3. 4 Calculated tensile strength for PP and PUL25-PP. (n=4).

Sample	Tensile Strength (N/cm ²)
PP	50.42±13.42
PUL25-PP	74.88±15.20



Figure 3. 12 Image of a PUL25-PP sample breaking after tensile test.

Tensile test revealed that there was no significant difference between PP and PUL25-PP samples' tensile strength. PP mesh has knitted form which created dog bone-shaped test samples to have varying knot distributions. Hence, high standard deviation was observed from both groups. Transverse tensile strength of human abdominal wall was stated as 9.2 N/cm² which takes thickness of abdominal wall into consideration (Hollinsky & Sandberg, 2007). On the other hand, tensile strength of intra-abdominal meshes were calculated as N/cm, without considering thickness of meshes (Pott et al., 2012). Therefore, rather than native tissue, commercially available products which are widely used in surgical operations were chosen for comparison. Prolene[®] (Johnson-Johnson, USA) and Surgimesh[®] (United States Surgical, USA) which are differently knitted meshes with different fiber diameters made of PP were reported to have 41.6 N/cm and 46.5 N/cm transverse tensile strength, respectively (Pott et al., 2012). Comparing provided and observed data, it was concluded that mechanical properties of mesh is effected by its physical properties. Moreover, as seen in Figure 3.13, after breaking of samples, PUL and PP layers were still intact. Hence it was concluded that integration between PUL and PP layers was successful.

3.3 Water Contact Angle Measurement

In order to determine hydrophilicity of 2 sides of intraperitoneal patch, water contact angle of F: COS layer, PUL-side and F: COS-side of the patch was measured (Figure 3.13). Water contact angle measurement was performed on assembled patch. F: COS-layer, alone was also included in measurements in order to address the possible effect of assembling on thin electrospun layer on water contact angle. Measurements revealed that water contact angle of F: COS layer was significantly higher than that of both F: COS-side and PUL-side of intraperitoneal patch. High value of water contact angle was related to hydrophobic surface property of a material (Gundersen, Leinaas, & Thaulow, 2014). Fibroin was referred as a hydrophobic biomaterial whereas COS was reported as a hydrophilic polymer (Nah et al., 2006; Vepari & Kaplan, 2007). Higher value of water contact angle of F: COS layer can be reasoned with the weight

ratio between hydrophilic portion and hydrophobic portion of F: COS layer. It was also observed that there was no significant difference between water contact angle values of PUL-side and F: COS-side of intraperitoneal patch. PUL was referred as a polymer with high hydrophilicity (Tabasum et al., 2018). Therefore, it was concluded that assembly of layers increased the hydrophilicity of F: COS surface. Surface hydrophilicity was considered as an important factor effecting cell viability (Chang & Wang, 2011). Cell viability on F: COS layer alone was investigated in this study, so far. Therefore, it was concluded that more research must be conducted to determine cell viability of F: COS-side of assembled intraperitoneal patch.

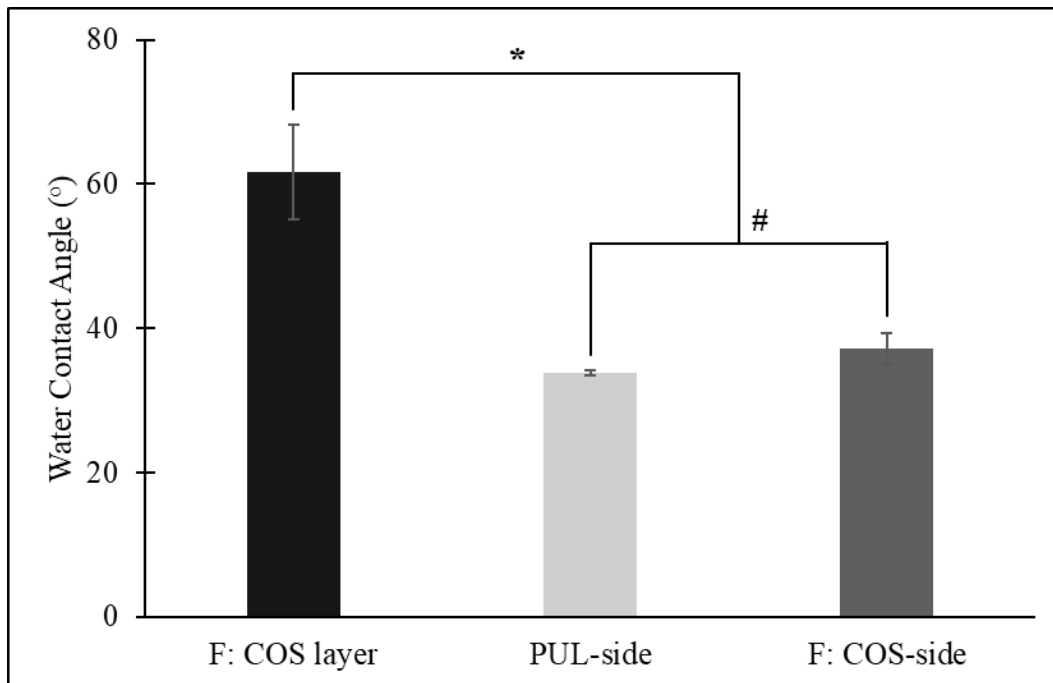


Figure 3. 13 Water contact angle values of PUL-side and F: COS-side of intraperitoneal patch and F: COS layer alone. PUL25 hydrogel was chosen for PUL-side while electrospun F: COS 90:10 (w/w) was chosen for F: COS-side of the intraperitoneal patch. “*” indicates statistical difference among groups whereas “#” stands for non-significant difference between groups (n=4, p<0.05).

3.4 Cell Culture Studies

3.4.1 Assessment of Cell Viability

3.4.1.1 Cell Viability on PUL Layer

Cell viability on PUL layer was assessed via Alamar Blue Assay. In preliminary studies, air-dried PUL20, PUL25, PUL30 and PUL35 hydrogels were used while TCPS was employed as positive control. Percent reduction values of Alamar Blue for TCPS and air-dried PUL20, PUL25, PUL30 and PUL35 are given in Figure 3.14.

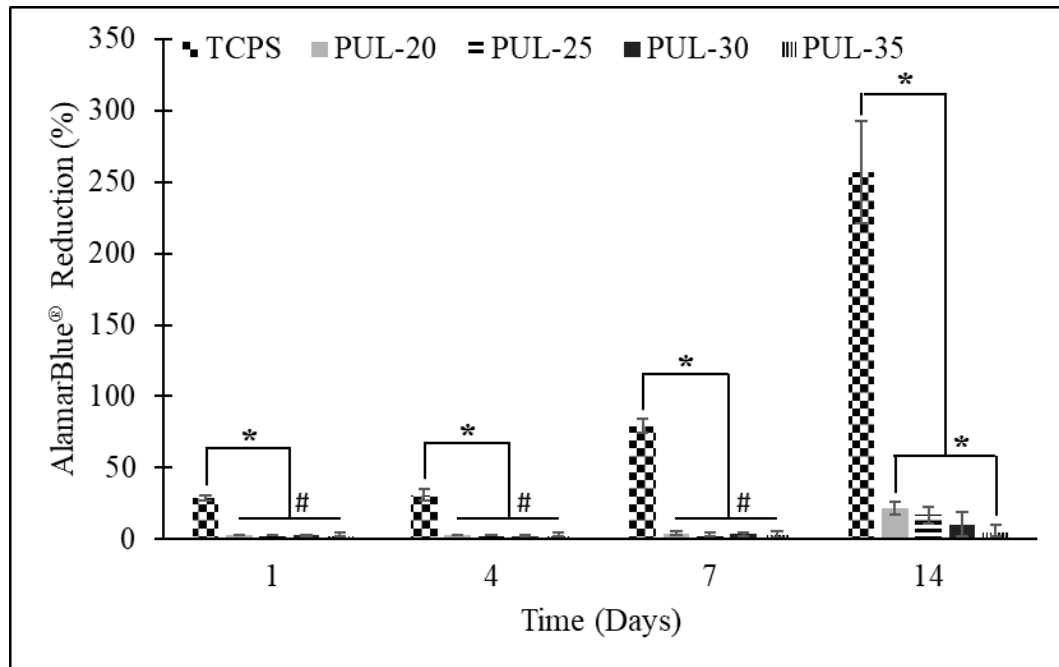


Figure 3. 14 Percent reduction of Alamar Blue for L929 cells seeded (25,000 cells/cm²) on TCPS, air-dried PUL20 hydrogels, PUL25, PUL30 and PUL35 hydrogels. Percent reduction Alamar Blue showed highest value at all given time points. Percent reduction of PUL hydrogels were non-significant at days 1,4 and 7. “*” indicates statistical significance whereas “#” stands for non-significant values (n=6, p<0.05).

Percent reduction of Alamar Blue was significantly lower for all PUL hydrogels compared to TCPS. Moreover, there was no significant difference between PUL hydrogels at days 1, 4 and 7. At day 14, percent reduction of Alamar blue PUL35 was the lowest whereas percent reduction values for PUL20, PUL25 and PUL30 were similar. Alamar Blue assay revealed that PUL hydrogels successfully acted as anti-adhesive layer. However, during experiments, hydrogels revealed significant change in dimension. Thus, considering integrity of layers, experiment was repeated with freeze dried PUL20 and PUL25 hydrogels. This way, effect of drying method on cell attachment was tested. Percent reduction of Alamar blue for TCPS, PUL20 and PUL25 is given in Figure 3.15.

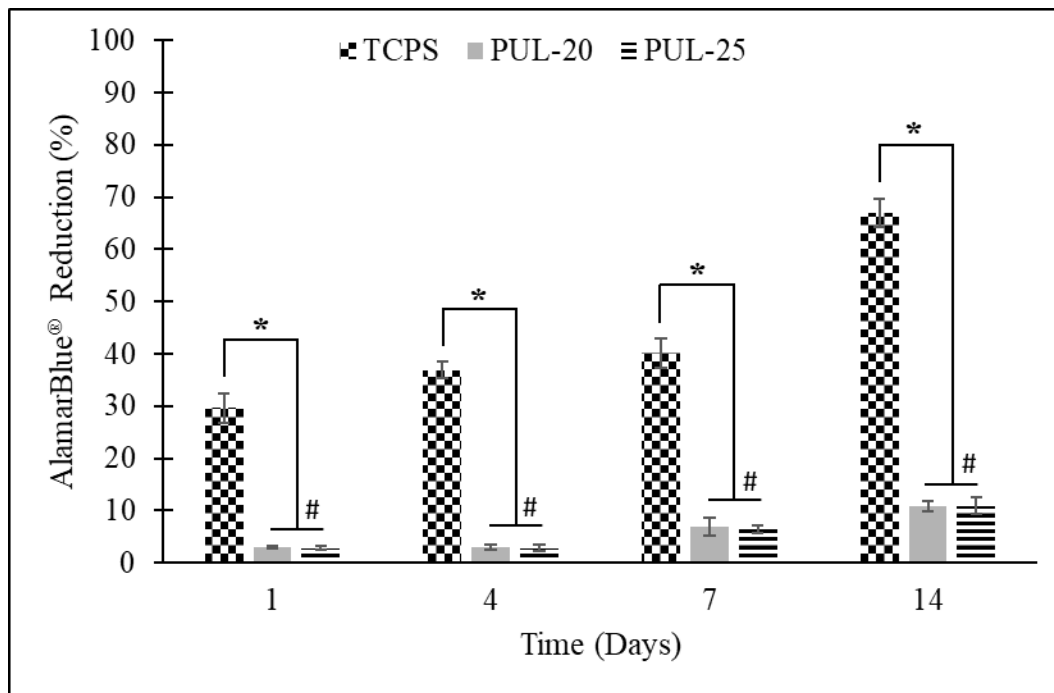


Figure 3. 15 Percent reduction of Alamar Blue by L929 cells seeded (25,000 cells/cm²) on TCPS, freeze-dried PUL20 hydrogels and freeze-dried PUL25 hydrogels. There was no statistical difference between percent reduction values observed between PUL20 and PUL25 hydrogel groups at all time points. Moreover, percent reduction values observed in both hydrogel groups was lower than observed in TCPS group, at all given time points. “*” indicates statistical difference between

groups whereas “#” stands for non-significant difference between groups (n=6, p<0.05).

In concordance with previous assay, compared to cells seeded on TCPS, cell viability was significantly lower for cells seeded on freeze dried PUL gels. Additionally, percent reduction of Alamar Blue measured for cells was similar for PUL20 and PUL25 hydrogels. In a similar study, Autissier, Letourneur & Le Visage (2007) cultured rabbit smooth muscle cells on 20% (w/v) PUL hydrogels cross-linked with STMP. It was claimed that PUL hydrogels promoted proliferation. However, cell viability assay was performed giving absorbance values at 590nm, without positive control, which makes results incomparable (Autissier et al., 2007). In another study, Bang et al. (2016) investigated potential of carboxymethyl PULL for prevention of intraperitoneal adhesions. Human epidermal fibroblasts were cultured on PUL hydrogels whereas *in vivo* experiments were performed on rats. It was shown that PUL hydrogel was able to prevent cell proliferation and intraperitoneal adhesions (Bang et al., 2016). Overall, it was shown that PUL hydrogels were able to reduce cell proliferation as percent reduction of PUL hydrogel groups were significantly lower than TCPS group at all given time points. This property of PUL hydrogel makes it suitable candidate for anti-adhesive layer.

3.4.1.2 Cell Viability on F: COS Layer

Viability of L929 cells seeded on electrospun F: COS layer with different polymer ratios (100:0, 95:5, 90:10, 80:20, 70:30, 60:40, 50:50, w/w) was assessed via Alamar Blue Assay at days 1, 4, 7 and 14. TCPS was used as positive control whereas not-seeded scaffolds were used as negative controls. Percent reduction values of Alamar Blue for TCPS, and electrospun F: COS scaffolds are given in Figure 3.16.

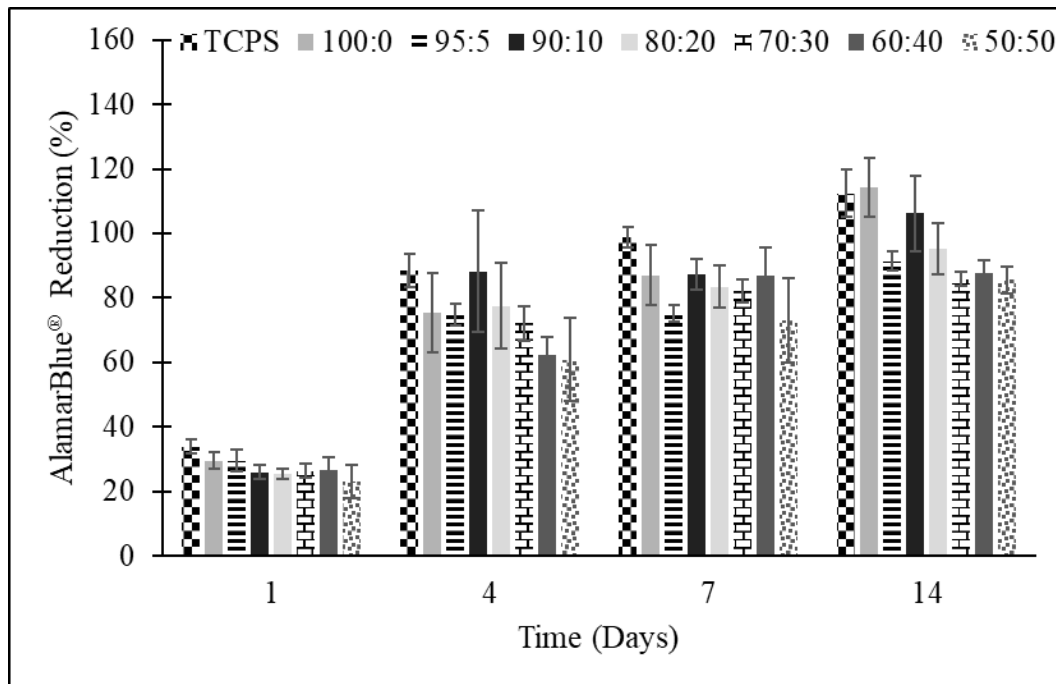


Figure 3. 16 Percent reduction of Alamar Blue by L929 cells seeded (25,000 cells/cm²) on TCPS and electrospun F: COS 100:0, 95:5, 90:10, 80:20, 70:30, 60:40 and 50:50 groups. “*” indicates significant difference between groups (n=6, p<0.05).

At day 1, there was no significant difference in the cell viability between TCPS and all F: COS groups whereas percent reduction observed in F: COS (50:50) group was significantly lower than observed in other groups and TCPS at day 4. Additionally, at day 7, percent reduction in both F: COS 95:5 and 50:50 was significantly lower than observed in other groups and TCPS group. Finally, at day 14, there was no significant difference between percent reduction values observed in TCPS group and F: COS 100:0, 90:10, 80:20 groups while percent reduction in F: COS 95:5, 70:30, 60:40 and 50:50 groups was significantly lower than TCPS group.

Cytocompatibility of electrospun fibroin was assessed by various groups. Park et al. (2016) reported that human dermal fibroblasts and keratinocytes were successfully cultivated on 3D electrospun fibroin scaffolds whereas Meinel et al. (2009) showed that electrospun fibroin was suitable for cultivation of human mesenchymal stem cells. Viability of L929 cells on electrospun fibroin was also assessed. Alessandrino et al.

(2008) tested cytocompatibility of electrospun fibroin fibers prepared with formic acid using L929 cells. Overall, it was observed that fibers containing more than 30 % (w/w) COS of total polymer led to a significant decrease in cell viability, which may be explained with increase in hydrophilicity of fibers with increasing concentration of COS (Nah et al., 2006; Vepari & Kaplan, 2007).

3.4.1.3 Assessment of Cell Morphology

SEM images of L929 cells on F: COS scaffolds after 14 days of incubation with with different polymer ratios (100:0, 95:5, 90:10, 80:20, 70:30, 60:40, 50:50, w/w) are given in Figure 3.17. Moreover, morphology of RAW 264.7 cells were also investigated to assess immunomodulation. SEM images of RAW 264.7 stimulated macrophage cells after 1 day of incubation on F: COS scaffolds with with different polymer ratios (100:0, 95:5, 90:10, 80:20, 70:30, 60:40, 50:50, w/w) are given in Figure 3.20.

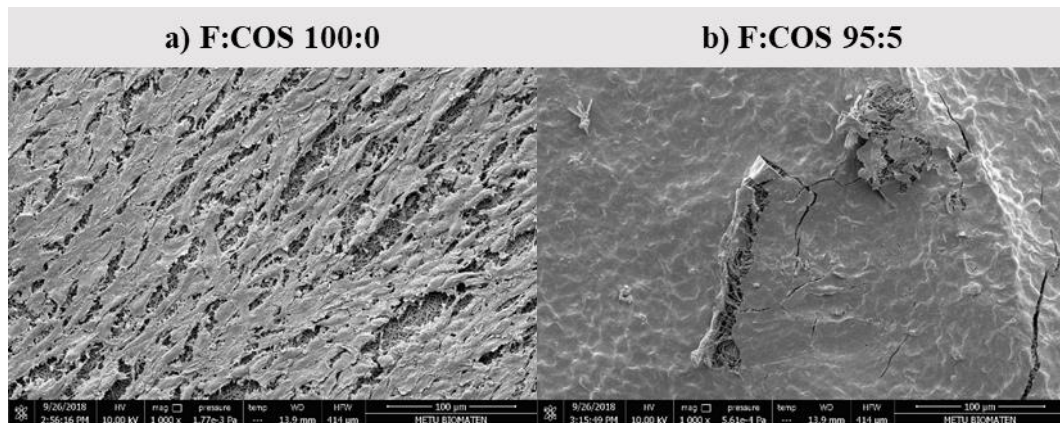


Figure 3. 17 SEM images of L929 cells seeded (25,000 cells/cm²) on electrospun F: COS with different polymer ratios. (Scale bar: 100 µm).

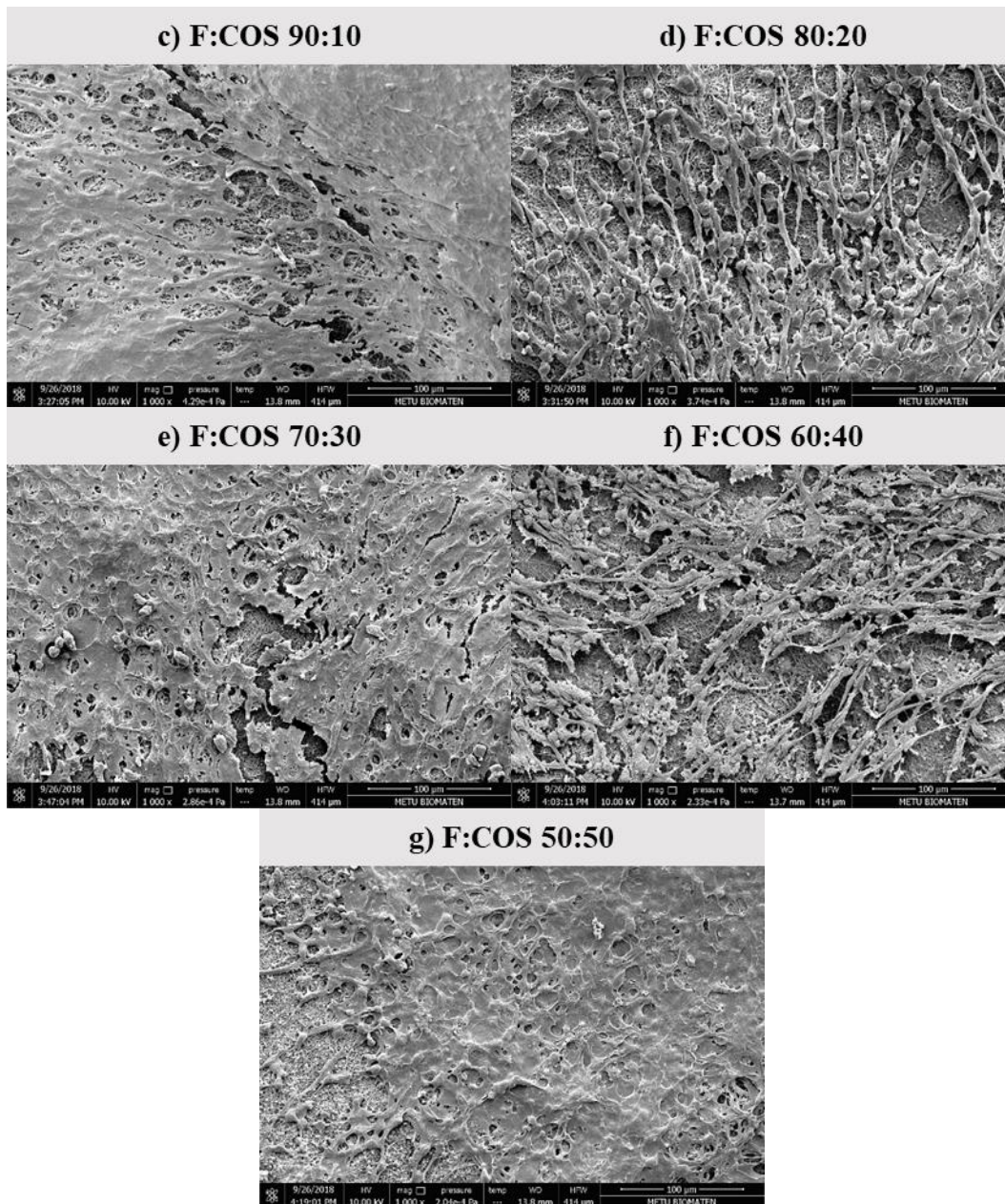


Figure 3.17 Continued SEM images of L929 cells seeded (25,000 cells/cm²) on electrospun F: COS with different polymer ratios. (Scale bar: 100 µm).

As seen in Figure 3.17, L929 cells spread on all F: COS scaffolds. Cells on all electrospun layers formed cell sheets consisting of spread and elongated morphology. Spread and elongated cells with long filopodia were referred as viable cells (Bahcecioglu, Hasirci, & Hasirci, 2018). Considering, the lowest value of Alamar

Blue[®] percent reduction among groups was 85% and cell sheet formation on F: COS layers together, high proliferation of L929 cells were confirmed. Moreover, F: COS 80:20, 60:40 and 50:50 samples presented both well-spread flattened cells and elongated rounder cells. elongated and rounder morphology of L929 cells were referred a migrating cells (Bahcecioglu et al., 2018). Therefore, it was considered that cells kept proliferating and migrating at day 14, on these layers. Overall, it was concluded that electrospun F: COS scaffolds presented suitable environment for proliferation of L929 cells which are of mesothelial origin as cells present in abdominal wall and hold potential for promotion of abdominal wall regeneration (Smith, 2002; Thonemann et al., 2002).

3.4.2 Assessment of Immunomodulatory Properties

Immunomodulatory property of F: COS layer of intraperitoneal patch was investigated by measuring NO⁻ concentration in culture media for varying F: COS polymer ratios. RAW 264.7 cells were stimulated with LPS to produce NO⁻. NO⁻ was detected by using a kit containing an enzyme converting nitrate (NO₃) to nitrite (NO₂). Amount of obtained nitrite is then detected by Griess reagent. Hence, NO⁻ was detected by total amount of NO₂ and NO₃ (Misko, Schilling, Salvemini, Moore, & Currie, 1993). In this case, enzyme from NO⁻ detection kit was not working as there was no difference in samples with and without enzyme (Data not shown). Moreover, calibration curve was constructed using nitrite standard. Hence other ingredients were not problematic. As a result, rather than NO⁻, amount of NO₂ was detected which is still useful for comparison. Concentration of NO⁻ produced by RAW 264.7 cells seeded on electrospun F: COS layers with different polymer ratios is given in Figure 3. 18.

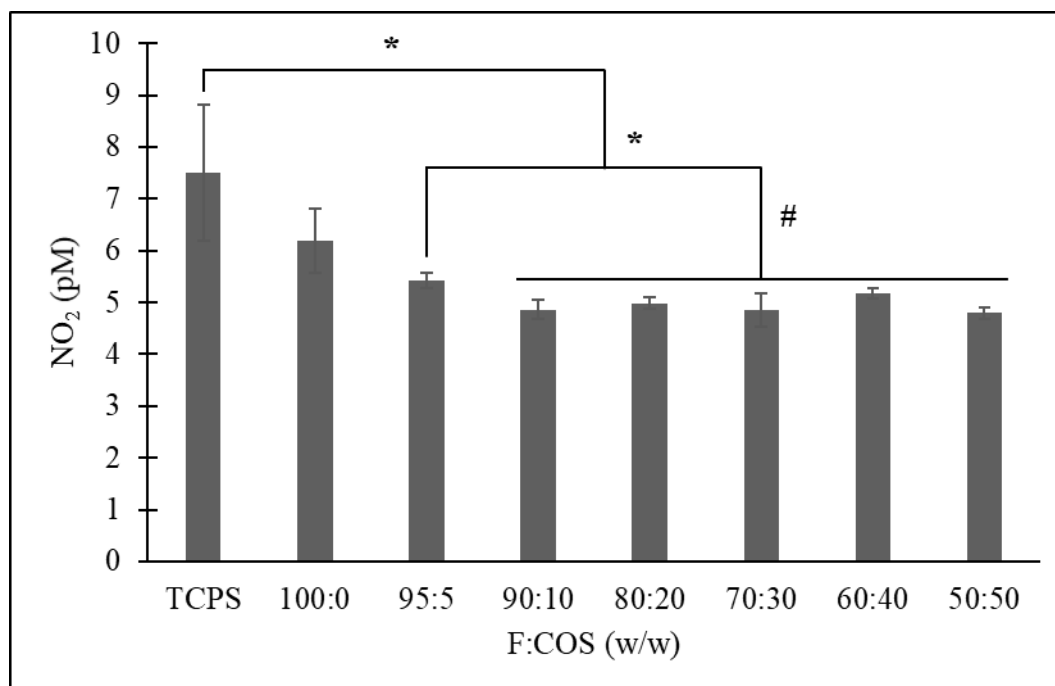


Figure 3. 18 Concentration of NO₂ produced by RAW 264.7 cells seeded on electrospun F: COS layers with different polymer ratios. “*” was used as a notification for statistically significant difference between the groups (n=6, p<0.05). “#” stands for non-significant difference between groups (n=6, p<0.05).

NO⁻ is synthesized by an enzyme called nitric oxide synthase, which is a mediator playing a major role in inflammation. Level of nitric oxide synthase is affected by levels of inflammatory molecules such as IFN- γ and TNF α (Ghasemian, Owlia, & Owlia, 2016). Hence, lowering of NO⁻ level was related to immunomodulation (H. K. Kim, Cheon, Kim, Kim, & Kim, 1999). As seen in Figure 3.15, NO⁻ concentration decrease as F: COS polymer ratio went down to 90:10 (w/w). It was also detected that further increase of COS did not lead to a significant decrease in NO⁻ production. Hence, it was concluded that F: COS 90:10 (w/w) achieved immunomodulation with the least amount of COS. Immunomodulatory activity of COS was reported before. Yoon et al. (2007) incorporated different amounts of COS in culture medium in order to determine immunomodulatory potential of COS. Inhibition of TNF- α and IL-6 gene expression as well as secretion of NO⁻ in RAW 264.7 macrophage cell line (Yoon et al., 2007) by COS was reported. In another study, Lee et al. (2009) investigated factors

affecting immunomodulatory effect of COS on RAW 264.7 macrophage cell line. Immunomodulation was evaluated by reduction of NO₂ level in cell culture media. It was found that degree of acetylation and molecular weight affected immunomodulatory effect the polymer (S. H. Lee et al., 2009). In thesis, high molecular weight COS with degree of acetylation over 90% was used. Results obtained were in concordance with literature. Considering both immunomodulatory effect and cell viability, F: COS 90:10 (^{w/w}) group was chosen as it provided significant immunomodulatory effect with minimum COS ratio and cell viability of L929 cells seeded on it was similar to that of TCPS.

CHAPTER 4

CONCLUSION

3-layered intraperitoneal patch consisting of polypropylene mesh within anti-adhesive pullulan (PUL) hydrogel with regenerative and immunomodulatory fibroin: chitosan oligosaccharide lactate (F: COS) electrospun layer on one side was fabricated for the first time. Water uptake and diameter change in PUL hydrogel were higher for lower hydrogel concentrations. Degradation and mechanical properties were proportional to hydrogel concentration. PUL hydrogels of different concentration showed similar anti-adhesiveness for fibroblasts. Hence PUL 25 was considered as most feasible hydrogel group. Macrophage cells seeded on F: COS 90:10 (^{w/w}) electrospun layer presented significantly lower NO⁻ production. Further increasing COS ratio did not produce any significant change in NO⁻ level. Thus, F: COS 90:10 (^{w/w}) was considered to be most suitable layer for immunomodulation.

As conclusion, our results showed that three layered peritoneal mesh composed of PP mesh embedded in PUL25 hydrogel with F: COS 90:10 (^{w/w}) electrospun layer on one side fulfilled the needs of anti-adhesiveness on one side and regeneration on the other side rat justified the need for *in vivo* tests in animal abdominal wall defect models for evaluation of potential clinical use of the proposed intraperitoneal patch.

REFERENCES

- Abed, A., Deval, B., Assoul, N., Bataille, I., Portes, P., Louedec, L., ... Meddahi-Pellé, A. (2008). A Biocompatible Polysaccharide Hydrogel–Embedded Polypropylene Mesh for Enhanced Tissue Integration in Rats. *Tissue Engineering Part A*, *14*(4), 519–527. <https://doi.org/10.1089/tea.2007.0134>
- Alessandrino, A., Marelli, B., Arosio, C., Fare, S., Tanzi, M. C., & Freddi, G. (2008). Electrospun Silk Fibroin Mats for Tissue Engineering. *Engineering in Life Sciences*, *8*(3), 219–225. <https://doi.org/10.1002/elsc.200700067>
- Andorko, J. I., & Jewell, C. M. (2017). Designing biomaterials with immunomodulatory properties for tissue engineering and regenerative medicine. *Bioengineering & Translational Medicine*, *2*(2), 139–155. <https://doi.org/10.1002/btm2.10063>
- Ar'Rajab, A., Mileski, W., Sentementes, J. T., Sikes, P., Harris, R. B., & Dawidson, I. J. A. (1996). The Role of Neutrophils in Peritoneal Adhesion Formation. *Journal of Surgical Research*, *61*(1), 143–146. <https://doi.org/10.1006/jsre.1996.0095>
- Artis, T., Artis, A. S., Arslan, E., Mutlu, F., Akay, A., & Deniz, K. (2016). Preventive Effect of Ethyl Pyruvate on Postoperative Adhesion Formation Following Abdominal Surgery. *Journal of Investigative Surgery*, *29*(5), 260–265. <https://doi.org/10.3109/08941939.2016.1149639>
- Arung, W., Meurisse, M., & Detry, O. (2011). Pathophysiology and prevention of postoperative peritoneal adhesions. *World Journal of Gastroenterology*, *17*(41), 4545–4553. <https://doi.org/10.3748/wjg.v17.i41.4545>
- Autissier, A., Letourneur, D., & Le Visage, C. (2007). Pullulan-based hydrogel for

- smooth muscle cell culture. *Journal of Biomedical Materials Research - Part A*, 82(2), 336–342. <https://doi.org/10.1002/jbm.a.30998>
- Azuma, K., Osaki, T., Minami, S., & Okamoto, Y. (2015). Anticancer and Anti-Inflammatory Properties of Chitin and Chitosan Oligosaccharides. *Journal of Functional Biomaterials*, 6(1), 33–49. <https://doi.org/10.3390/jfb6010033>
- Bahcecioglu, G., Hasirci, N., & Hasirci, V. (2018). Effects of microarchitecture and mechanical properties of 3D microporous PLLA-PLGA scaffolds on fibrochondrocyte and L929 fibroblast behavior. *Biomedical Materials*, 13(3), 035005. <https://doi.org/10.1088/1748-605X/aaa77f>
- Bang, S., Lee, E., Ko, Y. G., Kim, W. Il, & Kwon, O. H. (2016). Injectable pullulan hydrogel for the prevention of postoperative tissue adhesion. *International Journal of Biological Macromolecules*, 87, 155–162. <https://doi.org/10.1016/j.ijbiomac.2016.02.026>
- Basu, B., Katti, D. S., & Kumar, A. (2009). *Advanced Biomaterials. Advanced Biomaterials: Fundamentals, Processing, and Applications*. <https://doi.org/10.1002/9780470891315>
- Blázquez, R., Sánchez-Margallo, F. M., Álvarez, V., Usón, A., Marinaro, F., & Casado, J. G. (2018). Fibrin glue mesh fixation combined with mesenchymal stem cells or exosomes modulates the inflammatory reaction in a murine model of incisional hernia. *Acta Biomaterialia*, 71, 318–329. <https://doi.org/10.1016/j.actbio.2018.02.014>
- Brochhausen, C., Schmitt, V. H., Planck, C. N. E., Rajab, T. K., Hollemann, D., Tapprich, C., ... Kirkpatrick, C. J. (2012). Current Strategies and Future Perspectives for Intraperitoneal Adhesion Prevention. *Journal of Gastrointestinal Surgery*, 16(6), 1256–1274. <https://doi.org/10.1007/s11605-011-1819-9>
- Brochhausen, C., Schmitt, V. H., Rajab, T. K., Planck, C. N. E., Krämer, B., Wallwiener, M., ... Kirkpatrick, C. J. (2011). Intraperitoneal adhesions-An

ongoing challenge between biomedical engineering and the life sciences. *Journal of Biomedical Materials Research - Part A*, 98 A(1), 143–156. <https://doi.org/10.1002/jbm.a.33083>

Chang, H.-I., & Wang, Y. (2011). Cell Responses to Surface and Architecture of Tissue Engineering Scaffolds. *Regenerative Medicine and Tissue Engineering - Cells and Biomaterials*. <https://doi.org/10.5772/21983>

Chon, J. W., Kim, H., Jeon, H. N., Park, K., Lee, K. G., Yeo, J. H., ... Park, Y. K. (2012). Silk fibroin hydrolysate inhibits osteoclastogenesis and induces apoptosis of osteoclasts derived from RAW 264.7 cells. *International Journal of Molecular Medicine*, 30(5), 1203–1210. <https://doi.org/10.3892/ijmm.2012.1120>

Christo, S. N., Diener, K. R., Bachhuka, A., Vasilev, K., & Hayball, J. D. (2015). Innate Immunity and Biomaterials at the Nexus: Friends or Foes. *BioMed Research International*, 2015. <https://doi.org/10.1155/2015/342304>

Clarke, T., Katkhouda, N., Mason, R. J., Cheng, B. C., Algra, J., Olasky, J., ... Balouch, M. (2011). Fibrin glue for intraperitoneal laparoscopic mesh fixation: A comparative study in a swine model. *Surgical Endoscopy and Other Interventional Techniques*, 25(3), 737–748. <https://doi.org/10.1007/s00464-010-1244-2>

Cold Spring Harbor Protocols. (2007, February 1). HEPES-buffered Tyrode's solution. <https://doi.org/10.1101/pdb.rec10805>

Deeken, C. R., Faucher, K. M., & Matthews, B. D. (2012). A review of the composition, characteristics, and effectiveness of barrier mesh prostheses utilized for laparoscopic ventral hernia repair. *Surgical Endoscopy and Other Interventional Techniques*, 26(2), 566–575. <https://doi.org/10.1007/s00464-011-1899-3>

Dória, R. G. S., Freitas, S. H. de, Hayasaka, Y. de B., Hage, M. C. F. N. S., Strefezzi, R. de F., Carregaro, A. B., ... Müller, A. F. (2018). Evaluation of polyamide surgical mesh as an abdominal ventral implant in rabbits. *Acta Cirurgica*

Brasileira, 33(5), 454–461. <https://doi.org/10.1590/s0102-865020180050000008>

Dubick, M. A., Mayer, A. D., Majumdar, A. P., Mar, G., McMahon, M. J., & Geokas, M. C. (1987). Biochemical studies in peritoneal fluid from patients with acute pancreatitis. Relationship to etiology. *Dig Dis Sci*, 32(3), 305–312.

Dulong, V., Forbice, R., Condamine, E., Le Cerf, D., & Picton, L. (2011). Pullulan–STMP hydrogels: a way to correlate crosslinking mechanism, structure and physicochemical properties. *Polymer Bulletin*, 67(3), 455–466. <https://doi.org/10.1007/s00289-010-0435-2>

Emre, A., Akin, M., Isikgonul, I., Yuksel, O., Anadol, A. Z., & Cifter, C. (2009). Comparison of intraperitoneal honey and sodium hyaluronate-carboxymethylcellulose (Seprafilm™) for the prevention of postoperative intra-abdominal adhesions. *Clinics*, 64(4), 363–368. <https://doi.org/10.1590/S1807-59322009000400016>

Fatkhudinov, T., Tsedik, L., Arutyunyan, I., Lokhonina, A., Makarov, A., Korshunov, A., ... Sukhikh, G. (2018). Evaluation of resorbable polydioxanone and polyglycolic acid meshes in a rat model of ventral hernia repair. *Journal of Biomedical Materials Research Part B: Applied Biomaterials*, 1–12. <https://doi.org/10.1002/jbm.b.34158>

Fragiskos, F. D. (2007). *Principles of surgery. Oral Surgery*. https://doi.org/10.1007/978-3-540-49975-6_3

Garg, K., & Bowlin, G. L. (2011). Electrospinning jets and nanofibrous structures. *Biomicrofluidics*, 5(1), 13403. <https://doi.org/10.1063/1.3567097>

Geckil, H., Xu, F., Zhang, X., Moon, S., & Demirci, U. (2010). Engineering hydrogels as extracellular matrix mimics. *Nanomedicine*, 5(3), 469–484. <https://doi.org/10.2217/nnm.10.12>

Ghasemian, M., Owlia, S., & Owlia, M. B. (2016). Review of Anti-Inflammatory

- Herbal Medicines. *Advances in Pharmacological Sciences*, 2016, 1–11.
<https://doi.org/10.1155/2016/9130979>
- Gizaw, M., Thompson, J., Faglie, A., Lee, S.-Y., Neuenschwander, P., & Chou, S.-F. (2018). Electrospun Fibers as a Dressing Material for Drug and Biological Agent Delivery in Wound Healing Applications. *Bioengineering*, 5(1), 9.
<https://doi.org/10.3390/bioengineering5010009>
- Gobin, A. S., Butler, C. E., & Mathur, A. B. (2006). Repair and regeneration of the abdominal wall musculofascial defect using silk fibroin-chitosan blend. *Tissue Engineering*, 12(12), 3383–3394. <https://doi.org/10.1089/Ten.2006.12.3383>
- Gokal, R., & Nolph, K. D. (2009). *Nolph and Gokal's Textbook of Peritoneal Dialysis*. (R. Khanna & R. T. Krediet, Eds.). Boston, MA: Springer US.
<https://doi.org/10.1007/978-0-387-78940-8>
- Göpferich, A. (1996). Mechanisms of polymer degradation and erosion. *Biomaterials*, 17(2), 103–114. [https://doi.org/10.1016/0142-9612\(96\)85755-3](https://doi.org/10.1016/0142-9612(96)85755-3)
- Gu, B. K., Park, S. J., Kim, M. S., Kang, C. M., Kim, J. II, & Kim, C. H. (2013). Fabrication of sonicated chitosan nanofiber mat with enlarged porosity for use as hemostatic materials. *Carbohydrate Polymers*, 97(1), 65–73.
<https://doi.org/10.1016/j.carbpol.2013.04.060>
- Guillaume, O., Park, J., Monforte, X., Gruber-Blum, S., Redl, H., Petter-Puchner, A., & Teuschl, A. H. (2016). Fabrication of silk mesh with enhanced cytocompatibility: preliminary in vitro investigation toward cell-based therapy for hernia repair. *Journal of Materials Science: Materials in Medicine*, 27(2), 1–13. <https://doi.org/10.1007/s10856-015-5648-3>
- Gundersen, H., Leinaas, H. P., & Thaulow, C. (2014). Surface structure and wetting characteristics of Collembola cuticles. *PLoS ONE*, 9(2), e86783.
<https://doi.org/10.1371/journal.pone.0086783>
- Haul, R. (1982). S. J. Gregg, K. S. W. Sing: Adsorption, Surface Area and Porosity.

2. Auflage, Academic Press, London 1982. 303 Seiten, Preis: \$ 49.50. *Berichte Der Bunsengesellschaft Für Physikalische Chemie*, 86(10), 957–957. <https://doi.org/10.1002/bbpc.19820861019>
- He, Y. X., Zhang, N. N., Li, W. F., Jia, N., Chen, B. Y., Zhou, K., ... Zhou, C. Z. (2012). N-terminal domain of Bombyx mori fibroin mediates the assembly of silk in response to pH decrease. *Journal of Molecular Biology*, 418(3–4), 197–207. <https://doi.org/10.1016/j.jmb.2012.02.040>
- Hollinsky, C., & Sandberg, S. (2007). Measurement of the tensile strength of the ventral abdominal wall in comparison with scar tissue. *Clinical Biomechanics*, 22(1), 88–92. <https://doi.org/10.1016/J.CLINBIOMECH.2006.06.002>
- Howard, D., Buttery, L. D., Shakesheff, K. M., & Roberts, S. J. (2008). Tissue engineering: Strategies, stem cells and scaffolds. *Journal of Anatomy*, 213(1), 66–72. <https://doi.org/10.1111/j.1469-7580.2008.00878.x>
- Hu, M., Lin, X., Huang, R., Yang, K., Liang, Y., Zhang, X., ... Wu, D. (2018). Lightweight, Highly Permeable, Biocompatible, and Antiadhesive Composite Meshes for Intraperitoneal Repairs. *Macromolecular Bioscience*, 18(7), 1–8. <https://doi.org/10.1002/mabi.201800067>
- Jakovljevic, D., Vrvic, M. M., Radulovic, M., & Hranisavljevic-Jakovljevic, M. (2001). Fine structural analysis of the fungal polysaccharide pullulan elaborated by *Aureobasidium pullulans*, CH-1 strain. *Journal of the Serbian Chemical Society*, 66(6), 377–383.
- Jaleh, B., Parvin, P., Wanichapichart, P., Saffar, A. P., & Reyhani, A. (2010). Induced super hydrophilicity due to surface modification of polypropylene membrane treated by O₂ plasma. *Applied Surface Science*, 257(5), 1655–1659. <https://doi.org/10.1016/j.apsusc.2010.08.117>
- Jammalamadaka, U., & Tappa, K. (2018). Recent Advances in Biomaterials for 3D Printing and Tissue Engineering. *Journal of Functional Biomaterials*, 9(1), 22. <https://doi.org/10.3390/jfb9010022>

- Jenkins, E. D., Lerdsirisopon, S., Costello, K. P., Melman, L., Greco, S. C., Frisella, M. M., ... Deeken, C. R. (2011). Laparoscopic fixation of biologic mesh at the hiatus with fibrin or polyethylene glycol sealant in a porcine model. *Surgical Endoscopy*, 25(10), 3405–3413. <https://doi.org/10.1007/s00464-011-1741-y>
- Jiang, S., Wang, W., Yan, H., & Fan, C. (2013). Prevention of intra-abdominal adhesion by bi-layer electrospun membrane. *International Journal of Molecular Sciences*, 14(6), 11861–11870. <https://doi.org/10.3390/ijms140611861>
- Junge, K., Binnebösel, M., Rosch, R., Jansen, M., Kämmer, D., Otto, J., ... Klinge, U. (2009). Adhesion formation of a polyvinylidene fluoride/polypropylene mesh for intra-abdominal placement in a rodent animal model. *Surgical Endoscopy*, 23(2), 327–333. <https://doi.org/10.1007/s00464-008-9923-y>
- Kaleya, R. N. (2005). Evaluation of implant/host tissue interactions following intraperitoneal implantation of porcine dermal collagen prosthesis in the rat. *Hernia*, 9(3), 269–276. <https://doi.org/10.1007/s10029-005-0003-0>
- Kelly, M., Macdougall, K., Olabisi, O., & McGuire, N. (2017). In vivo response to polypropylene following implantation in animal models: a review of biocompatibility. *International Urogynecology Journal*, 28(2), 171–180. <https://doi.org/10.1007/s00192-016-3029-1>
- Kim, H. K., Cheon, B. S., Kim, Y. H., Kim, S. Y., & Kim, H. P. (1999). Effects of naturally occurring flavonoids on nitric oxide production in the macrophage cell line RAW 264.7 and their structure-activity relationships. *Biochemical Pharmacology*, 58(5), 759–765. [https://doi.org/10.1016/S0006-2952\(99\)00160-4](https://doi.org/10.1016/S0006-2952(99)00160-4)
- Kim, Y., Ko, H., Kwon, I. K., & Shin, K. (2016). Extracellular matrix revisited: Roles in tissue engineering. *International Neurourology Journal*, 20, S23–S29. <https://doi.org/10.5213/inj.1632600.318>
- Klink, C. D., Schickhaus, P., Binnebösel, M., Jockenhoevel, S., Rosch, R., Tolba, R., ... Klinge, U. (2013). Influence of 4% icodextrin solution on peritoneal tissue

- response and adhesion formation. *BMC Surgery*, 13(1), 34. <https://doi.org/10.1186/1471-2482-13-34>
- Koc, O., Duran, B., Topcuoglu, A., Bugdayci, G., Yilmaz, F., & Dönmez, M. (2009). Intraperitoneal administration of single dose type I collagen or low dose melatonin to prevent intraperitoneal adhesion formation: A comparative study. *European Journal of Obstetrics Gynecology and Reproductive Biology*, 145(2), 209–213. <https://doi.org/10.1016/j.ejogrb.2009.05.019>
- Konar, S., Guha, R., Kundu, B., Nandi, S., Ghosh, T. K., Kundu, S. C., ... Hazra, S. (2017). Silk fibroin hydrogel as physical barrier for prevention of post hernia adhesion. *Hernia*, 21(1), 125–137. <https://doi.org/10.1007/s10029-016-1484-8>
- Koombhongse, S., Liu, W., & Reneker, D. H. (2001). Flat polymer ribbons and other shapes by electrospinning. *Journal of Polymer Science, Part B: Polymer Physics*, 39(21), 2598–2606. <https://doi.org/10.1002/polb.10015>
- Kruse, C. R., Singh, M., Targosinski, S., Sinha, I., Sørensen, J. A., Eriksson, E., & Nuutila, K. (2017). The effect of pH on cell viability, cell migration, cell proliferation, wound closure, and wound reepithelialization: In vitro and in vivo study. *Wound Repair and Regeneration*, 25(2), 260–269. <https://doi.org/10.1111/wrr.12526>
- Kukleta, J. F., Freytag, C., & Weber, M. (2012). Efficiency and safety of mesh fixation in laparoscopic inguinal hernia repair using n-butyl cyanoacrylate: Long-term biocompatibility in over 1, 300 mesh fixations. *Hernia*, 16(2), 153–162. <https://doi.org/10.1007/s10029-011-0887-9>
- Kundu, B., Rajkhowa, R., Kundu, S. C., & Wang, X. (2013). Silk fibroin biomaterials for tissue regenerations. *Advanced Drug Delivery Reviews*, 65(4), 457–470. <https://doi.org/10.1016/j.addr.2012.09.043>
- Lack, S., Dulong, V., Le Cerf, D., Picton, L., Argillier, J. F., & Muller, G. (2004). Hydrogels based on pullulan crosslinked with sodium trimetaphosphate (STMP): Rheological study. *Polymer Bulletin*, 52(6), 429–436.

<https://doi.org/10.1007/s00289-004-0299-4>

- Lack, S., Dulong, V., Picton, L., Cerf, D. Le, & Condamine, E. (2007). High-resolution nuclear magnetic resonance spectroscopy studies of polysaccharides crosslinked by sodium trimetaphosphate: a proposal for the reaction mechanism. *Carbohydrate Research*, 342(7), 943–953. <https://doi.org/10.1016/j.carres.2007.01.011>
- Lanza, R. P. (Robert P., Langer, R. S., & Vacanti, J. (2013). *Principles of tissue engineering*. Academic Press.
- Ławniczak, P., Grobelski, B., & Pasieka, Z. (2011). Properties comparison of intraperitoneal hernia meshes in reconstruction of the abdominal wall - Animal model study. *Polski Przegląd Chirurgiczny/ Polish Journal of Surgery*, 83(1), 19–26. <https://doi.org/10.2478/v10035-011-0003-y>
- Leal-Serrano, G., Ruperez, P., & Leal, J. A. (1980). Acidic polysaccharide from *Aureobasidium pullulans*. *Transactions of the British Mycological Society*, 75(1), 57–62. [https://doi.org/10.1016/S0007-1536\(80\)80194-X](https://doi.org/10.1016/S0007-1536(80)80194-X)
- Lee, K., Silva, E. A., & Mooney, D. J. (2011). Growth factor delivery-based tissue engineering: General approaches and a review of recent developments. *Journal of the Royal Society Interface*, 8(55), 153–170. <https://doi.org/10.1098/rsif.2010.0223>
- Lee, S. H., Senevirathne, M., Ahn, C. B., Kim, S. K., & Je, J. Y. (2009). Factors affecting anti-inflammatory effect of chitooligosaccharides in lipopolysaccharides-induced RAW264.7 macrophage cells. *Bioorganic and Medicinal Chemistry Letters*, 19(23), 6655–6658. <https://doi.org/10.1016/j.bmcl.2009.10.007>
- Li, H., Yang, J., Hu, X., Liang, J., Fan, Y., & Zhang, X. (2011). Superabsorbent polysaccharide hydrogels based on pullulan derivate as antibacterial release wound dressing. *Journal of Biomedical Materials Research - Part A*, 98 A(1), 31–39. <https://doi.org/10.1002/jbm.a.33045>

- Lin, L. X., Yuan, F., Zhang, H. H., & Sun, Y. L. (2017). Work of separation — A method to assess intraperitoneal adhesion and healing of parietal peritoneum in an animal model. *Clinical Biomechanics*, *41*, 82–86. <https://doi.org/10.1016/j.clinbiomech.2016.12.010>
- Lyu, S., & Untereker, D. (2009, September 11). Degradability of polymers for implantable biomedical devices. *International Journal of Molecular Sciences*. Multidisciplinary Digital Publishing Institute (MDPI). <https://doi.org/10.3390/ijms10094033>
- Martín-Cartes, J., Morales-Conde, S., Suárez-Grau, J., López-Bernal, F., Bustos-Jiménez, M., Cadet-Dussort, H., ... Morales-Mendez, S. (2008). Use of hyaluronidase cream to prevent peritoneal adhesions in laparoscopic ventral hernia repair by means of intraperitoneal mesh fixation using spiral tacks. *Surgical Endoscopy and Other Interventional Techniques*, *22*(3), 631–634. <https://doi.org/10.1007/s00464-007-9423-5>
- Meinel, A. J., Kubow, K. E., Klotzsch, E., Garcia-Fuentes, M., Smith, M. L., Vogel, V., ... Meinel, L. (2009). Optimization strategies for electrospun silk fibroin tissue engineering scaffolds. *Biomaterials*, *30*(17), 3058–3067. <https://doi.org/10.1016/J.BIOMATERIALS.2009.01.054>
- Misko, T. P., Schilling, R. J., Salvemini, D., Moore, W. M., & Currie, M. G. (1993). A fluorometric assay for the measurement of nitrite in biological samples. *Analytical Biochemistry*, *214*(1), 11–16. <https://doi.org/10.1006/abio.1993.1449>
- Morent, R., De Geyter, N., Leys, C., Gengembre, L., & Payen, E. (2008). Comparison between XPS- And FTIR-analysis of plasma-treated polypropylene film surfaces. *Surface and Interface Analysis*, *40*(3–4), 597–600. <https://doi.org/10.1002/sia.2619>
- Nagiah, N., Madhavi, L., Anitha, R., Srinivasan, N. T., & Sivagnanam, U. T. (2013). Electrospinning of poly (3-hydroxybutyric acid) and gelatin blended thin films: Fabrication, characterization, and application in skin regeneration. *Polymer*

Bulletin, 70(8), 2337–2358. <https://doi.org/10.1007/s00289-013-0956-6>

- Nah et al. (2006). Anti-cancer agent loaded hydrophobic bile acid conjugated hydrophilic chitosan oligosaccharide nanoparticles and preparation method thereof. Retrieved from <https://patents.google.com/patent/WO2007086651A1/en>
- Nam, K. S., Kim, M. K., & Shon, Y. H. (2007). Inhibition of proinflammatory cytokine-induced invasiveness of HT-29 cells by chitosan oligosaccharide. *Journal of Microbiology and Biotechnology*, 17(12), 2042–2045. Retrieved from <http://www.ncbi.nlm.nih.gov/pubmed/18167453>
- Naseri-Nosar, M., & Ziora, Z. M. (2018). Wound dressings from naturally-occurring polymers: A review on homopolysaccharide-based composites. *Carbohydrate Polymers*, 189(November 2017), 379–398. <https://doi.org/10.1016/j.carbpol.2018.02.003>
- Nehéz, L., Tingstedt, B., Vödrös, D., Axelsson, J., Lindman, B., & Andersson, R. (2006). Novel treatment in peritoneal adhesion prevention: protection by polypeptides. *Scandinavian Journal of Gastroenterology*, 41(9), 1110–1117. <https://doi.org/10.1080/00365520600554550>
- Norowski, P. A., Mishra, S., Adatrow, P. C., Haggard, W. O., & Bumgardner, J. D. (2012). Suture pullout strength and in vitro fibroblast and RAW 264.7 monocyte biocompatibility of genipin crosslinked nanofibrous chitosan mats for guided tissue regeneration. *Journal of Biomedical Materials Research - Part A*, 100 A(11), 2890–2896. <https://doi.org/10.1002/jbm.a.34224>
- Olsen, J. V, Ong, S.-E., & Mann, M. (2004). Trypsin Cleaves Exclusively C-terminal to Arginine and Lysine Residues. *Molecular & Cellular Proteomics*, 3(6), 608–614. <https://doi.org/10.1074/mcp.T400003-MCP200>
- Panilaitis, B., Altman, G. H., Chen, J., Jin, H. J., Karageorgiou, V., & Kaplan, D. L. (2003). Macrophage responses to silk. *Biomaterials*, 24(18), 3079–3085. [https://doi.org/10.1016/S0142-9612\(03\)00158-3](https://doi.org/10.1016/S0142-9612(03)00158-3)

- Park, J. B., & Lakes, R. S. (2007). *Biomaterials*. New York, NY: Springer New York.
<https://doi.org/10.1007/978-0-387-37880-0>
- Park, J. H., Lee, H. W., Chae, D. K., Oh, W., Yun, J. D., Deng, Y., & Yeum, J. H. (2009). Electrospinning and characterization of poly(vinyl alcohol)/chitosan oligosaccharide/clay nanocomposite nanofibers in aqueous solutions. *Colloid and Polymer Science*, 287(8), 943–950. <https://doi.org/10.1007/s00396-009-2050-z>
- Park, K. H., Kim, T. J., Cheong, T. K., Kim, J. W., Oh, B. H., & Svensson, B. (2000). Structure, specificity and function of cyclomaltodextrinase, a multispecific enzyme of the α -amylase family. *Biochimica et Biophysica Acta - Protein Structure and Molecular Enzymology*, 1478(2), 165–185. [https://doi.org/10.1016/S0167-4838\(00\)00041-8](https://doi.org/10.1016/S0167-4838(00)00041-8)
- Park, Y. R., Ju, H. W., Lee, J. M., Kim, D.-K., Lee, O. J., Moon, B. M., ... Park, C. H. (2016). Three-dimensional electrospun silk-fibroin nanofiber for skin tissue engineering. *International Journal of Biological Macromolecules*, 93, 1567–1574. <https://doi.org/10.1016/j.ijbiomac.2016.07.047>
- Piasecka-Zelga, J., Zelga, P., Szulc, J., Wietecha, J., & Ciechańska, D. (2018). An in vivo biocompatibility study of surgical meshes made from bacterial cellulose modified with chitosan. *International Journal of Biological Macromolecules*, 116, 1119–1127. <https://doi.org/10.1016/j.ijbiomac.2018.05.123>
- Plencner, M., East, B., Tonar, Z., Otáhal, M., Prosecká, E., Rampichová, M., ... Amler, E. (2014). Abdominal closure reinforcement by using polypropylene mesh functionalized with poly- ϵ -caprolactone nanofibers and growth factors for prevention of incisional hernia formation. *International Journal of Nanomedicine*, 9(1), 3263–3277. <https://doi.org/10.2147/IJN.S63095>
- Pomilio Di Loreto, F., Mangione, A., Palmisano, E., Cerda, J. I., Dominguez, M. J., Ponce, G., ... Bianco, S. (2013). Dried human amniotic membrane as an antiadherent layer for intraperitoneal placing of polypropylene mesh in rats.

Surgical Endoscopy and Other Interventional Techniques, 27(4), 1435–1440.
<https://doi.org/10.1007/s00464-012-2604-x>

Pott, P. P., Schwarz, M. L. R., Gundling, R., Nowak, K., Hohenberger, P., & Roessner, E. D. (2012). Mechanical Properties of Mesh Materials Used for Hernia Repair and Soft Tissue Augmentation. *PLoS ONE*, 7(10), e46978.
<https://doi.org/10.1371/journal.pone.0046978>

Prudente, A., Fávaro, W. J., Filho, P. L., & Riccetto, C. L. Z. (2016). Host inflammatory response to polypropylene implants: Insights from a quantitative immunohistochemical and birefringence analysis in a rat subcutaneous model. *International Braz J Urol*, 42(3), 585–593. <https://doi.org/10.1590/S1677-5538.IBJU.2015.0289>

Qi, Y., Wang, H., Wei, K., Yang, Y., Zheng, R. Y., Kim, I. S., & Zhang, K. Q. (2017). A review of structure construction of silk fibroin biomaterials from single structures to multi-level structures. *International Journal of Molecular Sciences*, 18(3). <https://doi.org/10.3390/ijms18030237>

Reynvoet, E., Van Cleven, S., Van Overbeke, I., Chiers, K., De Baets, P., Troisi, R., & Berrevoet, F. (2015). The use of cyanoacrylate sealant as simple mesh fixation in laparoscopic ventral hernia repair: a large animal evaluation. *Hernia*, 19(4), 661–670. <https://doi.org/10.1007/s10029-015-1347-8>

Rockwood, D. N., Preda, R. C., Yücel, T., Wang, X., Lovett, M. L., & Kaplan, D. L. (2011). Materials fabrication from *Bombyx mori* silk fibroin. *Nature Protocols*, 6(10), 1612–1631. <https://doi.org/10.1038/nprot.2011.379>

Sadava, E. E., Krpata, D. M., Gao, Y., Rosen, M. J., & Novitsky, Y. W. (2014a). Wound healing process and mediators: Implications for modulations for hernia repair and mesh integration. *Journal of Biomedical Materials Research - Part A*, 102(1), 295–302. <https://doi.org/10.1002/jbm.a.34676>

Sadava, E. E., Krpata, D. M., Gao, Y., Rosen, M. J., & Novitsky, Y. W. (2014b). Wound healing process and mediators: Implications for modulations for hernia

- repair and mesh integration. *Journal of Biomedical Materials Research - Part A*.
<https://doi.org/10.1002/jbm.a.34676>
- Sahbaz, A., Isik, H., Aynioglu, O., Gungorduk, K., & Gun, B. D. (2014). Effect of intraabdominal administration of *Allium sativum* (garlic) oil on postoperative peritoneal adhesion. *European Journal of Obstetrics Gynecology and Reproductive Biology*, *177*, 44–47. <https://doi.org/10.1016/j.ejogrb.2014.03.018>
- Schaub, N. J., Le Beux, C., Miao, J., Linhardt, R. J., Alauzun, J. G., Laurencin, D., & Gilbert, R. J. (2015). The effect of surface modification of aligned poly-l-lactic acid electrospun fibers on fiber degradation and neurite extension. *PLoS ONE*, *10*(9), e0136780. <https://doi.org/10.1371/journal.pone.0136780>
- Shi, L., Le Visage, C., & Chew, S. Y. (2011). Long-term stabilization of polysaccharide electrospun fibres by in situ cross-linking. *Journal of Biomaterials Science, Polymer Edition*, *22*(11), 1459–1472. <https://doi.org/10.1163/092050610X512108>
- Shin, Y. C., Yang, W. J., Lee, J. H., Oh, J. W., Kim, T. W., Park, J. C., ... Han, D. W. (2014). PLGA nanofiber membranes loaded with epigallocatechin-3-O-gallate are beneficial to prevention of postsurgical adhesions. *International Journal of Nanomedicine*, *9*(1), 4067–4078. <https://doi.org/10.2147/IJN.S68197>
- Singh, R. S., Kaur, N., & Kennedy, J. F. (2015). Pullulan and pullulan derivatives as promising biomolecules for drug and gene targeting. *Carbohydrate Polymers*, *123*, 190–207. <https://doi.org/10.1016/j.carbpol.2015.01.032>
- Singh, R. S., Kaur, N., Rana, V., & Kennedy, J. F. (2017). Pullulan: A novel molecule for biomedical applications. *Carbohydrate Polymers*, *171*, 102–121. <https://doi.org/10.1016/j.carbpol.2017.04.089>
- Smith, J. A. (2002). Sabiston. Textbook of Surgery: The Biological Basis of Modern Surgical Practice. *ANZ Journal of Surgery*, *72*(3), 248–248. <https://doi.org/10.1046/j.1445-2197.2002.2362d.x>

- Sonmez, A., Lurie, D., & Chuong, C. J. (2000). Effects of pantothenic acid on postoperative adhesion formation in a rat uterine horn model. *Archives of Gynecology and Obstetrics*, 263(4), 164–167. <https://doi.org/10.1007/s004040050274>
- Stokes, I. A. F., Gardner-Morse, M. G., & Henry, S. M. (2010). Intra-abdominal pressure and abdominal wall muscular function: Spinal unloading mechanism. *Clinical Biomechanics (Bristol, Avon)*, 25(9), 859–866. <https://doi.org/10.1016/j.clinbiomech.2010.06.018>
- Su, D., Yao, M., Liu, J., Zhong, Y., Chen, X., & Shao, Z. (2017). Enhancing Mechanical Properties of Silk Fibroin Hydrogel through Restricting the Growth of β -Sheet Domains. *ACS Applied Materials & Interfaces*, 9(20), 17489–17498. <https://doi.org/10.1021/acsami.7b04623>
- Tabasum, S., Noreen, A., Maqsood, M. F., Umar, H., Akram, N., Nazli, Z.-H., ... Zia, K. M. (2018). A review on versatile applications of blends and composites of pullulan with natural and synthetic polymers. *International Journal of Biological Macromolecules*, #pagerange#. <https://doi.org/10.1016/j.ijbiomac.2018.07.154>
- Taylor, M., Urquhart, A. J., Zelzer, M., Davies, M. C., & Alexander, M. R. (2007). Picoliter water contact angle measurement on polymers. *Langmuir*, 23(13), 6875–6878. <https://doi.org/10.1021/la070100j>
- Thonemann, B., Schmalz, G., Hiller, K.-A., & Schweikl, H. (2002). Responses of L929 mouse fibroblasts, primary and immortalized bovine dental papilla-derived cell lines to dental resin components. *Dental Materials*, 18(4), 318–323. [https://doi.org/10.1016/S0109-5641\(01\)00056-2](https://doi.org/10.1016/S0109-5641(01)00056-2)
- Thornton, M. H., Johns, D. B., Campeau, J. D., Hoehler, F., & Dizerega, G. S. (1998). Clinical evaluation of 0.5% ferric hyaluronate adhesion prevention gel for the reduction of adhesions following peritoneal cavity surgery: Open-label pilot study. *Human Reproduction*, 13(6), 1480–1485. <https://doi.org/10.1093/humrep/13.6.1480>

- Tsai, S. W., Fang, J. F., Yang, C. L., Chen, J. H., Su, L. T., & Jan, S. H. (2005). Preparation and evaluation of a hyaluronate-collagen film for preventing post-surgical adhesion. *Journal of International Medical Research*, *33*(1), 68–76. <https://doi.org/10.1177/147323000503300106>
- Van Der Maarel, M. J. E. C., Van Der Veen, B., Uitdehaag, J. C. ., Leemhuis, H., & Dijkhuizen, L. (2002). Properties and applications of starch-converting enzymes of the α -amylase family. *Journal of Biotechnology*, *94*(2), 137–155. [https://doi.org/10.1016/S0168-1656\(01\)00407-2](https://doi.org/10.1016/S0168-1656(01)00407-2)
- Vasconcelos, D. M., Gonçalves, R. M., Almeida, C. R., Pereira, I. O., Oliveira, M. I., Neves, N., ... Barbosa, M. A. (2016). Fibrinogen scaffolds with immunomodulatory properties promote in vivo bone regeneration. *Biomaterials*, *111*, 163–178. <https://doi.org/10.1016/j.biomaterials.2016.10.004>
- Vepari, C., & Kaplan, D. L. (2007). Silk as a Biomaterial. *Progress in Polymer Science*, *32*(8–9), 991–1007. <https://doi.org/10.1016/j.progpolymsci.2007.05.013>
- Vishwakarma, A., Bhise, N. S., Evangelista, M. B., Rouwkema, J., Dokmeci, M. R., Ghaemmaghami, A. M., ... Khademhosseini, A. (2016). Engineering Immunomodulatory Biomaterials To Tune the Inflammatory Response. *Trends in Biotechnology*, *34*(6), 470–482. <https://doi.org/10.1016/j.tibtech.2016.03.009>
- Wang, F., Qiao, L., Chen, L., Zhang, C., Wang, Y., Wang, Y., ... Zhang, N. (2016). The immunomodulatory activities of pullulan and its derivatives in human pDC-like CAL-1 cell line. *International Journal of Biological Macromolecules*, *86*, 764–771. <https://doi.org/10.1016/j.ijbiomac.2016.02.013>
- Wittaya-Areekul, S., & Prahsarn, C. (2006). Development and in vitro evaluation of chitosan-polysaccharides composite wound dressings. *International Journal of Pharmaceutics*, *313*(1–2), 123–128. <https://doi.org/10.1016/j.ijpharm.2006.01.027>
- Wong, V. W., Rustad, K. C., Galvez, M. G., Neofytou, E., Glotzbach, J. P., Januszyk,

- M., ... Gurtner, G. C. (2011). Engineered Pullulan–Collagen Composite Dermal Hydrogels Improve Early Cutaneous Wound Healing. *Tissue Engineering Part A*, 17(5–6), 631–644. <https://doi.org/10.1089/ten.tea.2010.0298>
- Wotton, F. T., & Akoh, J. A. (2009). Rejection of Permacol® mesh used in abdominal wall repair: A case report. *World Journal of Gastroenterology*, 15(34), 4331–4333. <https://doi.org/10.3748/wjg.15.4331>
- Xu, Y., Zou, L., Lu, H., & Kang, T. (2017). Effect of different solvent systems on PHBV/PEO electrospun fibers. *RSC Advances*, 7(7), 4000–4010. <https://doi.org/10.1039/c6ra26783a>
- Yetkin, G., Uludag, M., Citgez, B., Karakoc, S., Polat, N., & Kabukcuoglu, F. (2009). Prevention of peritoneal adhesions by intraperitoneal administration of vitamin E and human amniotic membrane. *International Journal of Surgery (London, England)*, 7(6), 561–565. <https://doi.org/10.1016/j.ijso.2009.09.007>
- Yoon, H. J., Moon, M. E., Park, H. S., Im, S. Y., & Kim, Y. H. (2007). Chitosan oligosaccharide (COS) inhibits LPS-induced inflammatory effects in RAW 264.7 macrophage cells. *Biochemical and Biophysical Research Communications*, 358(3), 954–959. <https://doi.org/10.1016/j.bbrc.2007.05.042>
- You, R., Li, X., Liu, Y., Liu, G., Lu, S., & Li, M. (2014). Response of filopodia and lamellipodia to surface topography on micropatterned silk fibroin films. *Journal of Biomedical Materials Research - Part A*, 102(12), 4206–4212. <https://doi.org/10.1002/jbm.a.35097>
- Yu, H. Y., Liu, L. Q., Tang, Z. Q., Yan, M. G., Gu, J. S., & Wei, X. W. (2008). Surface modification of polypropylene microporous membrane to improve its antifouling characteristics in an SMBR: Air plasma treatment. *Journal of Membrane Science*, 311(1–2), 216–224. <https://doi.org/10.1016/j.memsci.2007.12.016>
- Zhang, W., Li, Y., Jiang, D., Xie, S., Zeng, M., Chen, J., ... Zou, X. (2018). Promotion of Hernia Repair with High-Strength, Flexible, and Bioresorbable Silk Fibroin Mesh in a Large Abdominal Hernia Model. *ACS Biomaterials Science and*

Engineering, 4(6), 2067–2080. <https://doi.org/10.1021/acsbiomaterials.7b00666>

Zhang, Z., Ni, J., Chen, L., Yu, L., Xu, J., & Ding, J. (2011). Biodegradable and thermoreversible PCLA-PEG-PCLA hydrogel as a barrier for prevention of post-operative adhesion. *Biomaterials*, 32(21), 4725–4736. <https://doi.org/10.1016/j.biomaterials.2011.03.046>

Zhang, Z., Ni, J., Chen, L., Yu, L., Xu, J., & Ding, J. (2012). Encapsulation of cell-adhesive RGD peptides into a polymeric physical hydrogel to prevent postoperative tissue adhesion. *Journal of Biomedical Materials Research - Part B Applied Biomaterials*, 100 B(6), 1599–1609. <https://doi.org/10.1002/jbm.b.32728>

APPENDIX

CALIBRATION CURVES

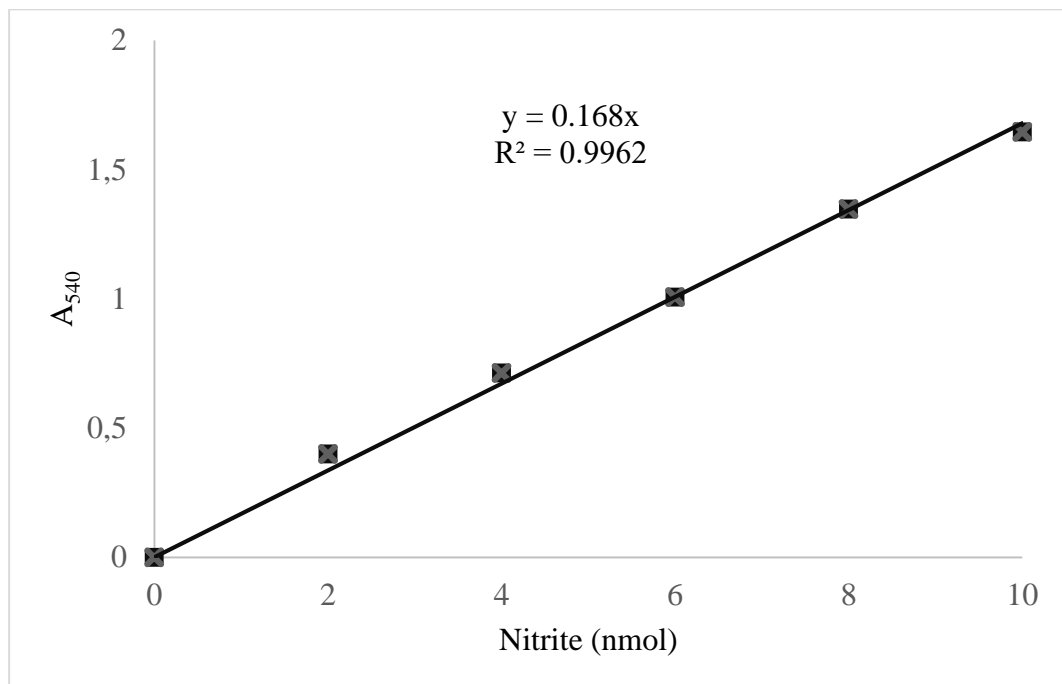


Figure A. 1 Standard curve for NO⁻ detection assay constructed with nitrite (NO₂) standards (0-10ng).